

NONLINEAR PERFORMANCE ANALYSIS OF STEEL LATTICE ENERGY
DISTRIBUTION TOWERS

A THESIS SUBMITTED TO
THE GRADUATE SCHOOL OF NATURAL AND APPLIED SCIENCES
OF
MIDDLE EAST TECHNICAL UNIVERSITY

BY

YUNUS ANIL KÖŞKER

IN PARTIAL FULFILLMENT OF THE REQUIREMENTS
FOR
THE DEGREE OF MASTER OF SCIENCE
IN
CIVIL ENGINEERING

FEBRUARY 2022

Approval of the thesis:

**NONLINEAR PERFORMANCE ANALYSIS OF STEEL LATTICE
ENERGY DISTRIBUTION TOWERS**

submitted by **YUNUS ANIL KÖŞKER** in partial fulfillment of the requirements for the degree of **Master of Science in Civil Engineering, Middle East Technical University** by,

Prof. Dr. Halil Kalıpçılar
Dean, Graduate School of **Natural and Applied Sciences**

Prof. Dr. Erdem Canbay
Head of the Department, **Civil Engineering**

Prof. Dr. Eray Baran
Supervisor, **Civil Engineering**

Examining Committee Members:

Prof. Dr. Uğurhan Akyüz
Civil Engineering METU

Prof. Dr. Eray Baran
Civil Engineering, METU

Prof. Dr. Oğuzhan Hasançebi
Civil Engineering, METU

Prof. Dr. Afşin Sarıtaş
Civil Engineering, METU

Prof. Dr. Tolga Akış
Civil Engineering, Atılım University

Date: 03.02.2022

I hereby declare that all information in this document has been obtained and presented in accordance with academic rules and ethical conduct. I also declare that, as required by these rules and conduct, I have fully cited and referenced all material and results that are not original to this work.

Name Last name : Yunus Anıl Köşker

Signature :

ABSTRACT

NONLINEAR PERFORMANCE ANALYSIS OF STEEL LATTICE ENERGY DISTRIBUTION TOWERS

Köşker, Yunus Anıl
Master of Science, Civil Engineering
Supervisor: Prof. Dr. Eray Baran

February 2022, 100 pages

Steel lattice tower structures play a vital role in overhead energy transmission and distribution networks. The safety of the towers has a great significance in order to keep power systems functioning. Despite their crucial function, these structures are susceptible to damage and sometimes total collapse as a result of environmental overloading. The collapse of tower structures in varying magnitude has been reported due to changing global weather patterns in the past few years. On January 16th, 2019, strong wind and heavy precipitation were predominant in Tufanbeyli, Turkey, and resulted in the collapse of 45 steel lattice distribution towers. In this thesis, some of these collapsed towers were taken as a case study and an investigation was carried out to evaluate the structural performance, estimate the load-carrying capacity, and determine the collapse mechanism of the structures under different loading conditions and modeling assumptions. On this basis, linear analyses were performed on eighteen suspension towers and three tension towers under the design loads and the failure condition loads to identify the exact cause of tower failures. Failure condition analyses of the towers were conducted by considering the loading cases of conductor break and ice with wind. Measured material capacities for tower steel

members and conductors were incorporated in these analyses in an attempt to accurately simulate the actual conditions. The realistic conditions that the towers were likely to experience on the day of the incident were predicted based on meteorological data. Numerical results reveal that under design level loads and the specified loading cases the towers possess the safety level intended by the related design documents. However, at the time of the incident, ice accumulation around the conductors was multiple in size compared to the specified value by the design code. According to site inspections and field reports, the tower members experiencing failure were predicted accurately by failure condition analyses. Further studies were performed on the selected towers, focusing on the nonlinear properties to reveal the full collapse mechanism of the towers and failure sequence of the structural members. The nonlinear static pushover analysis with lumped plasticity approach was employed by modeling axial hinges with piece-wise linear force-deformation characteristics. The capacity curves of the towers were investigated and the most vulnerable parts of the towers were demonstrated. Results obtained from nonlinear analyses indicate that the tower response is governed by buckling of leg members in the tower body under ice and wind interaction condition, while for conductor break loading case the response is governed mostly by bolt bearing deformation of horizontal and brace members located near crossarms. It was determined that bolt bearing capacity provides a more ductile failure mechanism compared to sudden collapse due to member buckling.

Keywords: Steel Lattice Towers, Static Nonlinear Analysis, Plastic Hinge, Overhead Energy Distribution Lines

ÖZ

ÇELİK KAFES ENERJİ DAĞITIM DİREKLERİNİN DOĞRUSAL OLMAYAN PERFORMANS ANALİZİ

Köşker, Yunus Anıl
Yüksek Lisans, İnşaat Mühendisliği
Tez Yöneticisi: Prof. Dr. Eray Baran

Şubat 2022, 100 sayfa

Çelik kafes direk yapıları, havai enerji iletim ve dağıtım hattı ağlarında hayati bir rol oynamaktadır. Güç sistemlerinin çalışır durumda kalması için direklerin güvenliği büyük önem taşımaktadır. Son yıllarda değişen küresel hava koşulları nedeniyle dünya çapında çeşitli direk yıkılmaları rapor edilmiştir. 16 Ocak 2019'da Türkiye'nin Tufanbeyli ilçesinde düşük sıcaklıkta şiddetli rüzgâr ve yoğun bir kar yağışı etkili olmuştur ve 45 adet çelik kafes enerji dağıtım direği yıkılmıştır. Bu tezde Tufanbeyli'deki direkler örnek alınmıştır ve farklı yükleme koşulları ve modelleme varsayımları altında direklerin yapısal performans değerlendirilmesi gerçekleştirilerek yük taşıma kapasitesi ve direklerin göçme mekanizmasının belirlenmesine yönelik çalışmalar yapılmıştır. Bu doğrultuda, kesin yıkılma sebeplerini belirlemek için tasarım yükleri ve gerçekçi durum yükleri altında 18 adet taşıyıcı ve 3 adet durdurucu çelik kafes direk üzerinde çalışmalar yapılmıştır. Gerçekçi durum yükleri, direklerin ve iletkenlerin yıkılma anında maruz kaldıkları dış yükleri yansıtmaktadır ve analizlerde iletken kopması ve buzlu iletkenlere rüzgâr etkimesi olmak üzere iki farklı yükleme koşulu dikkate alınmıştır. Doğrusal analiz sonuçlarına göre direkler güncel tasarım şartnamesini sağlamıştır. Buna karşın,

yıkılma anında, iletkenlerin etrafındaki buz kalınlığının, tasarım şartnamesinde belirtilen değere kıyasla oldukça fazla olduğu belirlenmiştir. Yıkılma mekanizmasını ve yapısal elemanların göçme sırasını ortaya çıkarmak için doğrusal olmayan statik itme analizi yöntemi ile daha ileri çalışmalar yapılmıştır. Yığılı plastik davranış modeli aksel mafsallar ile modellenmiştir ve direklerdeki kritik elemanlar belirlenmiştir. Analiz sonuçlarına göre, buzlu iletkenlere rüzgâr yüklemesi koşulu direğin gövdesinde bulunan bacak elemanlarında burkulmaya sebep olurken, iletken kopması yüklemesi koşulu direğin konsolları arasındaki yatay ve çapraz eleman birleşimlerinde göçmeye sebep olmaktadır. İletken kopması koşulunda daha sünek bir davranış görülürken, buzlu iletkenlere rüzgâr koşulunda burkulma sebebiyle yapıların kapasite eğrilerinde ani bir göçme tespit edilmiştir.

Anahtar Kelimeler: Çelik Kafes Direkler, Statik Doğrusal Olmayan Analiz, Plastik Mafsal, Havai Enerji Dağıtım Hattı

To My Family

ACKNOWLEDGMENTS

I would like to thank and express my heartfelt gratitude to my thesis supervisor, Prof. Dr. Eray Baran, for his valuable guidance, encouragement, and patience throughout the preparation of this thesis. His educative comments and constructive criticism have been extremely helpful for my self-development in academic and professional life.

Toroslar Elektrik Dağıtım A.Ş. provided financial and technical support for this study. Help from numerous administrative and technical staff, especially Hülya Akinç and Gökhan Eyigün, is gratefully acknowledged.

This thesis would not have been possible without the support of my family. I owe my deepest appreciation to my parents, Seher and Osman Köşker, for their endless care, understanding, and love they have given me during my life. A special thank you to my lovely fiancé Yağmur Ölmez for her love and encouragement. I would like to sincerely thank my dearest brother Yavuz Arda Köşker for his priceless support.

Lastly, I would like to extend my thanks to my cousin Berkcan Köşker and my friends Soner Gürsan and Ahmet Özlemiş for their great friendship and encouragement. I also would like to express my gratitude to dear Eser Çabuk for giving moral and valuable support during this study.

TABLE OF CONTENTS

ABSTRACT.....	v
ÖZ	vii
ACKNOWLEDGMENTS	x
TABLE OF CONTENTS.....	xi
LIST OF TABLES	xiii
LIST OF FIGURES	xiv
1 INTRODUCTION	1
1.1 Steel Lattice Transmission and Distribution Towers	3
1.2 Thesis Objectives and Scope.....	5
1.3 Organization of the Thesis	6
2 LITERATURE REVIEW	7
2.1 Failure Mechanisms of Collapsed Towers	7
2.2 Linear and Nonlinear Tower Analysis Approaches	9
2.3 Tower Loading Conditions.....	12
2.4 Strengthening and Retrofitting of Tower Structures	14
3 INVESTIGATION OF TUFANBEYLI TOWERS	17
3.1 Description of Investigated Power Distribution Line.....	17
3.2 Site Inspections on Towers	20
3.3 Analyses of Towers	20
3.3.1 Numerical Modeling of Towers.....	24

3.3.2	Analysis of Towers under Design Level Loads	25
3.3.3	Analysis of Towers under Failure Condition	35
4	NONLINEAR ANALYSIS OF TOWERS	47
4.1	Background and Objective.....	47
4.1.1	Pushover Analysis	49
4.1.2	Modeling of Plastic Hinges	51
4.2	Nonlinear Performance of the Towers.....	56
4.2.1	Ice and Wind Interaction (IWI) Load Case	56
4.2.2	Middle Conductor Break (MCB) Load Case.....	62
4.2.3	Comparison of Numerically Predicted and Observed Failures	68
5	CONCLUSIONS	71
	REFERENCES	75
	APPENDICES	81
A.	Appendix A - Schematic Figures of RU and DU Type of Towers.....	81
B.	Appendix B - Investigated Failed Towers During Site Visit.....	82
C.	Appendix C – Structural Properties of No.106 Tower	85

LIST OF TABLES

Table 3.1 Nominal section properties of the conductors used in the investigated power distribution line (TEDAŞ, 2000).....	18
Table 3.2 Properties of the angle sections used in Tufanbeyli towers.....	19
Table 3.3 Design properties of Tufanbeyli towers and observed damage.....	22
Table 3.4 Loading cases specified for suspension towers (TEDAŞ, 2008).....	26
Table 3.5 Loading cases specified for tension towers (TEDAŞ, 2008).....	27
Table 3.6 Maximum member capacity ratios obtained for suspension towers.....	33
Table 3.7 Maximum capacity ratios obtained for tension towers.....	34
Table 3.8 Material properties of the specimens.....	37
Table 3.9 Loading cases for failure condition analysis.....	39
Table 3.10 Failure condition loads.....	40
Table 3.11 Failure condition analysis results.....	42
Table 4.1 Load-carrying capacities and ultimate displacements under IWI loading case.....	61
Table 4.2 Load-carrying capacities and ultimate displacements under MCB loading case.....	68

LIST OF FIGURES

Figure 1.1. 154 kV Bosphorus crossing steel lattice transmission tower	1
Figure 1.2. Examples of reported tower failures: (a) Kefallonia Island, Greece, 2006; (b) Hainan, China, 2014; (c) Münsterland, Germany, 2005.....	2
Figure 1.3. Components and parts of transmission/distribution towers: (a) components of an energy line; (b), (c) typical tower parts	4
Figure 3.1. Meteorological data from Tufanbeyli station for January 2019	17
Figure 3.2. Observations during the day of the incident: (a) ice sleeves around conductors; (b) a collapsed tower; (c) staff removing ice on conductors.....	18
Figure 3.3. Locations of the failed towers along the power distribution line.....	21
Figure 3.4. Wind and weight spans for towers	23
Figure 3.5. Structural analysis model of RU-2 type tower	24
Figure 3.6. Conductor break loading cases used for suspension towers	28
Figure 3.7. Conductor break loading cases used for tension towers	28
Figure 3.8. Ice load map of Turkey (TEDAŞ, 2008).....	30
Figure 3.9. Loading cases and calculated loads (kN) on tower No.112 (RU-4 type tower).....	31
Figure 3.10. Loading cases and calculated loads (kN) on tower No. 119 (DU+0 type tower).....	32
Figure 3.11. Tensile testing of conductor steel and aluminum wires	35
Figure 3.12. Tension testing of steel coupon samples: (a) sample in the testing machine; (b) coupon samples extracted from the steel angle section; (c) tested coupon samples	36
Figure 3.13. Stress-strain curves of the test specimens	37
Figure 3.14. Results for tower No.106: (a) damage observed in the field; (b) member capacity ratios in MCB loading case; (c) member capacity ratios in TCB loading case	43

Figure 3.15. Member capacity ratios obtained under IWI loading case with 60 km/h wind.....	44
Figure 4.1. Generic linear and nonlinear force-deformation relationships	48
Figure 4.2. Monitored joints and degrees of freedom for IWI and MCB loading cases	51
Figure 4.3. Generalized hinge curve for steel members (FEMA, 2000).....	52
Figure 4.4. Type-I Hinge Properties	54
Figure 4.5. Type-II Hinge Properties	54
Figure 4.6. Type-III Hinge Properties.....	54
Figure 4.7. Load-displacement response of Tower No.106 under IWI loading case	57
Figure 4.8. Progression of damage in Tower No.106 under IWI loading case.....	57
Figure 4.9. Load-displacement response of Tower No.107 under IWI loading case	58
Figure 4.10. Progression of damage in Tower No.107 under IWI loading case.....	58
Figure 4.11. Load-displacement response of Tower No.108 under IWI loading case	59
Figure 4.12. Progression of damage in Tower No.108 under IWI loading case.....	59
Figure 4.13. Pushover curves of the towers under IWI loading case.....	62
Figure 4.14. Load-displacement response of Tower No.106 under MCB loading case.....	64
Figure 4.15. Progression of damage in Tower No.106 under MCB loading case ..	64
Figure 4.16. Load-displacement response of Tower No.107 under MCB loading case.....	65
Figure 4.17. Progression of damage in Tower No.107 under MCB loading case ..	65
Figure 4.18. Load-displacement response of Tower No.108 under MCB loading case.....	66
Figure 4.19. Progression of damage in Tower No.108 under MCB loading case ..	66
Figure 4.20. Pushover curves of the towers under MCB loading case	67
Figure 4.21. Observed and predicted collapse of No.106 tower.....	69

Figure 4.22. Observed and predicted collapse of No.107 tower	69
Figure 4.23. Observed and predicted collapse of No.108 tower	70

CHAPTER 1

INTRODUCTION

Energy transmission and distribution line systems have a crucial role in modern life as they provide the essential links between power plants and communities. Steel lattice towers, which have been widely used for many other functions, including telecommunication and wind turbines, are the vital component of overhead energy transmission and distribution systems. The primary role of transmission/distributions towers is to transfer the power for long distances safely with sufficient height from ground (Figure 1.1).



Figure 1.1. 154 kV Bosphorus crossing steel lattice transmission tower

Steel lattice towers are backbones in the operation of electrical transmission/distribution grids. They are considered as one of the most critical components of the power networks. The safety of these structures has a great significance in order to keep power systems functioning properly. Although steel lattice towers are very efficient structures for resisting the external load actions arising from environmental effects and weight of the line components, these structures are vulnerable to extensive damage due to natural hazards. Failures in transmission/distribution towers in varying magnitude have been reported during the past few decades due to changes in global weather patterns with extreme winds and heavy ice actions (Alminhana et al., 2018; Klinger et al., 2011; Xie and Sun, 2012). In Figure 1.2, some of the recently occurred failure examples on towers are shown.



a)



b)



c)

Figure 1.2. Examples of reported tower failures: (a) Kefallonia Island, Greece, 2006; (b) Hainan, China, 2014; (c) Münsterland, Germany, 2005

Various environmental effects may cause cascading tower failures along a line, as the failure of a tower usually propagates the collapse along with the adjacent towers. This leads to severe damage to the entire energy line architecture and results in economic losses associated with power disruption. In order to mitigate the damage resulting from natural hazards, determination of collapse mechanism under different failure modes as well as an accurate prediction of the structural capacity of steel lattice towers are essential for the reliability of energy transmission/distribution networks.

1.1 Steel Lattice Transmission and Distribution Towers

Steel lattice transmission/distribution towers are self-supported space truss frame structures composed of main structural members and bracing systems. Lattice towers are very efficient structural systems for resisting high lateral forces and practical at the same time due to ease of construction applications. Towers are typically constructed using standard single or built-up steel angle members with the ends connected to other members through bolted joints, either directly or through gusset plates. Towers are typically composed of leg, brace, and horizontal members, as illustrated in Figure 1.3.

The components of a typical transmission/distribution line are as follows: conductors through which power is transmitted, tower structures, and insulators that isolate the electricity and connect conductors to the tower. Typical layout of these components is shown in Figure 1.3.

Transmission/distribution towers come in many shapes and sizes due to different operational purposes. Parts of a typical transmission tower are tower body, cage, crossarm, waist, and peak (Figure 1.3). On the other hand, distribution towers usually have relatively simple architecture and smaller size compared to transmission towers. The reason for the difference in the overall geometry of transmission and distribution towers is the voltage level. Higher voltage levels used in transmission

lines require the towers to be relatively tall and crossarms to be wide in order to satisfy the electrical clearance requirements. Increased tower height, together with large diameter conductors, result in higher level of design forces in transmission towers as compared to the towers utilized in distribution networks. Such a high level of design forces dictates the use of members with relatively large cross sections.

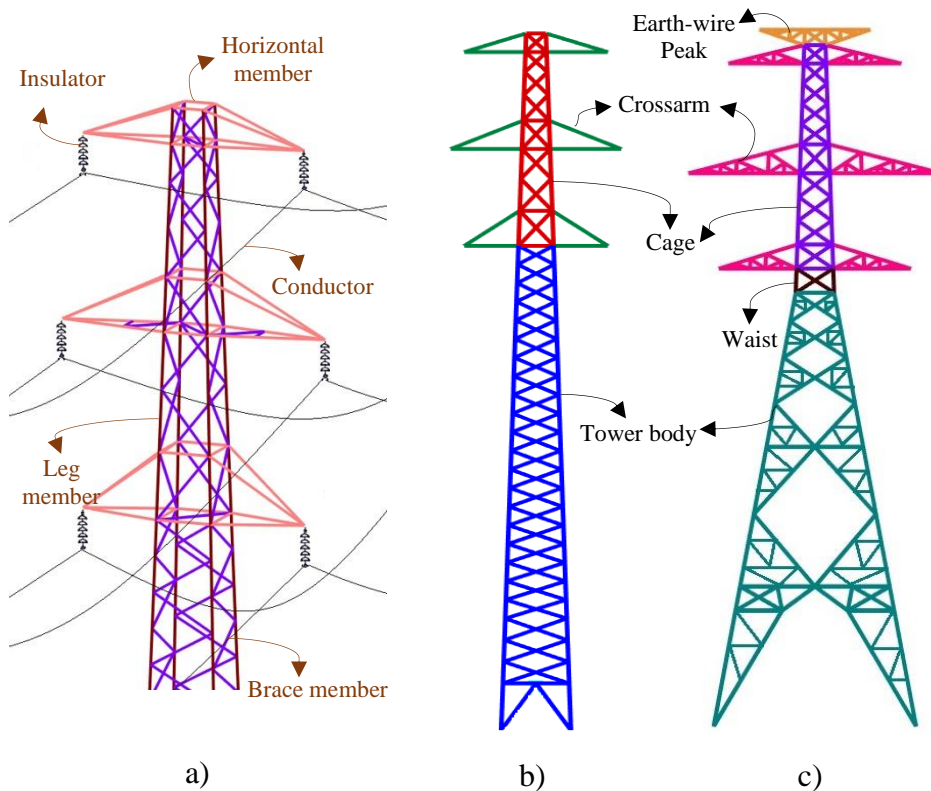


Figure 1.3. Components and parts of transmission/distribution towers: (a) components of an energy line; (b), (c) typical tower parts

In a typical power transmission/distribution line, towers vary based on their roles and can be classified as suspension, tension, and terminal towers. Suspension towers, which constitute the majority of transmission/distribution towers in service, are intended to carry only the weight of the conductors and insulators. The conductors are simply suspended from the towers through insulators. Suspension towers are used on straight sections of the energy line or when the angle of line deviation is small. They are lightweight and therefore more economical structures compared to tension and terminal towers. Tension towers are designed to support the additional tension

loads develop in conductors as a result of line stringing operation. This type of towers can be used at any location but are usually preferred at turning points of the line where the line deviation angle is relatively large. Tension towers are utilized in power transmission/distribution lines in a less frequent pattern than suspension towers. Terminal towers are the heaviest structures in a transmission/distribution line and are located at the end of the line. On one side of terminal towers, the conductors are connected to the electrical substation. Therefore, these towers are subjected to one-side tension loads exerted by the conductors.

Transmission/distribution towers are subjected to external loads due to various sources during their service lives. Loads that are considered in structural design include self-weight of the power line components (i.e., tower, conductors, insulators), wind and ice loads on the conductors, wind loads on the insulators, wind loads on the tower members, and tension loads induced by line deviation and conductor break or unbalanced loading conditions. ASCE 74 (2010), ASCE 10-15 (2015), and EN50341 (2012) are the primary design guides and provisions considered for the determination of loads and also structural design of towers. In Turkey, the current technical specification by the Turkish Power Distribution Agency (TEDAŞ, 2008) is the key document providing guidelines on loading and design of steel lattice distribution towers.

1.2 Thesis Objectives and Scope

The main focus of this thesis is on the investigation of failure conditions of steel lattice distribution towers by comparing the current design code assumptions and actual failure conditions observed in the field. A part of the investigation, the recent collapse of the 34.5 kV voltage capacity distribution towers in Tufanbeyli district was taken as the case study, and linear and nonlinear analyses of the towers were performed. The case-study towers were investigated by linear analyses in an attempt to evaluate the compliance of their structural design according to the loading cases specified by the related design document (TEDAŞ, 2008). Nonlinear analyses were

conducted under the “realistic” loading conditions that the selected collapsed towers were subjected to at the time of the incident. In this way, the safety levels of the towers were determined by considering two different loading conditions determined by site inspections and meteorological data. The load conditions were described as middle conductor break (MCB) and ice and wind interaction (IWI). In these realistic condition analyses, measured material properties for the tower members and conductors were used. The response of the towers determined this way was compared with the site-observed conditions of both the collapsed and intact towers.

1.3 Organization of the Thesis

In addition to the Introduction chapter, there are four more chapters in this thesis. Chapter 2 gives a review of the current literature on various aspects of transmission/distribution towers and nonlinear analysis approaches, as well as strengthening applications. In Chapter 3, results from linear analysis of the towers under design and failure conditions are presented. Additionally, this chapter gives the results of material testing on the conductor sample and samples extracted from steel angle sections taken out from the collapsed towers. In Chapter 4, response of the selected towers performed under two different loading conditions in nonlinear analyses is discussed. Conclusions of the study are summarized in Chapter 5.

CHAPTER 2

LITERATURE REVIEW

There exist several studies in the literature on steel lattice towers, and the studies differ depending on the various design needs of the structures. In this thesis, the literature review is focused on several topics to summarize the essential characteristics of the structures. First, the studies on the structural capacity assessment of collapsed towers are presented, and the failure mechanisms are reviewed. The comparison of the failed conditions and numerical results are discussed. Next, the nonlinear analysis approaches applied on tower structures are overviewed, followed by tower loading condition assumptions. Lastly, strengthening and retrofitting applications applied on steel lattice towers are reviewed.

2.1 Failure Mechanisms of Collapsed Towers

Transmission/distribution tower failures in varying magnitudes have been reported during the past few years. Investigation on these failures has been documented by different researchers. Anagnostatos et al. (2013) investigated the collapse of transmission towers in Kefallonia, Greece in 2006. A total of ten 150 kV steel lattice towers collapsed as a result of 89-102 km/h wind speeds and excessive ice accumulation on conductors. It was reported that the diameter of the ice-covered conductors reached 15 cm at the time of the failure, which is approximately 2.42 times the value specified in EN 50341 (2012) design guide. Therefore, the acting wind loads on conductors were increased and consequently the towers were collapsed. Collapse of 110 kV double circuit tension towers was investigated by Jian et al. (2013). The towers were reported to fail due to the wind loads exceeding design values. Based on their findings, Anagnostatos et al. and Jian et al. recommend revision of the design regulations in order to reflect the changing meteorological

conditions in recent years. Another recommendation provided as a result of these investigations is to keep the tower spans shorter in newly constructed lines.

In a study by Klinger et al. (2011), a total of eleven collapsed transmission towers in Münsterland, Germany in 2005 were analyzed under (1) the design regulations at the time of the construction, (2) the current design code, and (3) the real failure loading conditions. The towers were reported to collapse due to unbalanced ice loading on conductors with a wind speed of 65 km/h. Additionally, embrittlement of brace members due to ageing accelerated the failure process, which has been determined by experimental studies. It was suggested that the assessment of same type of existing transmission towers should be conducted in order to evaluate the compliance of the design loads specified in EN 50341 (2012).

Zhang and Xie investigated the failure mechanism of a tower collapsed during a typhoon and indicated that the failure was triggered by overloading of brace members (2019). Therefore, even though these are secondary members special attention should be paid on design of these components. A similar observations was also reported by Yang, et al. in the study on wind-induced destruction of power transmission towers (2016).

Edgar and Sordo (2017) reported a study on two 400 kV transmission towers to assess their vulnerability under the extreme loading induced by Hurricane Wilma that hit Yucatan Peninsula in 2005. The results were discussed under the action of load patterns from four wind design codes, and a good correspondence among the compared codes is stated. Full-scale testing and numerical analyses of a 400 kV steel lattice transmission tower with built-up cruciform leg members were investigated by Shukla et al. (2021) in order to determine the effect of bending moments induced by eccentric loading at the connections. Results from the numerical model indicated that the collapse of the tower may have been caused by the small eccentricity between the main member axial forces.

2.2 Linear and Nonlinear Tower Analysis Approaches

There are different approaches available in the literature that have been used to determine the structural characteristics of tower structures by several researchers. The linear analyses approach is mostly used to evaluate the compliance of the tower design with the design standards (Anagnostatos et al., 2013; Klinger et al., 2011). As one of the first comprehensive studies on nonlinear analysis of steel lattice transmission towers, Al-Bermani and Kitipornchai (1992) developed an analytical technique to evaluate the ultimate strength of steel lattice tower. The method that they employed considers both geometric and material nonlinearities using an equivalent tangent stiffness matrix of the members. The lumped plasticity approach was adopted for the expected inelastic response of the members. Rao and Kalyanaraman (2001) investigated the nonlinear structural modeling approach on a panel of the transmission tower by employing both beam-column elements and plate elements. Effects of member eccentricity and rotational rigidity of joints, as well as material nonlinearity were taken into account. Good agreement was obtained between the numerical predictions and test results.

Fu and Li (2018) and Wang et al. (2019) conducted static nonlinear analyses considering the initial eccentricity and geometric imperfections obtained from linear buckling analysis by uniform imperfection mode method. The capability of nonlinear analysis with material nonlinearity and imperfections in the structural capacity assessment was addressed. The failure modes determined by nonlinear analysis using bilinear isotropic hardening model in ANSYS software were confirmed with the experimental observations.

Tian et al. (2018) conducted nonlinear pushover analyses and full-scale tests on two different types of towers under thirteen load cases considering 27 m/s wind speed and 15 mm ice thickness. The towers were modelled with ABAQUS software by using beam elements. In nonlinear static analysis, the progression of failure was modeled using the birth-to-death element approach and arc-length method was used for solution control. A user-defined material model was created to introduce member

instability in the model accurately. Results indicated that the collapse of the investigated towers occurred due to buckling of the leg members located in the lower part of the towers.

Displacement-controlled pushover analyses on two types of tension towers were carried out by Edgar and Sordo (2017) to evaluate the failure sequence and determine the safety level of the structures. Structural members were modeled as beam-column elements represented by lumped plastic hinges in SAP2000 software. Based on the numerical results, an evaluation of wind load patterns provided in different design codes was provided.

Although static nonlinear analysis models are generally adopted for towers, there are also a number of researchers considering dynamic actions on steel lattice transmission towers. Zhang et al. (2019) investigated the wind speeds that resulted in failure by employing static and dynamic nonlinear analysis by using ANSYS software. The numerical results suggest that as the members vibrate under the dynamic external loads, the load distribution in the tower changes. In a study by Li et al. (2017) the dynamic impact effects resulting from the conductor break were investigated, and the results indicate that the dynamic instability occur earlier than the static instability. Hence, it was suggested to consider the dynamic effects in the failure investigations.

Tian et al. (2019) and Wang et al. (2014) developed an incremental dynamic analysis (IDA) procedure for numerical analysis of steel power transmission towers. In this respect a transmission line consisting of two towers and three spans were modelled in ABAQUS software. For the structural models, beam and truss elements were adopted for tower members and conductors, respectively. The critical wind speed that causes the collapse of a long-span transmission tower was determined by considering the probability of failure in various wind attack angles. According to the results of the comparative studies, it was stated that the capacity values obtained from dynamic analysis were lower than those obtained from static analysis. Loss of

stability was observed to occur earlier under dynamic load effects compared to the static case.

The collapse analysis of a long-span transmission tower-line system subjected to the 1999 Chi-Chi earthquake was investigated by Tian et al. (2017). The IDA procedure was adopted by considering the geometrical and material nonlinearities. The Tian-Ma-Qu material model (Tian et al., 2018) was used to introduce the nonlinear properties to the members. It was concluded that more attention should be paid to seismic design of this type of towers due to some tower segments possessing a relatively high probability of damage under seismic effects. Shear deformations contributed to the failure of diagonal and horizontal members, while bending deformations led to buckling of leg members. It was stated that the failure of a diagonal or horizontal member may accelerate the total collapse of the structure.

More than 20 steel lattice transmission towers were failed by progressive collapse due to the 2008 Wenchuan earthquake. Tian et al. (2016) simulated the progressive collapse of these towers under earthquake excitation. Failure path, fracture position, and collapse resistance of the towers were investigated. The results indicated that the diagonal brace members are more vulnerable to overloading than the main leg members. It was also reported that analysis under multi-component seismic excitation is more prone to collapse than longitudinal seismic excitation. On this basis, Alminhana et al. (2018) conducted a study on multi-span transmission line sections under progressive failure scenarios. Two case studies were presented to assess the anti-cascade load case and examine the vulnerability of an existing transmission tower. The static and dynamic analyses were performed on guyed and freestanding towers. The towers were modeled with conductor, insulator sets, and steel lattice supports fully discretized into finite elements. The static analysis results were compared with the dynamic responses of the line section under the conductor break condition. The proposed dynamic analysis technique was reported to predict the main causes resulting in the collapse of the investigated towers.

2.3 Tower Loading Conditions

Analysis of steel power transmission lines under different loading effects has been presented by several researchers. Li et al. (2017) investigated the conductor break loading condition on a transmission line consisting of three towers and two spans of conductors. On this basis, parametric research was performed to observe the influence of the ice thickness accumulated around conductors, weight span, and insulator length. Based on pushover analysis results it was clarified that longer weight spans and larger conductor tensions due to ice sleeves lead to smaller load-carrying capacity. Similarly, use of shorter insulators negatively affected the static load bearing capability. In other studies by Li et al. (2018, 2020) similar findings were determined for the insulator break loading condition. It was concluded that the insulator breakage leads to unbalanced loads, which resulted in an increase of the vertical load on the towers.

Tian et al. (2018) investigated the ultimate capacity and failure mechanism of two types of power transmission towers subjected to conductor break as well as ice and wind interaction (IWI) loading conditions. The study included numerical analyses combined with full-scale tests. Based on the numerical and experimental results, the tower segments close to the crossarms were reported to be more susceptible to failure under the investigated loading conditions. An extensive investigation was conducted by Vincent et al. (2004) on a line segment including 12 towers and 11 spans of conductors. The results obtained by tests compared with nonlinear dynamic analyses results under several failure conditions. The results indicated that, the calculated longitudinal loads were smaller than the loads originating from conductor failure. The failure mode was reported to be a determining factor in the amplification of loading due to dynamic response of the tower and line system.

The effects of wind attack angle on the towers and the ice thickness on the conductors were investigated under ice and wind interaction (IWI) loading conditions by Liu et al. (2018). The most unfavorable wind direction was determined as perpendicular to the power line under the ice loading. In this loading conditions, a 30 mm ice thickness

around the conductors resulted in overloading in some of the members in the upper part of the tower.

A parametric study was carried out by Fu and Li (2018) to demonstrate the failure sequence of a 500 kV transmission tower with the uncertainties of material properties and section dimensions. The failure of each structural member under different wind directions was analyzed, and it was stated that the most critical section is the middle part of the tower body, while the most unfavorable wind attack angle is perpendicular to the power line. Another probabilistic study to predict the response of a power transmission line under wind loading and excitations induced by rain loading was conducted by Fu et al. (2019). Uncertainties associated with material properties and section dimensions were included in the analyses. For the investigated towers the main failure pattern included overloading of main leg members. It was concluded that the presence of rainfall decreased the wind speed capacity of the towers. The rainfall effect was observed to increase significantly with increasing number of connector bundles.

To study the seismic risk evaluation, probabilistic fragility analysis of latticed steel tubular transmission towers subjected to near-field ground motions, was conducted by Pan et al. (2020). It was determined that the fragility of the tower is greatly affected by the seismic incident angle. The direction corresponding to the longitudinal direction of the line was reported to be the most unfavorable direction for the towers under the investigated ground motions. It was also concluded that neglecting the coupling between the tower and the conductors may lead to overestimation of tower seismic capacity. The influence of various sources of uncertainty on the probabilistic seismic demands of towers was numerically investigated by Tian et al. (2019) and Fu et al (2022). Random samples of different uncertainty parameters, including ground motion variability and structural modeling uncertainties, were generated. Seismic fragility curves were determined through a nonlinear IDA procedure. The results indicated that deterministic structural parameters are acceptable for estimating seismic fragility of the investigated towers. The collapse simulation of a steel lattice transmission tower subjected to a

unidirectional earthquake ground motion was further investigated by seismic fragility analyses by Long et al. (2018). It was reported that the determined seismic collapse probability of the investigated tower meets the demand dictated by the Chinese seismic code.

2.4 Strengthening and Retrofitting of Tower Structures

Several researchers have contributed to the literature with theoretical and experimental studies in order to increase the load capacity of existing transmission towers. There are mainly two reinforcing methods that are used in practice. Providing a number of horizontal diaphragms along the tower's height is the first retrofitting approach (Al-Bermani et al., 2004; Xie and Sun, 2012). Al-Bermani et al. (2004) conducted a study on tower strengthening by providing additional diaphragms, and different types of diaphragm systems were investigated for single panel of a tower. The effects of the diaphragm geometry on the structure have been evaluated by prototype tests and nonlinear analyses. Based on the obtained results, an existing telecommunication tower was retrofitted with additional diaphragms, and the structural capacity was increased by 40%.

Xie and Sun (2012) conducted an experimental study to investigate the behavior of a 500 kV capacity transmission tower with additional diaphragms provided to increase the load carrying capacity. It was stated that load-carrying capacity and ductility of the tower have been enhanced significantly with the presence of diaphragms. The increase in the ultimate load capacity was approximately 18%. The results indicated that the out-of-plane deformations of the brace members were reduced by providing additional diaphragms. Similar findings were also represented by Cai et al. (2016) in the wind tunnel testing of 500 kV tower prototypes. It was reported that the most vulnerable part of the towers are the leg members at lower panels, and with the introduction of diaphragms the ultimate bearing capacity of the tower is enhanced under wind actions. The maximum wind speed that resulted in a collapse of the tower was increased by 33% with the addition of diaphragms. The

vibration properties of the towers with and without diaphragms were reported to be similar. Li et al. (2017) also noted that a diaphragm system could improve the buckling capacity of tower leg members. In the study by Yang et al. (2016), tower retrofit by providing additional diaphragms was investigated by using a collapsed transmission tower as a case study. Results obtained from both static and dynamic nonlinear analyses demonstrated that providing additional diaphragms and braces in lower part of the tower results in member forces and tower deformations.

The second approach for tower strengthening is by increasing the cross section of the existing tower members. This is usually achieved by bolting new steel profiles to the existing members. In this way, the load-carrying capacity of the leg members can significantly be improved (Shukla et al., 2021). Mills et al. (2012), Zhuge et al. (2012), and Lu et al. (2014) focused on retrofitting of steel angle main leg members in lattice transmission towers by bolted angle reinforcing members. The experimental results verified the effectiveness of the reinforcement method. Depending on the number of panels reinforced within the tower the increase in tower load capacity could be as high as 105%. The load sharing between the existing and the reinforcement member was studied, and it was reported that an effective load transfer can be achieved by using a bolted splice type connection. Numerical analysis of the proposed strengthening system was also conducted, and the numerical results were compared with the results from axial load testing of tower members. The numerical model included the connection details, including bolt pretension and slip response. It was reported that the investigated tower retrofit is an efficient method, and the level of strength increase can be predicted accurately through numerical analysis.

CHAPTER 3

INVESTIGATION OF TUFANBEYLI TOWERS

3.1 Description of Investigated Power Distribution Line

Tufanbeyli District of Adana Province in Turkey receives energy via a 34.5 kV voltage level double circuit power distribution line. The energy line is 76 km long and was established in 1976. On January 16th, 2019, strong wind and heavy snowfall were predominant in the district and resulted in the collapse of a total of 45 steel lattice towers located on the power distribution network. Out of these 45 towers, 24 towers were part of the double circuit line, while the remaining towers were part of a separate single-circuit line. The investigation conducted as part of this thesis focus on the Tufanbeyli part of the double-circuit distribution line, where fifteen tower failures occurred.

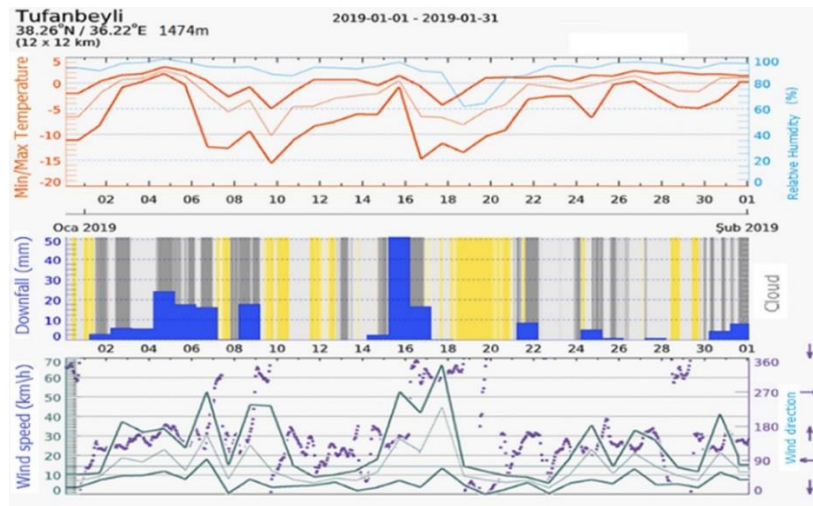


Figure 3.1. Meteorological data from Tufanbeyli station for January 2019

The meteorological data obtained from Tufanbeyli station indicates wind speeds of up to 60 km/h and a minimum temperature of approximately -15°C (Figure 3.1). In addition to the meteorological data, photographs taken by field staff indicate thick

ice sleeves around conductor wires during the day of the incident (Figure 3.2). The investigated part of the Tufanbeyli double-circuit distribution line utilizes 3/0 AWG (Pigeon) type conductors made up of aluminum strands with steel core (ACSR). The corresponding conductor properties are given in the TEDAŞ Technical Manual on Design of Distribution Lines (TEDAŞ, 2000) and presented in Table 3.1.

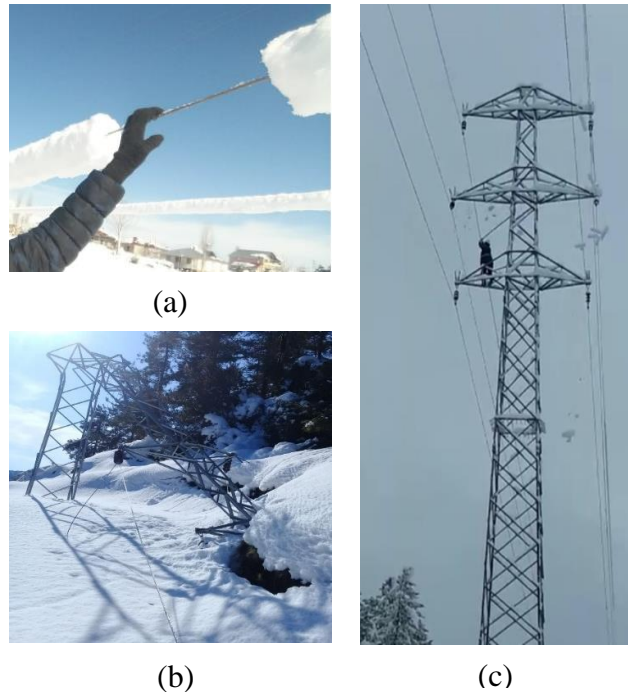


Figure 3.2. Observations during the day of the incident: (a) ice sleeves around conductors; (b) a collapsed tower; (c) staff removing ice on conductors

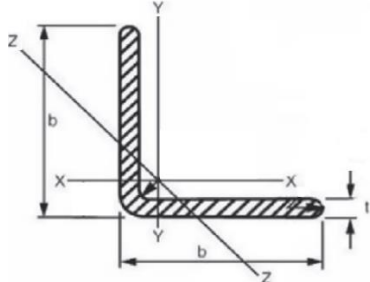
Table 3.1 Nominal section properties of the conductors used in the investigated power distribution line (TEDAŞ, 2000)

Property	
Diameter (d)	12.75 mm
Self-weight per unit length (P)	3.36 N/m
Cross sectional area (S)	99.23 mm ²
Ultimate Tension Capacity (F_u)	29.72 kN
Maximum Design Force (F_T) *	10.71 kN

* 8.96 kN shall be used for ice region I

The investigated line consists of four types of towers, which are BU, DU, RU, and SU type. These tower types have been commonly used in power distribution networks in rural areas of Turkey. Structural design of these towers are based on steel angle members made of St 37 class steel (Table 3.2) (TEDAŞ, 2000). Due to their relatively old design and poor documentation, the geometrical properties of BU and SU type towers were not available at the beginning of the investigation. Therefore, these tower types were excluded from the current study and the investigation focused only on the DU and RU type towers. Geometrical details are illustrated for the RU type suspension towers and DU type tension towers in Appendix A. In order to accommodate the changes in the topography, towers are usually designed for different heights in a modular pattern. For instance, RU type towers can be constructed as RU-8, RU-6, RU-4, RU-2, RU+0, RU+2, RU+4, or RU+6. The numbers in this type of designation indicate the increase or decrease in tower height (in meters) compared to the geometry of the nominal tower.

Table 3.2 Properties of the angle sections used in Tufanbeyli towers



Section Type	b (mm)	t (mm)	A_g (mm ²)	$r_{x,y}$ (mm)	r_z (mm)
L40x4	40	4	308	121	77
L50x5	50	5	480	151	97
L60x6	60	6	690	182	117
L65x7	65	7	870	196	126
L70x7	70	7	940	212	136

3.2 Site Inspections on Towers

A condition assessment of the existing intact towers and failure investigation of some of the five damaged towers were performed during the site visit to Tufanbeyli on August 22nd, 2019. Locations of the towers along the investigated power distribution line are shown in Figure 3.3. Superimposed on the same figure are the marks of the fifteen failed towers and photographs of the observed failure patterns. Among all failed towers, photographs are provided only for towers No.106, No.107, No.108, No.116, and No.127, because the other failed towers had already been dismantled before the site visit.

During the site visit, verification of the presence of structural members and examinations for configurational problems in the towers are made with a hands-on investigation. Visual inspection of the towers indicated no signs of corrosion or surface deterioration, improper connections, or foundation damage on the failed and intact towers. Two main failure modes observed on the towers are (1) torsional deformation of the tower cage between the middle and lower crossarms and (2) buckling of leg members at a location below the lower crossarm. In some parts of the line, broken conductors were also observed. Photographs of the inspected failed towers are given in Appendix B.

3.3 Analyses of Towers

Two types of loading conditions, namely design condition and failure condition, were performed in an attempt to determine the exact cause of the tower collapses and to investigate the safety level of the existing towers. The investigation focused on the part of the towers between No.100-No.130, because this was part of the line with the most observed damage. Fourteen of the fifteen failed towers were located in this part of the line. As evident in Figure 3.3 this part of the line has a straight profile with no deviation. Characteristic design properties of the towers as well as the damage condition on the towers and conductors are presented in Table 3.3.

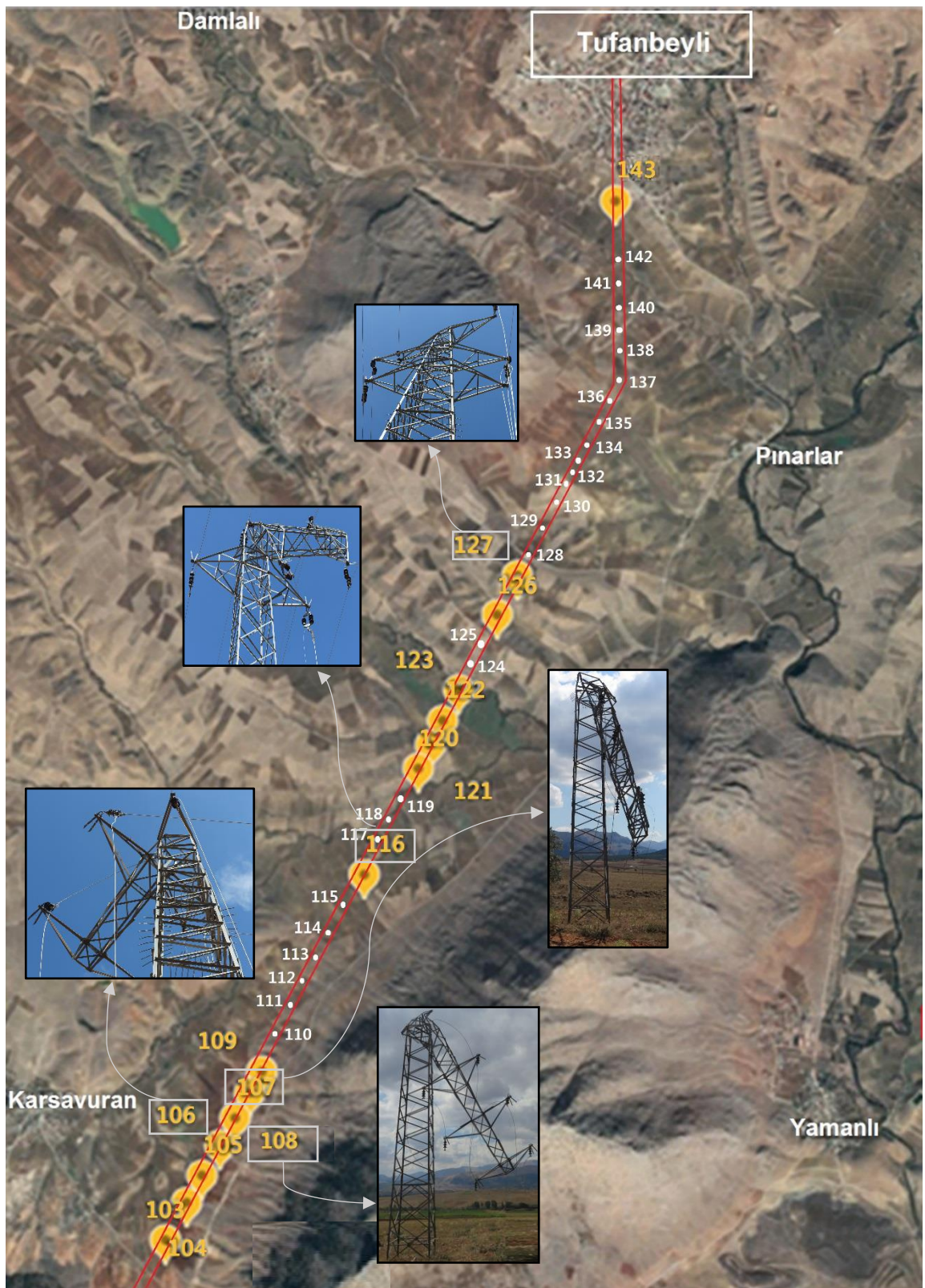


Figure 3.3. Locations of the failed towers along the power distribution line

Table 3.3 Design properties of Tufanbeyli towers and observed damage

Tower	Type	Height (m)	Back Span (m)	Wind Span, a_w (m)	Weight Span, a_g (m)	Damage Condition	
						Tower	Conductor
100	RU-2	20.7	240	219	127	x	x
101	RU+0	22.7	198	227	234	x	x
102	SU+6	28.5	256	252	284	x	Broken
103	SU+4	26.5	247	287	249	Damaged	Broken
104	SU+4	26.5	326	283	279	Damaged	Broken
105	RU+4	26.7	240	260	257	Damaged	Broken
106	RU+4	26.7	280	265	280	Damaged	Broken
107	RU-4	18.7	250	237	212	Damaged	Broken
108	RU-2	20.7	224	209	195	Damaged	Broken
109	RU+4	26.7	193	227	231	Damaged	Broken
110	BU+6	27.7	260	247	304	x	x
111	SU+6	28.5	234	247	236	x	x
112	RU-4	18.7	260	240	228	x	x
113	RU+2	24.7	220	210	258	x	x
114	RU+0	22.7	200	224	174	x	x
115	DU+2	23.3	247	303	333	x	x
116	SU+4	26.5	359	326	335	Damaged	x
117	SU+2	24.5	293	265	256	x	Broken
118	RU-2	20.7	237	232	227	x	Broken
119	DU+0	21.3	227	227	205	x	x
120	RU-2	20.7	226	225	212	Damaged	x
121	RU-2	20.7	224	224	177	Damaged	x
122	SU+4	24.7	223	259	352	Damaged	x
123	RU-2	20.7	294	258	213	Damaged	x
124	RU+0	22.7	221	227	150	x	x
125	RU+2	24.7	232	246	256	x	x

Table 3.3 (cont'd) Design properties of Tufanbeyli towers and observed damage

Tower	Type	Height (m)	Back Span (m)	Wind Span, a_w (m)	Weight Span, a_g (m)	Damage Condition	
						Tower	Conductor
126	SU+4	24.5	259	318	402	Damaged	x
127	SU-6	26.5	377	270	199	Damaged	Broken
128	DU+0	21.3	162	182	230	x	x
129	RU-2	20.7	201	196	250	x	x
130	RU-2	20.7	190	95	185	x	x

Among the properties given in Table 3.3, back span is the distance between the tower that is considered and the previous tower along the line. Weight span (a_g) is the horizontal distance between the lowest point of the conductor on either side of the tower. Weight span is used for determination of the total conductor weight supported by each tower. Wind span (a_w) is the distance between middle points of the span on either side of the tower. Wind span is used for determination of the lateral load supported by each tower due to the wind load on conductors. Determination of weight and wind spans for a sample power line is illustrated in Figure 3.4. As illustrated, the wind spans of towers T2 and T3 are a_{w-T2} and a_{w-T3} , and the weight spans are a_{g-T2} and a_{g-T3} .

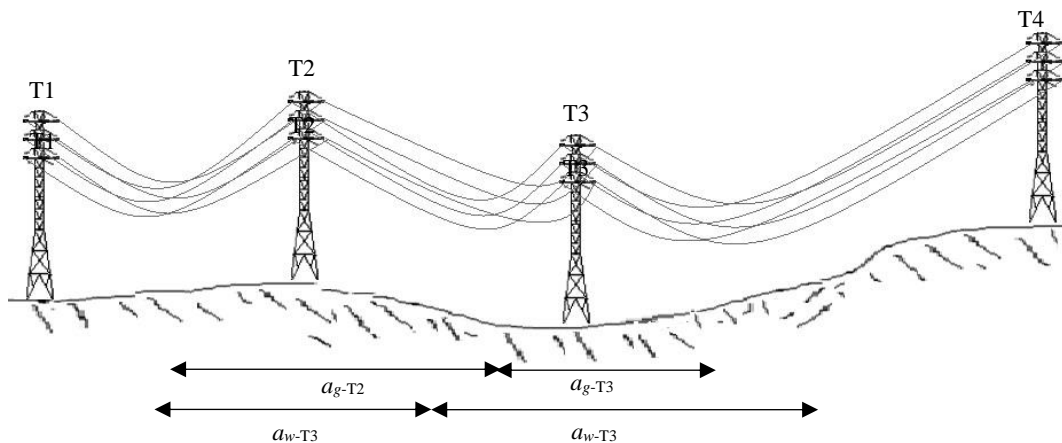


Figure 3.4. Wind and weight spans for towers

3.3.1 Numerical Modeling of Towers

Structural modeling and numerical analysis of the towers were conducted within PLS-TOWER and SAP 2000 software. PLS-TOWER software was used for verification of the results obtained from the SAP2000 models. After similar responses were achieved for a suspension type RU+4 tower, modeling and analysis of the towers were continued with SAP2000 software, as it allows for a rapid model buildup and post-processing of the analysis results. Eighteen RU type and three DU type towers were modeled according to the design and construction drawings (TEDAŞ, 2000). A separate 3-dimensional numerical model was prepared for each tower by utilizing 2-node frame elements. Brace and horizontal members were modeled as pinned connected elements. As mentioned earlier, this is the general approach used in modeling of lattice type distribution towers, since the structural response is close to ideal pinned behavior due to the members being connected usually with a single bolt. Leg members were modeled as continuous elements. The weight of the connection components was neglected in the study since they have no significant contribution to the response. Tower bases were modeled as pinned with all three translational degrees of freedom being restrained. Several views from the numerical model of the RU-4 suspension tower are shown in Figure 3.5.

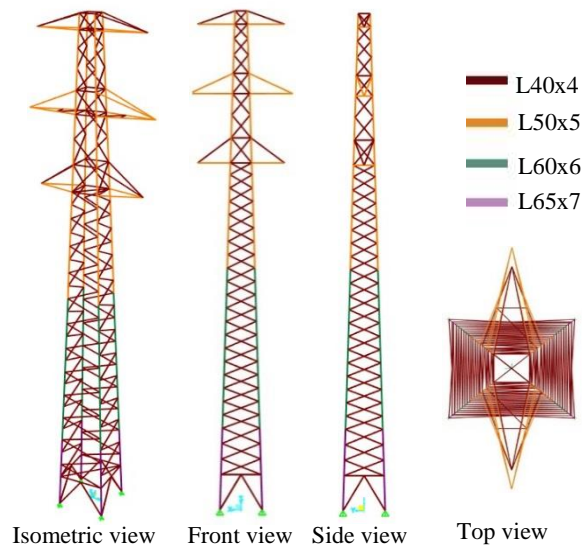


Figure 3.5. Structural analysis model of RU-2 type tower

As part of the structural analysis of towers, member forces were determined by linear elastic analysis with the axially loaded member and small deformation assumptions. Comparison of the axial load bearing capacity with the axial force demand produces the capacity ratio for each tower member. A properly designed tower should have capacity ratio of less than 1.0 for all members. Axial load capacities of the tower members were determined by considering the limit states of buckling, net section yielding, bolt bearing and bolt shear, as described in ASCE 10-15 (2015). Effective lengths of the structural members were also determined with respect to corresponding tower geometry according to ASCE 10-15 (2015). The load capacity of an axially loaded member under compression is governed by the most unfavorable limit state among the limit states of buckling, bolt bearing, and bolt shear. Similarly, for a member under tension, the load capacity is governed by the most unfavorable limit state among the limit states of net section yielding, bolt bearing, and bolt shear limit states.

3.3.2 Analysis of Towers under Design Level Loads

The technical specification by Turkish Power Distribution Agency (TEDAŞ, 2008) is the key document providing guidelines on design loads for steel lattice type power distribution towers. Due to the design and construction of the investigated towers dating back to the 1970s, it was deemed necessary to check the structural behavior of the towers under design loads. In this regard, towers were analyzed in order to evaluate the compliance of the design according to the current design practice.

TEDAŞ Specification identifies the loading cases to be considered for structural design of power distribution towers. There are three loading cases for suspension towers and five loading cases for tension towers that should be considered in the design. These loading cases are summarized, respectively in Table 3.4 and Table 3.5. A factor of safety value of 1.5 is specified for all of these loading cases for both types of towers (TEDAŞ, 2008). Loading cases specified for suspension towers are (1) transverse wind with no ice, (2) longitudinal wind with no ice, and (3) conductor

break. For tension towers, loading cases to be considered in design are (1) unbalanced loading due to ice-covered conductors, (2) transverse wind with no ice, (3) conductor break, (4) opposite lift, and (5) uplift. Conductor break loading case considers breaking of a single ice-covered conductor for suspension towers. On the other hand, breaking of two neighboring ice-covered conductors is considered for tension towers. Therefore, for the investigated towers, which are part of a double-circuit line, structural analysis under conductor break loading case were conducted in three loading cases for suspension towers and ten loading cases for tension towers. These loading cases are illustrated in Figure 3.6 and Figure 3.7.

Table 3.4 Loading cases specified for suspension towers (TEDAŞ, 2008)

Loading Case	Transverse Loads	Longitudinal Loads	Vertical Loads
Transverse Wind, no Ice, +5 C°	- Wind loads on conductors, insulator and tower body	No load	- Self-weight of the Insulators, tower and conductors with no ice
Longitudinal Wind with no Ice, +5 C°	No load	- One sided tension load by 2% of max design force of conductors - Wind loads on insulator - Wind loads on tower	- Self-weight of the Insulators, tower and conductors with no ice
Conductor Break, -5 C°	No load due to small angle of line deviation	- 1/3 of max design force of the broken conductor	- 2/3 of weight of the ice-covered broken conductor - Weight of the ice- covered conductors - Self-weight of the insulators and tower

Table 3.5 Loading cases specified for tension towers (TEDAŞ, 2008)

Loading Case	Transverse Loads	Longitudinal Loads	Vertical Loads
Unbalanced Loading, -5 C°	No load due to small angle of line deviation	- 40% of max design force of the broken conductor	- Weight of the ice covered conductors - Self-weight of the insulators and tower
Transverse Wind, no Ice, +5 C°	- Wind loads on conductor - Wind loads on insulator - Wind loads on tower	No load	- Self-weight of the conductors with no ice, insulators and tower
Conductor Break, -5 C°	No load due to small angle of line deviation	- 75% of max design force of the broken conductor	- 2/3 of weight of the ice-covered broken conductor - Weight of the ice-covered other conductors - Self-weight of the insulators and tower
Opposite Lift, -5 C	No load due to small angle of line deviation	No load	- Weight of the ice-covered conductors with opposite weight span in back and fore of the tower
Uplift, -5 C	No load due to small angle of line deviation	No load	- Weight of the ice-covered conductors with uplift weight span

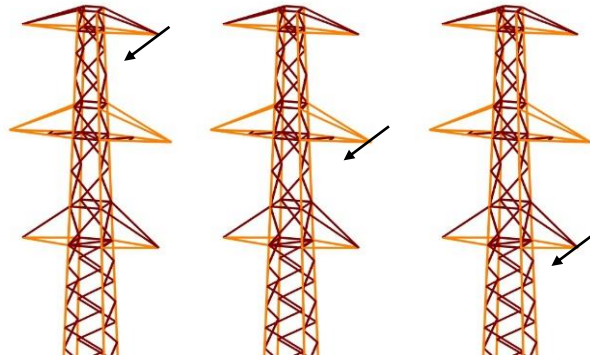


Figure 3.6. Conductor break loading cases used for suspension towers

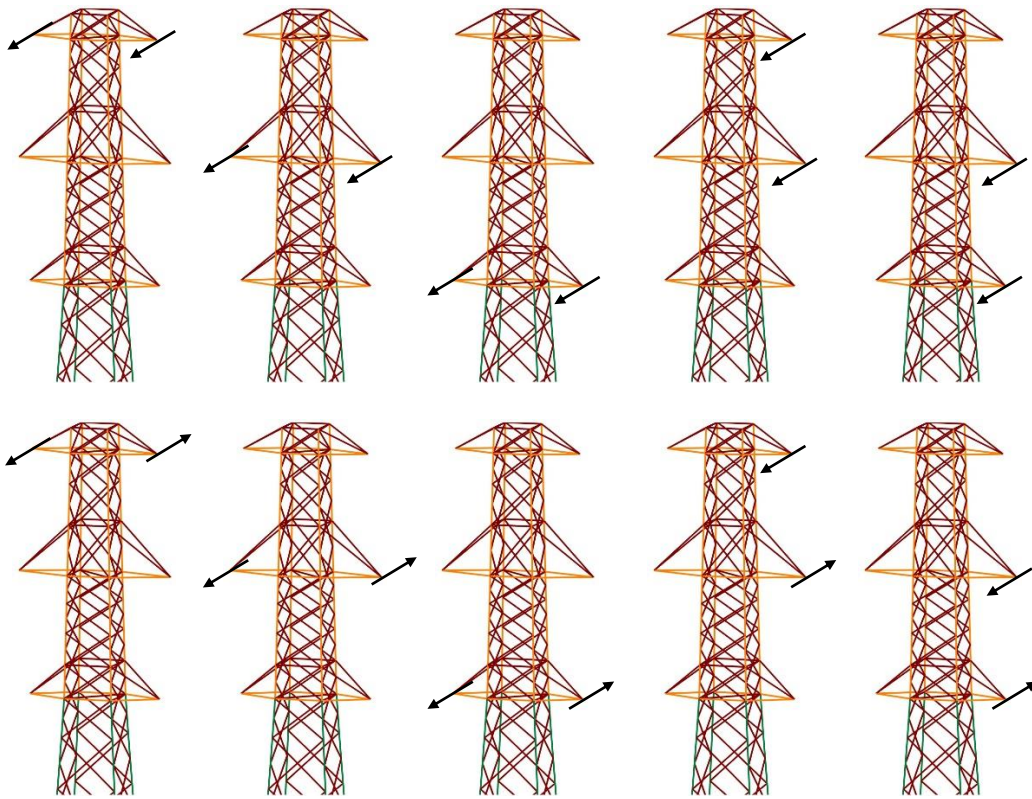


Figure 3.7. Conductor break loading cases used for tension towers

Design loads in the specified loading cases are described as (1) self-weight of the line components, (2) ice loads on conductors, (3) wind loads on conductors, insulators, and tower members, and (4) tension loads due to conductor break. Additionally, a 0.98 kN (100 kgf) of maintenance load in conductor attachment joints is to be included in loading cases (TEDAŞ, 2008).

Wind force that is expected to act on the surface of the energy line components can be computed by using the equation shown in Eqn. (3.1). In this equation, W is the horizontal wind force, c is dynamic wind pressure coefficient, q is dynamic wind pressure, and A is the wind-affected area of a conductor, insulator, or tower member. Recommended values of these parameters are specified in the TEDAŞ design document based on the power line properties. For conductors with no ice, the wind-affected area (A) is simply determined as the wind span multiplied by the diameter of the conductor.

$$W = c \cdot q \cdot A \quad (3.1)$$

$$q = V^2/16 \quad (3.2)$$

Dynamic wind pressure coefficient (c) depends on the shape, size, and horizontal characteristics of a component under the effect of wind. The value of q is given as 2.8 for tower members and 1.1 for conductors with a diameter between 12.5 mm and 15.8 mm. In addition, dynamic wind pressure (q) is specified as 0.52 kN/m² (53 kgf/m²) for conductors and 0.69 kN/m² (70 kgf/m²) for tower members and insulators located at an elevation between 15 m and 40 m. Relation between dynamic wind pressure (q) and wind speed (V) is given by Eqn. (3.2). Based on this relation, the 0.52 kN/m² wind pressure corresponds to a wind speed of 128 km/h on conductors by taking into account the safety factor of 1.5.

Ice loading on unit length of the conductor (Pb) is calculated as shown in Eqn. (3.3). In this equation, d is the conductor diameter and k has a value of 0, 0.2, 0.3, 0.5, or 1.2 depending on the geographic location of the tower specified in ice load map of Turkey (Figure 3.8). The investigated towers are located in ice region III with a corresponding k value of 0.3. Once the weight of ice accumulation per unit length of conductor is determined the total vertical force on the tower due to conductor and ice weight (Wc) can be calculated by making use of Eqn. (3.4). In this equation P is the self-weight per unit length of the conductors.

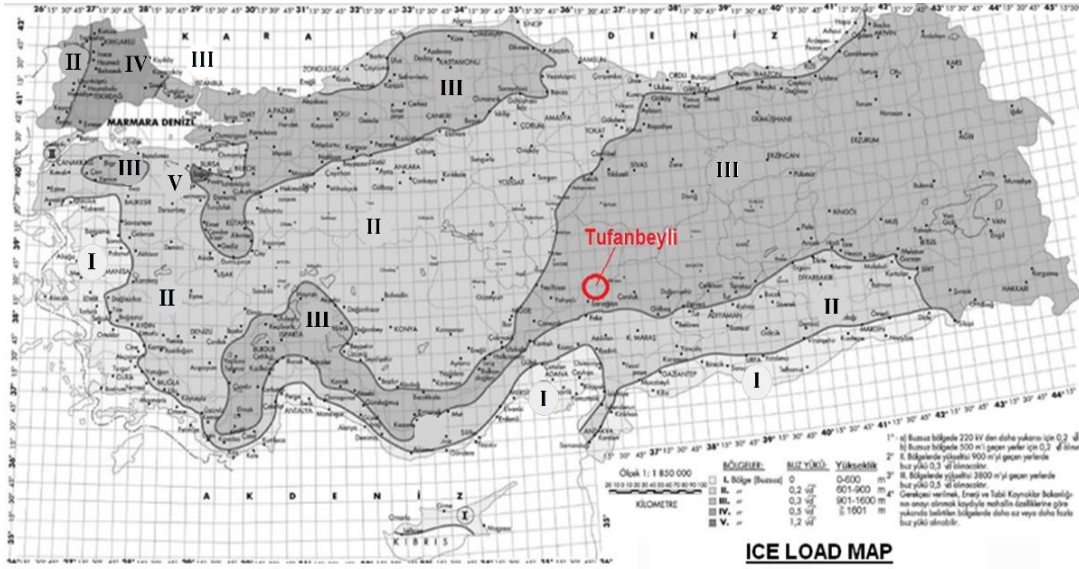


Figure 3.8. Ice load map of Turkey (TEDAŞ, 2008)

$$Pb = k \cdot \sqrt{d} \quad (3.3)$$

$$Wc = ag \cdot (Pb + P) \quad (3.4)$$

$$db = (d^2 + 2122 \cdot Pb)^{0.5} \quad (3.5)$$

In Eqn. (3.5) relation between ice loading on unit length of conductors (Pb) and diameter of ice-covered conductor (db) is represented. This relation is based on a unit weight of 5.89 kN/m^3 for unit weight of ice forming around the conductor. Considering the location and altitude of the investigated towers, the design ice load was calculated to be 10.5 N/m (1.07 kgf/m), which corresponds to a 23.5 mm thick ice cover around the $3/0 \text{ AWG}$ conductor by taking into account the safety factor of 1.5.

Figures 3.9 and 3.10 respectively show the calculated external loads (without the 1.5 safety factor) for each loading case in a suspension tower (tower No. 112) and tension tower (tower No. 119). In conductor break loading case, only top conductor break (TCB) condition (i.e., one of the top conductors in the suspension tower and top two conductors in the tension tower) is illustrated as an example. It should be noted that wind loading acting on tower members is not included in the load trees

shown in Figure 3.9 and 3.10 for the sake of clarity. In structural models of the towers, wind loading acting on tower members was applied to each joint based on the tributary lengths.

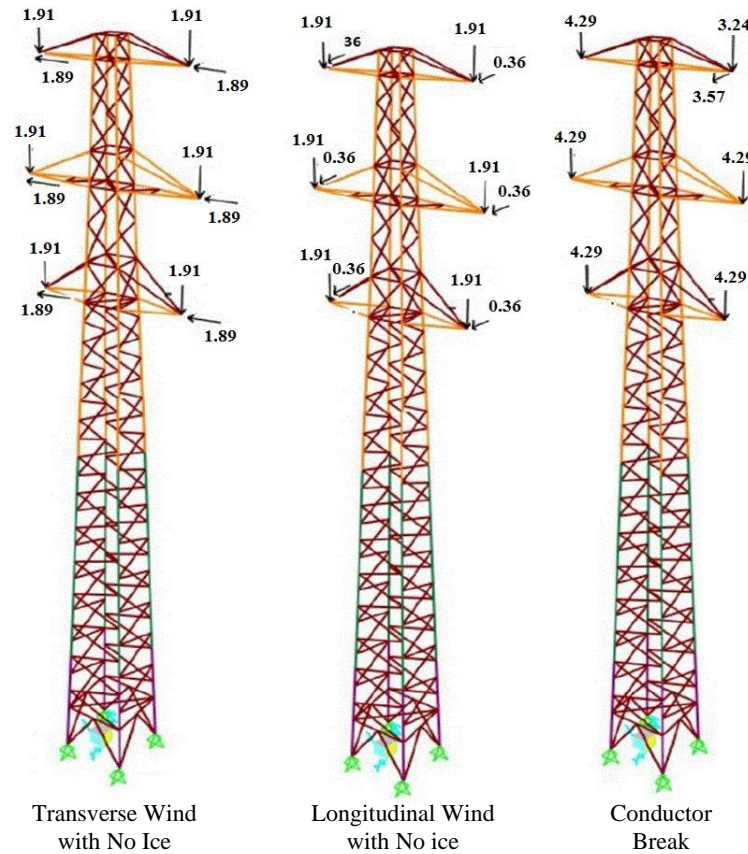


Figure 3.9. Loading cases and calculated loads (kN) on tower No.112 (RU-4 type tower)

Analysis results for the investigated suspension and tension towers are presented respectively in Table 3.6 and 3.7. In these tables, the maximum value of the calculated capacity ratios for every member in each tower are given with the elevation of the corresponding member along the tower height.

The capacity ratio results of the investigated suspension towers indicate that axial forces in members are significantly below the expected capacity of the corresponding members under longitudinal wind with no ice and conductor break loading cases. On the other hand, considerably high capacity ratios, which are between 80%-98%, were

calculated under transverse wind with no ice loading case. Moreover, under this loading case, the locations of the members with the maximum capacity ratio correspond to the locations where the leg member's cross section changes from L60x6 to L50x5. This observation is valid for all of the investigated suspension towers. For the leg members, buckling limit state was observed to be the governing mode. Therefore, a stronger wind can cause leg buckling in these towers under transverse wind with no ice loading case. Another observation that is valid in the results presented in Table 3.6 is that members in the cage and crossarm parts of the towers have relatively high capacity ratios under the conductor break loading case. In this loading case, the governing limit states were bolt bearing and buckling of the members.

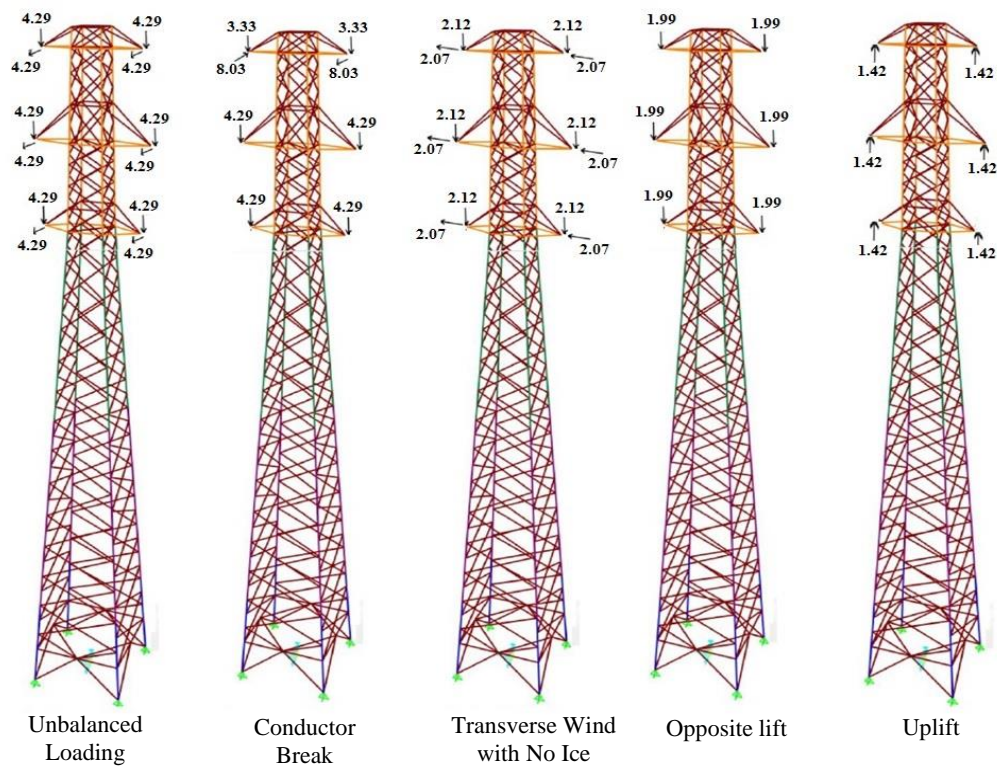


Figure 3.10. Loading cases and calculated loads (kN) on tower No. 119 (DU+0 type tower)

Table 3.6 Maximum member capacity ratios obtained for suspension towers

Tower	Loading Cases		
	Transverse Wind with No Ice*	Longitudinal Wind with No Ice*	Conductor Break*
100	0.81 (11 m)	0.36 (1 m)	0.58 (16.8 m)
101	0.87 (7.1 m)	0.44 (0.5 m)	0.63 (21.7 m)
105	0.97 (17 m)	0.46 (0.5 m)	0.61 (25.7 m)
106	0.98 (17 m)	0.47 (0.5 m)	0.61 (25.7 m)
107	0.90 (3.1 m)	0.39 (3.1 m)	0.72 (18.1 m)
108	0.83 (5.1 m)	0.40 (1 m)	0.62 (19.7 m)
109	0.88 (4.1 m)	0.46 (0.5 m)	0.62 (25.7 m)
112	0.90 (3.1 m)	0.39 (3.1 m)	0.73 (18.2 m)
113	0.85 (2.1 m)	0.46 (0.5 m)	0.61 (23.7 m)
114	0.87 (7.1 m)	0.43 (0.5 m)	0.63 (21.7 m)
118	0.89 (5.1 m)	0.40 (1 m)	0.62 (19.7 m)
120	0.87 (5.1 m)	0.40 (1 m)	0.62 (19.7 m)
121	0.87 (5.1 m)	0.39 (1 m)	0.62 (19.7 m)
123	0.96 (11 m)	0.40 (1 m)	0.62 (19.7 m)
124	0.88 (13 m)	0.44 (0.5 m)	0.63 (21.7 m)
125	0.93 (2 m)	0.46 (0.5 m)	0.61 (23.7 m)
129	0.79 (5.1 m)	0.40 (1 m)	0.61 (19.7 m)
130	0.80 (5.1 m)	0.40 (1 m)	0.62 (19.7 m)

*Numbers in parenthesis indicate the elevation of the member producing the maximum capacity ratio

Table 3.7 Maximum capacity ratios obtained for tension towers

Tower	Loading Cases				
	Unbalanced Loading*	Transverse Wind with No Ice*	Conductor Break*	Opposite Lift*	Uplift*
115	0.81 (1 m)	0.84 (18 m)	0.66 (2 m)	0.13 (18.5 m)	0.25 (20 m)
119	0.76 (3.5 m)	0.69 (16 m)	0.56 (1 m)	0.10 (20.8 m)	0.07 (18.5 m)
128	0.77 (3.5 m)	0.69 (16 m)	0.51 (1 m)	0.10 (21.3 m)	0.13 (18.5 m)

*Numbers in parenthesis indicate the elevation of the member producing the maximum capacity ratio

The tension tower member capacity ratios presented in Table 3.7 indicate that the maximum demand occurs under the unbalanced loading and transverse wind with no ice loading cases. Under these loading cases, the governing limit states for tower members were observed to be buckling and net section yielding. In general, the tension towers possess smaller capacity ratios than the suspension towers, indicating a higher safety level for the investigated tension towers.

The applicable loading cases with the specified design level loads produced capacity ratios that are all less than 1.0, indicating that the towers possess the safety level intended by the related design documents. Although structural design of the towers was verified based on the assumed design loads and loading cases, the failures occurred on January 16th, 2019, indicate that the towers were subjected to higher levels of loading. Therefore, response of the towers should be further studied by utilizing the actual loading conditions that may have occurred on the day of the incident.

3.3.3 Analysis of Towers under Failure Condition

3.3.3.1 Material Tests

Material tests are frequently used in validation studies for the failure investigation of structures since the analytical solutions may not represent the in-place material properties. In order to guarantee accurate modeling of failure condition for the investigated towers, two series of tensile loading tests were conducted on samples taken from the investigated line. The first of these tests was conducted on a piece of 3/0 AWG conductor. This type of conductor is formed by six aluminum wires that are wrapped around a central steel wire. Tensile loading tests were conducted on these steel and aluminum wires using the setup shown in Figure 3.11. Based on the results obtained from these tests the ultimate tensile capacity of the conductor was determined to be 36.19 kN. This measured strength is 22% higher than the nominal ultimate tension capacity of 29.72 kN specified in TEDAŞ Technical Manual on Design of Distribution Lines (TEDAŞ, 2000).



Figure 3.11. Tensile testing of conductor steel and aluminum wires

The second series of material tests were conducted on coupon samples extracted from two L40x4 and one L70x7 steel angle profiles that were taken from the failed towers. It should be noted that even though taken from failed towers, the angle profiles themselves were virtually undamaged. Six coupon samples were tested as part of this series. Details of the tests are shown in Figure 3.12. Complete stress-strain curves obtained from these tests are given in Figure 3.13 with the yield and ultimate tensile strength values tabulated in Table 3.8. The average yield and tensile strengths were determined to be 310 MPa and 440 MPa, respectively. As mentioned earlier, the investigated towers were designed based on St37 steel class. The minimum specified yield and tensile strengths for this class of steel are 240 MPa and 370 MPa, respectively. Based on these values, it can be concluded that the investigated towers were constructed out of a steel class that is higher than the St37 class assumed in design.

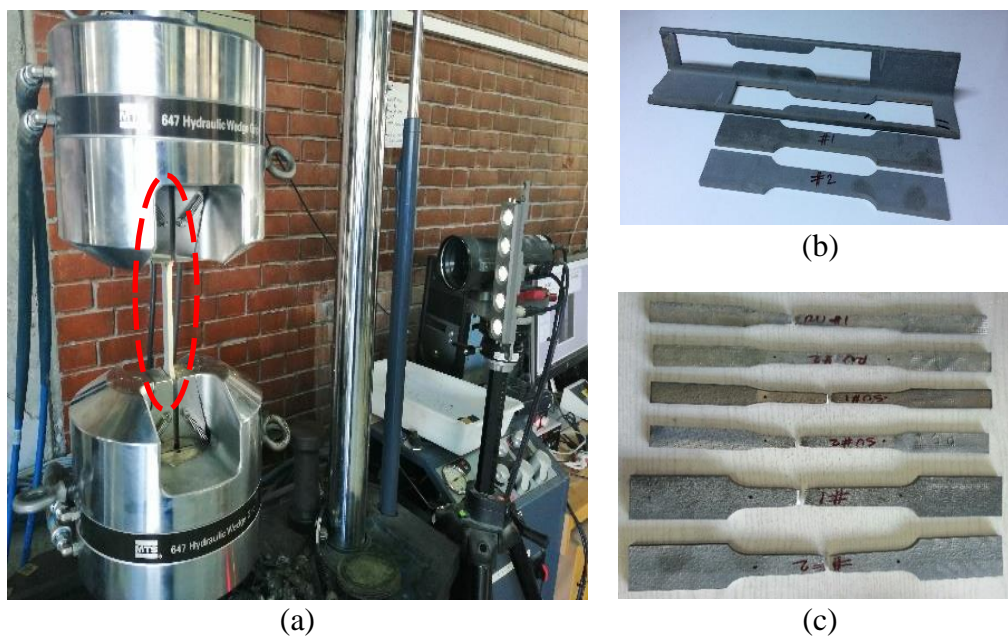


Figure 3.12. Tension testing of steel coupon samples: (a) sample in the testing machine; (b) coupon samples extracted from the steel angle section; (c) tested coupon samples

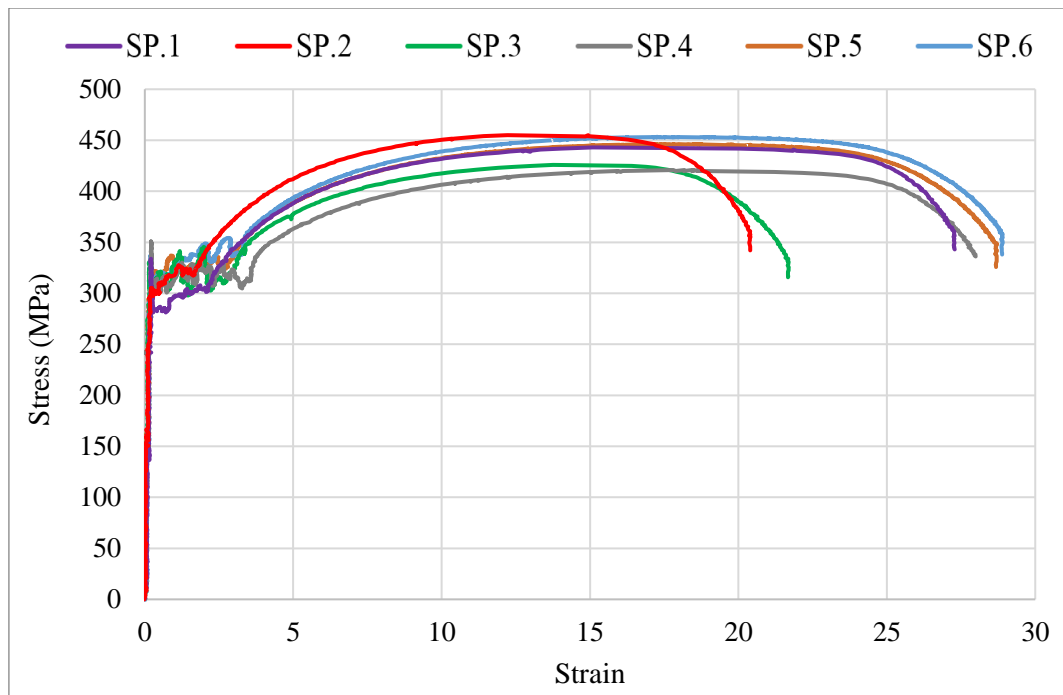


Figure 3.13. Stress-strain curves of the test specimens

Table 3.8 Material properties of the specimens

Specimens	Tensile Yield Stress (MPa)	Ultimate Stress (Mpa)
SP.1 (L40x4, RU)	320	445
SP.2 (L40x4, RU)	310	455
SP.3 (L40x4, SU)	320	425
SP.4 (L40x4, SU)	315	420
SP.5 (L70x4, RU)	285	445
SP.6 (L70x4, RU)	300	455
Average value	310	440

Experimentally determined yield and tensile strengths were used for determination the member axial load capacities in the towers as part of the failure condition analyses explained in the following sections.

3.3.3.2 Failure Condition Loads

As part of the failure investigation of the towers, the actual loading conditions that the towers were likely to experience on the day of the incident were predicted based on meteorological data. As mentioned earlier, this data (Figure 3.1) indicates wind speeds of as much as 60 km/h together with the temperatures as low as -15°C . In addition, heavy snowfall and significant ice accumulation on the conductors were reported at several locations along the investigated power distribution line.

The presence of high wind, precipitation, and low temperature altogether during the day of the incident requires the consideration of a loading case that represents the ice and wind interaction (IWI) in the failure condition analyses. Although IWI loading case is accounted for in the design of transmission towers, it is not considered as a design load condition for distribution towers (TEDAŞ, 2008).

In this study, the IWI loading case, as shown in Table 3.9, was included in the failure condition analyses. Based on the meteorological data, two wind speeds of 50 km/h and 60 km/h were considered in the failure condition analyses under the IWI loading case. Wind loads were determined using Eqn. (3.1) by calculating dynamic wind pressure (q) for 50 km/h and 60 km/h wind speed according to Eqn. (3.2). Dynamic wind pressure coefficient (c) was adopted as 1.0 based on TEİAŞ technical document. Wind loads acting on the conductors were determined by considering the wind area of the ice-covered conductors, which is equal to wind span (a_w) for the investigated tower multiplied by the total diameter of the ice-covered conductor. Therefore, the actual thickness of the ice sleeve that formed around the conductor prior to the failure of the towers has to be determined accurately for the failure condition analyses.

The conductor break loading case specified in TEDAŞ Technical Specification considers the horizontal load on the tower in terms of the maximum design force of the conductor. Based on TEDAŞ Technical Manual on Design of Distribution Lines (TEDAŞ, 2000) the maximum design force for the conductor type used in the

investigated line (i.e., 3/0 AWG (Pigeon) type conductor) is 10.71 kN. This value corresponds to 36% of the nominal ultimate tension capacity of the conductor ($F_u=29.72$ kN). Load testing conducted on the conductor sample taken from the failed line however indicated an ultimate tensile capacity of 36.19 kN. Occurrence of a conductor break in a line can be considered as an indication that the tensile force in the conductor reached the ultimate tensile capacity. For this reason, for the failure condition analyses under IWI and conductor break loading cases, the force in the conductor just before the collapse of the investigated towers was considered to be equal to the experimentally determined ultimate tensile capacity of the 3/0 AWG (Pigeon) type conductor.

Table 3.9 Loading cases for failure condition analysis

Loading Case	Transverse Loads	Longitudinal Loads	Vertical Loads
Ice and Wind Interaction (IWI), -15 C°	- Wind loads on ice-covered conductors	No load	- Weight of the ice covered conductors
	- Wind loads on ice accumulated insulators		- Self-weight of the insulators and tower
Conductor Break, -15 C°	No load	- 1/3 of tensile capacity of the broken conductor	- 2/3 of weight of the ice-covered broken conductor
			- Weight of ice-covered other conductors
			- Self-weight of the insulators and tower
			- Maintenance load

The actual ice loading on conductors with the temperature of -15°C were also determined by considering the condition that the tensile force in the ice-covered conductor is equal to the experimentally determined ultimate tensile capacity of 36.19 kN. The ice load and the corresponding ice thickness determined this way are given in Table 3.10. As evident the actual ice load and ice thickness values are significantly larger than the design ice load of 10.5 N/m and the corresponding ice thickness of 23.5 mm. This is an indication that the broken conductors in the investigated line were subjected to loading levels that are significantly beyond the design load levels. The weight of ice-covered conductors, and transverse wind loads shown in Table 3.10 act on the corresponding tower at each end of crossarms, where conductors are attached.

Table 3.10 Failure condition loads

Tower	Ice Load (N/m)	Ice Thickness (mm)	Weight of Ice-Covered Conductors (kN)	50 km/h wind on Ice Covered Conductors, (kN)	60 km/h wind on Ice Covered Conductors (kN)
100	89.86	63.6	71.11	21.77	31.35
101	60.77	51.3	90.16	18.59	26.77
105	58.15	50.1	95.04	20.83	30.01
106	55.76	48.9	99.20	20.80	29.96
107	63.92	56.8	85.76	21.24	30.60
108	67.05	54.2	82.44	17.92	25.82
109	61.18	51.5	89.52	18.61	26.80
112	61.62	51.7	88.84	19.79	28.50
113	58.12	50.0	95.13	16.82	24.23
114	71.89	56.3	78.62	19.89	28.64
115	52.73	47.4	112.15	23.13	33.32
118	61.72	51.5	112.59	19.05	27.44
119	65.21	53.3	84.29	19.20	27.66

Table 3.10 (cont'd) Failure condition loads

Tower	Ice Load (N/m)	Ice Thickness (mm)	Weight of Ice-Covered Conductors (kN)	50 km/h. Wind on Ice Covered Conductors, (kN)	60 km/h. Wind on Ice Covered Conductors (kN)
120	63.99	52.8	85.69	18.90	27.22
121	71.23	56.0	79.08	19.80	28.51
123	63.85	52.7	85.92	21.61	31.12
124	79.52	59.5	74.56	21.19	30.51
125	58.27	50.1	94.81	19.69	28.36
128	61.34	51.6	89.26	14.93	21.51
129	58.88	50.4	93.54	15.76	22.70
130	69.25	55.1	80.54	17.43	25.10

3.3.3.3 Failure Condition Analysis Results

The towers were analyzed under the ice and wind loads determined using the procedure explained in the previous sections in accordance with the IWI and conductor break loading cases. Similar to the assessment under design level loads, the maximum axial load in the tower members were compared with the axial load capacity of the members determined according to ASCE 10-15 (2015).

The maximum member capacity ratios determined this way are presented in Table 3.11, along with the observed damage on towers and conductors. The three conditions considered for the conductor break loading case are top conductor break (TCB), middle conductor break (MCB), and bottom conductor break (BCB). Only the towers with reported conductor break were analyzed under the conductor break loading case. On the other hand, the IWI loading case was applied to all of the investigated towers.

Table 3.11 Failure condition analysis results

Tower	Field Reports		Member Capacity Ratio from Analyses				
	Damage Status		Conductor Break*			IWI*	
	Tower	Conductor	BCB	MCB	TCB	50 km/h	60 km/h
100	x	x	x	x	x	0.84	1.12
101	x	x	x	x	x	0.81	1.04
105	Cage	Broken	<0.75	1.06	1.13	0.88	1.15
106	Cage	Broken	0.78	1.08	1.19	0.89	1.16
107	Legs	Broken	<0.75	1.11	1.16	0.86	1.14
108	Legs	Broken	<0.75	1.07	1.17	<0.75	1.01
109	Cage	Broken	<0.75	1.07	1.35	<0.75	1.05
112	x	x	x	x	x	<0.75	1.04
113	x	x	x	x	x	0.79	0.98
114	x	x	x	x	x	0.81	1.07
115	x	x	x	x	x	<0.50	<0.75
118	x	Broken	<0.75	1.09	1.32	0.82	1.06
119	x	x	x	x	x	<0.75	<0.75
120	Legs	x	x	x	x	0.80	1.04
121	Legs	x	x	x	x	0.81	1.07
123	Legs	x	x	x	x	0.88	1.16
124	x	x	x	x	x	0.83	1.11
125	x	x	x	x	x	0.85	1.10
128	x	x	x	x	x	<0.75	<0.75
129	x	x	x	x	x	<0.75	0.94
130	x	x	x	x	x	<0.75	0.97

* Bold numbers indicate cases where member capacity ratio exceeds 1.0

Analyses with the actual material properties and loading indicate no failure for tension towers. Similarly, for suspension towers the analyses indicate no failure under the BCB loading case and IWI loading case with 50 km/h wind. All of the

towers investigated under MCB and TCB loading cases experienced a maximum member capacity ratio greater than 1.0, indicating at least one member failure. These numerically predicted failures are in agreement with the field observations.

In suspension towers analyzed under conductor break loading case, some of the members were observed to be overloaded. Furthermore, results indicate that the critical members are located between the middle and upper crossarms in TCB load case, and between middle and lower crossarms in MCB loading case. In these cases, tower failure occurred due to bolt bearing of the horizontal and brace members in cage part of the towers. For a representation of the general behavior, analysis results from MCB and TCB loading cases are compared with the observed damage for tower No.106 in Figure 3.14. As evident, the predicted damage as a result of conductor break is consistent with the actual damage observed in the field.

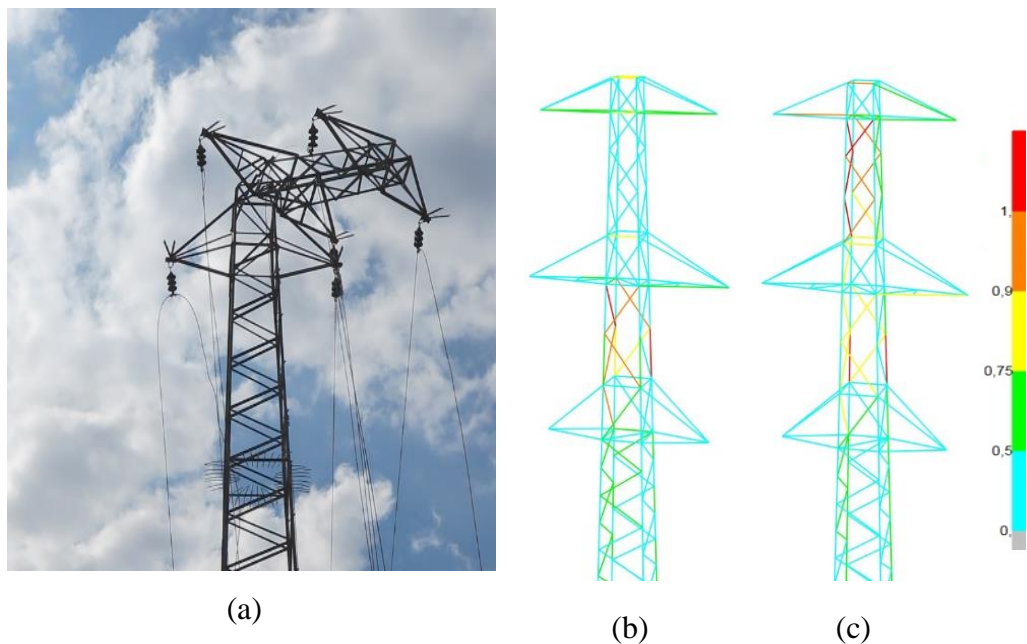


Figure 3.14. Results for tower No.106: (a) damage observed in the field; (b) member capacity ratios in MCB loading case; (c) member capacity ratios in TCB loading case

As evident in Table 3.11, member overloading occurred in some of the suspension towers in the IWI loading case with 60 km/h wind. Analysis models for some of these towers are shown in Figure 3.15. As evident in figures, the overloaded leg members are located at the location where member cross-section changes. The governing limit state for these leg members is buckling under compressive axial load.

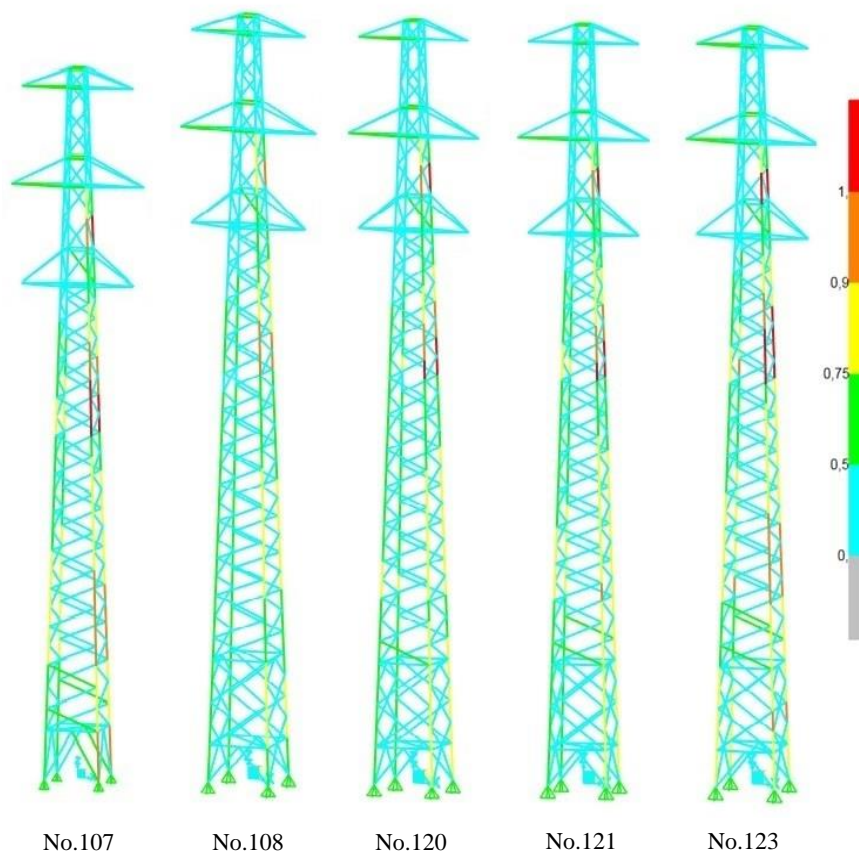


Figure 3.15. Member capacity ratios obtained under IWI loading case with 60 km/h wind

Based on the results presented above, it can be concluded that excessive ice accumulation was the main cause of the investigated tower failures. Ice weights determined based on the measured conductor tensile capacity are 3.4-5.7 times what is specified by the design documents. As a result, thickness of the ice layer accumulated around the conductors increases significantly compared to the design assumption of 23.5 mm. Effects of the ice accumulation on tower loading are

twofold. Increased weight of the conductors due to ice accumulation imposes additional vertical loading at crossarm ends. Ice accumulation around conductors also increases the wind area and leads to larger horizontal loading to be imposed on towers. This latter effect can cause tower failure even at relatively mild wind speeds. For example, the design wind speed of 128 km/h with no ice condition, as specified by the TEDAŞ design specification, is safer than the ice+wind loading case with 60 km/h wind speed for the investigated towers.

CHAPTER 4

NONLINEAR ANALYSIS OF TOWERS

4.1 Background and Objective

Investigation of linear analysis results provided useful insights on identifying the failure of Tufanbeyli towers. Although the linear analysis that is based on ASCE10-15 (2015) design standards clarified the failed members in the structures, it did not produce sufficient knowledge to make a definite conclusion on the progression of damage within towers. A nonlinear analysis incorporating nonlinear material and geometric effects is required in order to identify the mechanism leading to failure of the towers.

In a linear elastic analysis, it is assumed that the deformation is very small, there are no topological changes, the material stress-strain relationship is linearly described by Hooke's law and thus stiffness of the structure is constant during the loading process (Rao and Kalyanaraman, 2001). With this type of modelling approach, it is assumed that the applied load and the resulting deflections are linearly dependent to each other in equilibrium equations.

An illustration of a generic force-displacement relationships for a linear and nonlinear analysis is shown in Figure 4.1. For the nonlinear analysis force-deformation slope starts to decrease with the initiation of material and/or geometric nonlinearity, while the slope is always constant in the linear analysis. In this type of behavior force-deformation curve often referred to as failure path.

In structural analysis, nonlinearity is mostly considered as being related to two main effects which are material and geometrical nonlinearities (Alam, 1993; Al-Bermani and Kitipornchai, 1992). Geometrical nonlinearity, which usually occurs due to large deformation of the structure and P-Delta effects, results in changes in the stiffness

matrix of the structure. In this case, the equilibrium equations are formed considering the deformed geometry. On the other hand, material nonlinearity is associated with the changes in the slope of the material-stress-strain response at a given instant. The steel material used in power distribution tower structures behaves linearly at low strain values, but at higher strains once the yield limit is reached under loading the slope of the stress-strain response decrease gradually.

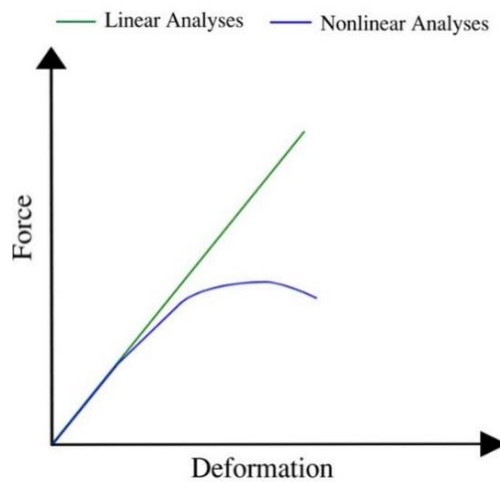


Figure 4.1. Generic linear and nonlinear force-deformation relationships

A static nonlinear analysis procedure was adopted to further study the response of the investigated towers within the post-elastic response region. For this purpose, a set of displacement-controlled pushover analyses with lumped plastic hinges was conducted by using the SAP2000 structural analysis program. Three suspension towers (No.106, No.107 and No.108) located within the investigated power distribution line were selected for the nonlinear analysis. These towers were among those reported to collapse during the January 2019 ice storm and were visually inspected during the site visit as mentioned in Chapter 3.2. Therefore, a reliable comparison and evaluation can be possible between the nonlinear analysis results of the towers and site observations.

In nonlinear analysis, failure condition loads were considered for the selected towers and the results from these analyses were compared with site observations as well as the linear design approach. As discussed in Chapter 3, failure condition loads were

induced on towers by excessive icing on conductors and wind loads acting on the distribution line components. In this regard, two sets of nonlinear loading cases were determined for the nonlinear pushover analyses, which were ice and wind interaction (IWI) loading case and middle conductor break (MCB) loading case.

4.1.1 Pushover Analysis

Pushover analysis has become a useful procedure for the evaluation of expected performance of structural systems by estimating the capacity present within the system considering the progression of damage. This type of analysis can provide significant insights about potential weaknesses of the structural system, which cannot be obtained by linear elastic analysis (Edgar and Sordo, 2017; Mara and Hong, 2013; Tapia-Hernández et al., 2017).

Pushover analysis involves application of monotonically increasing patterns of loads to the structure up to a predetermined value or state. Potential sources of nonlinearities within the structural systems are reflected in the analysis model and the loading is applied sequentially in a step-by-step fashion. At each step a nonlinear static analysis is conducted and the response of the structure at the end of each load increment is evaluated. This type of iterative analysis is continued until the target displacement or force is reached, and the progression of damage within the structural system is monitored. In this way strength and ductility properties and more importantly, the change in the overall load-carrying capability of the structure can be determined.

In the pushover analysis of the investigated towers, the two sets of nonlinear loading cases applied were (1) ice and wind interaction (IWI) loading case and (2) middle conductor break (MCB) loading case. The IWI loading case includes the actual wind load acting on the towers and ice-covered conductors. The meteorological data of the failure day, given in Figure 3.1, reveals a maximum wind speed of approximately 60 km/h. Based on this observation, the 60 km/h wind speed was used for the IWI

loading case. The MCB loading case considers breaking of the conductor attached to the middle cross arm of the towers. The fact that the damage on the failed towers was localized in the region between the lower and middle cross arms indicates breaking of the middle conductor in the field (Figure 3.14). For this reason, only the middle conductor break case was included in the numerical investigation.

As stated earlier, No.107 and No.108 towers suffered from buckling of leg members and No.106 tower failed due to conductor break condition. In pushover analysis, both IWI and MCB loading cases were applied on all three towers in an attempt to provide a comparison between the numerically predicted and observed failure patterns under these two loading cases.

Pushover analysis was conducted in two stages for each loading case. The first stage can be defined as service stage, and it was considered that only gravity loads are acting on the tower. The vertical loading considered in the first stage were weight of the ice accumulated conductors, weight of the insulators and self-weight of the tower. Second stage of the analysis includes the pushover loading. In this stage, lateral and vertical loads induced by conductor break condition were introduced to MCB loading case and lateral wind loads were introduced to IWI loading case. In this two-stage analysis procedure the condition of the tower obtained at the end of the first stage (including the stiffness matrix, member forces, and deformations) was used as the initial condition for the subsequent nonlinear analysis in the second stage.

In the first stage of pushover analysis, force-controlled method was adopted since the structure was expected to remain in the elastic range of behavior under vertical loads applied in this stage. In the second stage, however, the analysis was run as displacement-controlled in order to accurately capture the inelastic response of towers including stiffness degradation and strength deterioration.

In principle, any joint can be chosen for monitoring target displacement in a pushover analysis. The joints and degrees of freedom used for monitoring the progression of the analysis in MCB and IWI loading cases are demonstrated in Figure 4.2. Joint 171, which was located at the left end of the middle cross arm, was chosen for MCB

loading case. Displacement of this joint in the direction parallel to the line was monitored during the analysis, because this was the main deformation mode expected to occur under the broken conductor loading. For the IWI loading case, on the other hand, the main deformation mode was in the direction perpendicular to the line. For this reason, displacement at the tip of the top cross arm in the direction perpendicular to the line (i.e., at joint 165) was monitored for the IWI loading case.

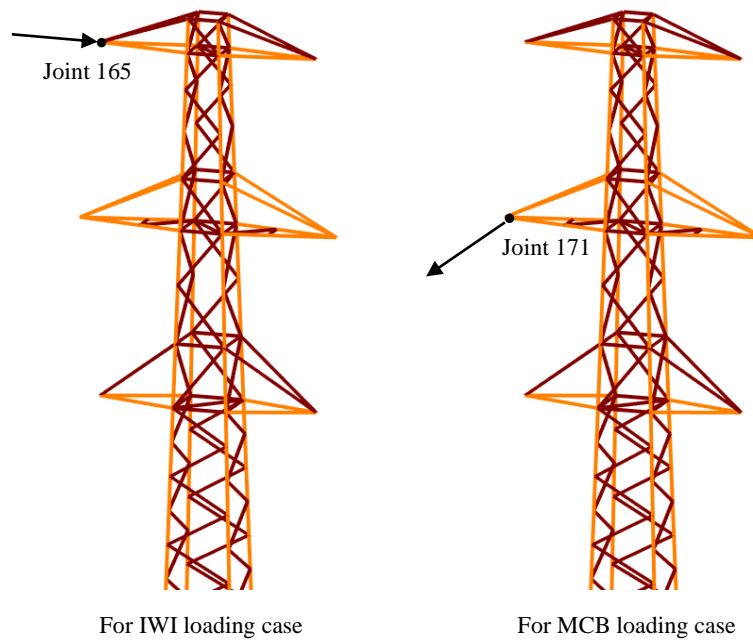


Figure 4.2. Monitored joints and degrees of freedom for IWI and MCB loading cases

4.1.2 Modeling of Plastic Hinges

In static nonlinear analysis, representation of the expected force-deformation relation of individual members is one of the key steps to achieve reliable structural response. Using localized plastic hinges is one of the approaches commonly used for this purpose. The plastic hinges are supposed to represent the nonlinear material properties and any other sources of inelastic response of the corresponding member. The load capacity of individual members that are part of a truss system is governed by a series of limit states, such as buckling, yielding over net cross-sectional area,

bolt bearing, and bolt shear. Which one of these limit states will govern the load capacity depends on the geometry of the member as well as the details used at the connection region.

In the towers investigated in the current study, plastic hinge properties for the members were calculated according to FEMA356 (FEMA, 2000), which provides extensive recommendations for the load-deformation modeling of individual elements. A generalized force-deformation hinge model specified by FEMA 356 is shown in Figure 4.3. The load Q and total displacement Δ are normalized by limit load Q_y , and limit deformation Δ_y respectively in generalized hinge curve. The post-yield response is defined by parameters a , b , and c , for which the numerical values are provided in FEMA 356. Five points (A-E) are marked on the force-deformation curve, based on the parameters a , b , and c .

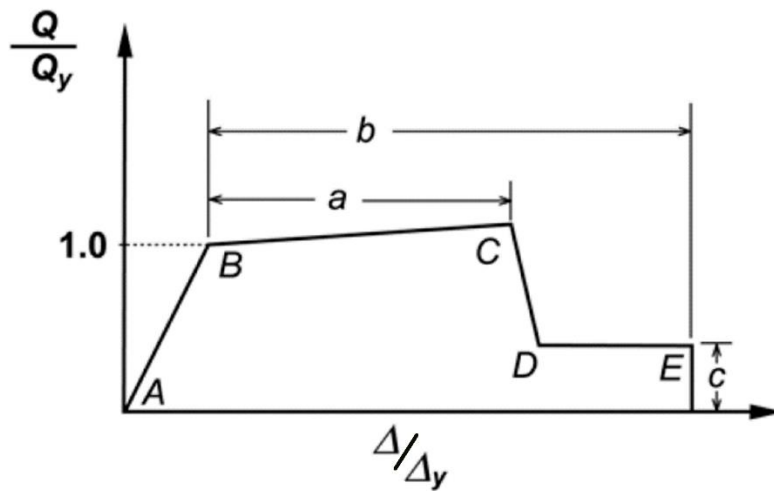


Figure 4.3. Generalized hinge curve for steel members (FEMA, 2000)

As illustrated in Figure 1.3 (a), transmission/distribution line towers consist of leg members, brace members and horizontal members. During structural design it is traditionally assumed that no moment transfer occurs through the connections used at the ends of structural members. Therefore, no moment is present in the members, and the design is usually based on the pure axially loaded member assumption (Da Silva et al., 2005). On the other hand, leg members are connected to each other with splice connections and they can carry small moments in addition to axial

compression and tension loads. Even though some moments are always present in leg members of existing towers, they are generally neglected when evaluating the behavior of the structures (Alam, 1993; Jiang et al., 2011). In structural analysis, external loads acting on the towers are applied to joints only and not in between joints along the members. Thus, no bending is expected to develop in the members. Moreover, it is usually assumed that a well detailed lattice tower does not have excessive eccentricities at the connections and therefore does not have significant bending moments in the members.

Based on the axially loaded member assumption, axial type plastic hinges in the form of load-deformation response were provided at middle length of all structural members in the analysis models. As discussed earlier, the load capacity of tower members is governed by a series of limit states depending on the geometry of the member. Therefore, different set of hinge properties should be defined for each frame member for nonlinear analyses. Plastic hinge properties used for each member in No.106 tower is presented in Appendix C, together with computed load capacities for all applicable limit states.

Axial hinges used for the members in the investigated towers were grouped as Type-I, Type-II, and Type-II, as shown in Figure 4.4 to Figure 4.6. These hinge properties were assigned to the built-in zero-length elements that are located at the center of each structural member in the investigated towers. As evident, the axial hinges used for the members have different behavior in tension and compression.

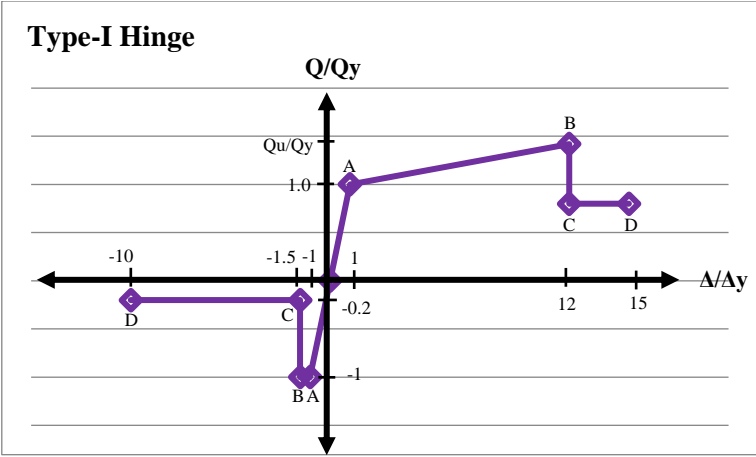


Figure 4.4. Type-I Hinge Properties

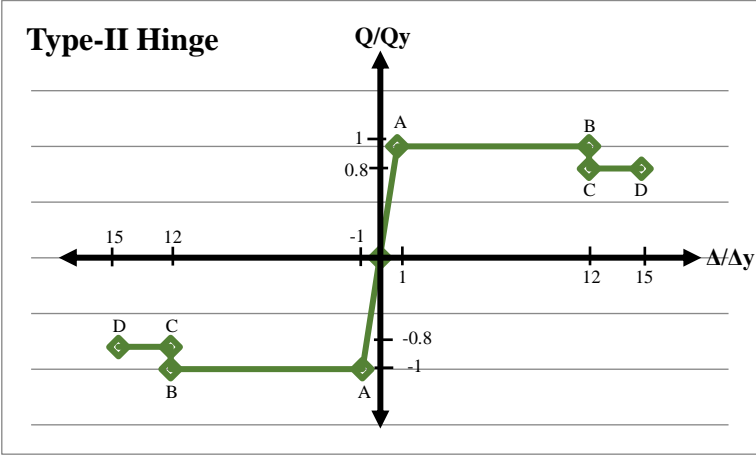


Figure 4.5. Type-II Hinge Properties

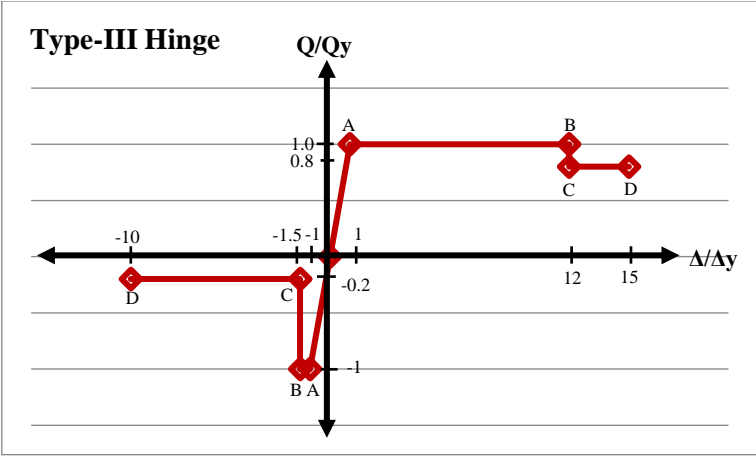


Figure 4.6. Type-III Hinge Properties

Type-I hinge was considered for leg members. For compression case, the failure mode is buckling instability of leg members. The load capacity Q_y in tension is dictated by net section yielding at member ends. The load capacity Q_u in tension is dictated by the most unfavorable limit state of net section rupture, bolt bearing, or bolt shear. This means that tension response of the plastic hinge changes according to the section type of steel members. In the investigated towers, the load capacity Q_u in tension of leg members is governed by net section rupture limit for L50x5 and L60x6 cross sections, while bolt bearing is the governing limit state for L65x7 and L70x7 cross sections. For this reason, for Type-I hinge shown, in Figure 4.4, the value of Q_u/Q_y is taken as 1.15 for L70x7, 1.28 for L65x7, and 1.42 for L50x5 and L60x6 cross sections.

Bolt bearing limit state governs the load capacity of horizontal members and most of the brace members for both tension and compression cases. This type of behavior was modeled by Type-II hinge. As the characteristic structural behavior is represented by bolt bearing limit state, a yield plateau is formed in the hinge curve after the yield load is achieved.

Type-III hinge was used to represent the nonlinear behavior of slender brace members. Brace members located near tower base possess larger slenderness than those located in upper parts of towers. This is mainly due to the overall geometry of the towers, where the horizontal distance between neighboring leg members decreases with increasing elevation. Therefore, for brace members located near tower base the predominant limit state under compression is buckling limit state. In addition, bolt bearing limit state governs the load capacity of the brace members for tension case.

4.2 Nonlinear Performance of the Towers

4.2.1 Ice and Wind Interaction (IWI) Load Case

Three sets of pushover analyses under IWI loading case was performed for No.106, No.107, and No.108 towers and the corresponding lateral load versus displacement curves (NL-GH) were determined, as shown in Figure 4.7, 4.9, and 4.11. The load values in these plots represent the total wind load acting on the tower, while the displacement values represent the lateral displacement of Joint-165 shown in Figure 4.2. In each plot, the curve labelled as NL-GH indicates the case where both material and geometric nonlinearities were considered in the analysis. the curve labelled as NL-H, on the other hand, indicates the case where only material nonlinearity was present in the analysis. Linear response of the tower is represented by the line labelled as LA.

Several points are marked on the nonlinear load-displacement curves in order to illustrate the progression of damage on the towers under pushover loading. The extent of damage in terms of the formation of plastic hinging in individual members at these points are shown in Figure 4.8, 4.10, and 4.12, respectively for towers No.106, No.107, and No.108. The percentage of applied load and the corresponding deformed shapes are given in the figures. Members that suffer damage in each tower at the end of the analysis are also indicated in the figures, with “*L*” indicating leg members and “*B*” indicating brace members.

According to pushover curves, it is seen that the linear behavior is valid until the formation of the first hinging in a leg member, which corresponds to buckling of this member. This damage results in a decrease in the lateral stiffness of towers. The load-carrying ability of the towers continues to increase until the formation of hinging in multiple members. After the ultimate capacity is reached, the towers cannot tolerate the load redistribution of failed members and total collapse occurs suddenly.

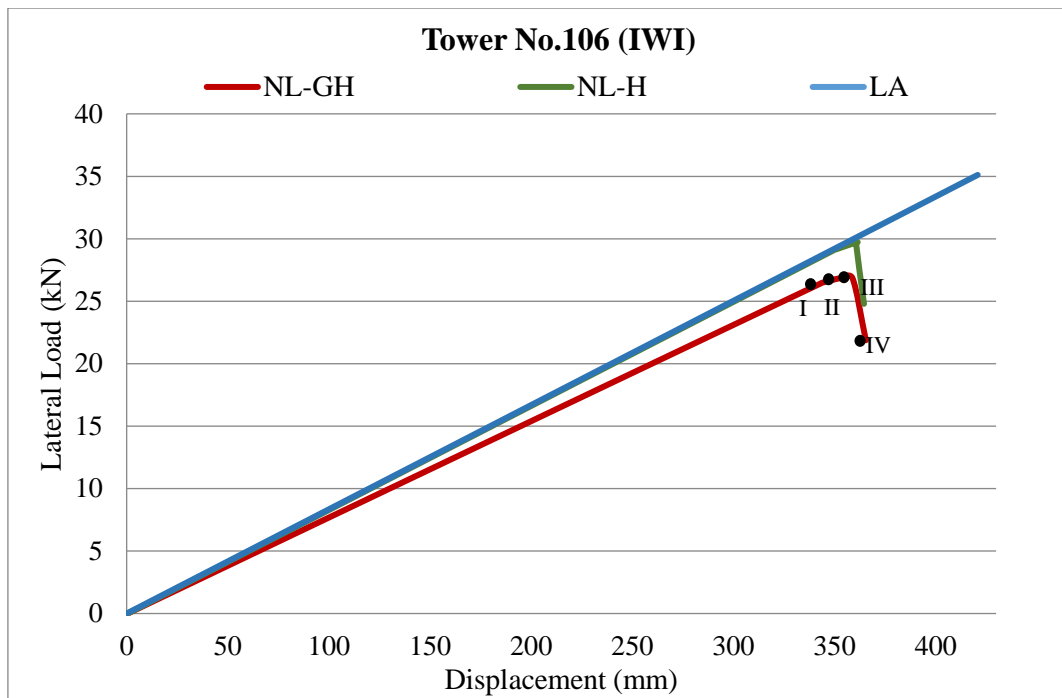


Figure 4.7. Load-displacement response of Tower No.106 under IWI loading case

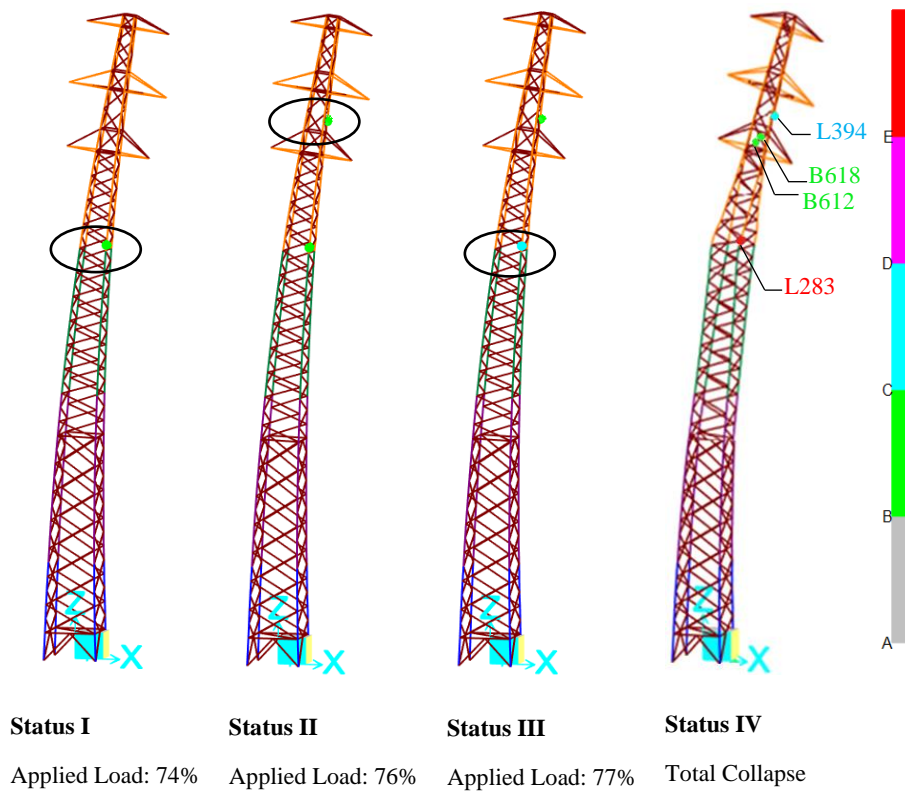


Figure 4.8. Progression of damage in Tower No.106 under IWI loading case

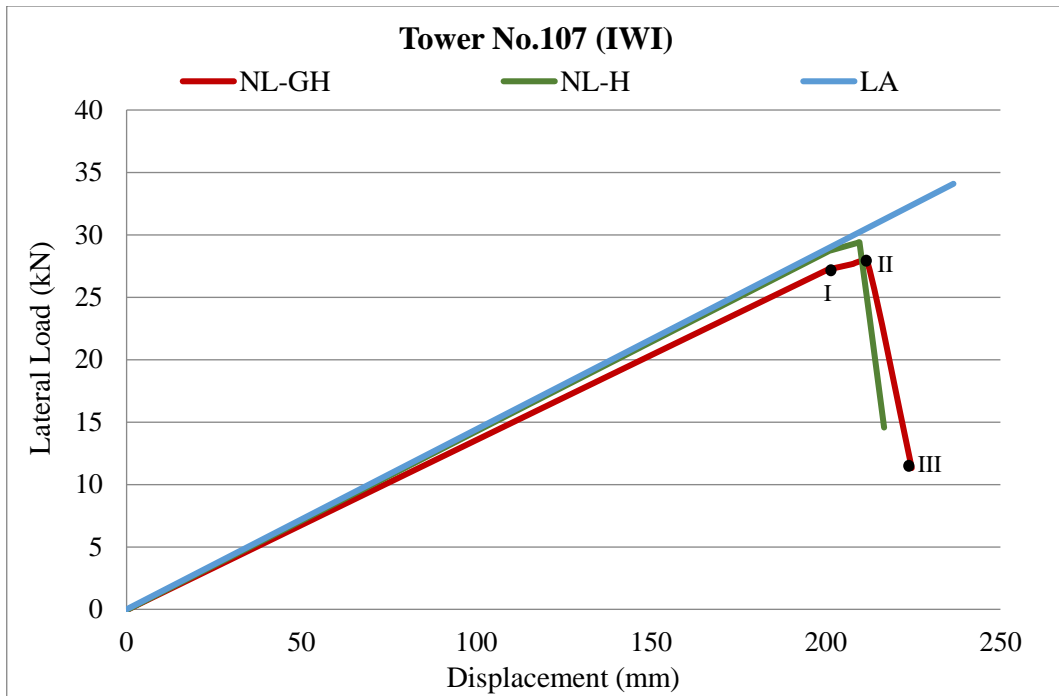


Figure 4.9. Load-displacement response of Tower No.107 under IWI loading case

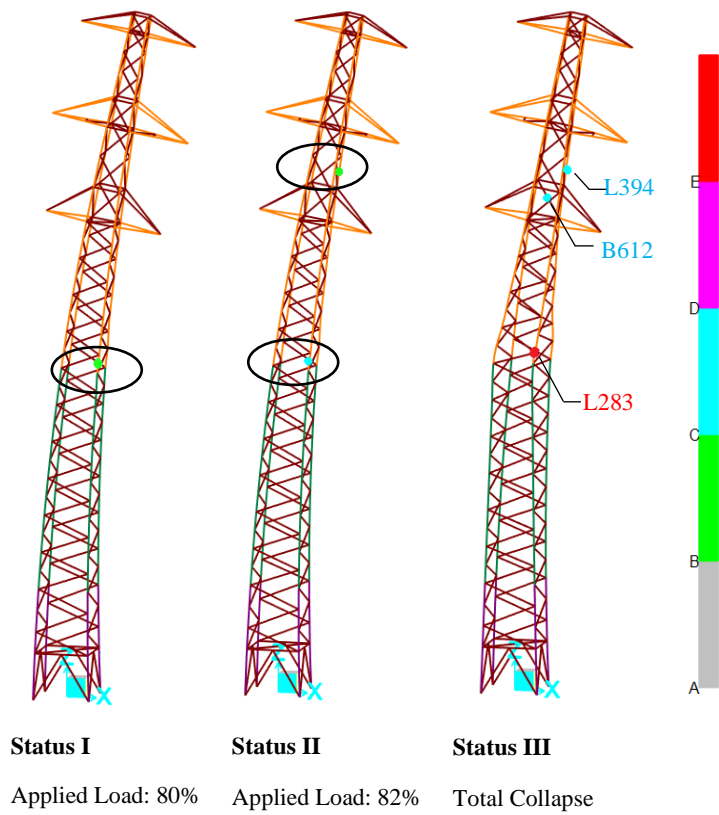


Figure 4.10. Progression of damage in Tower No.107 under IWI loading case

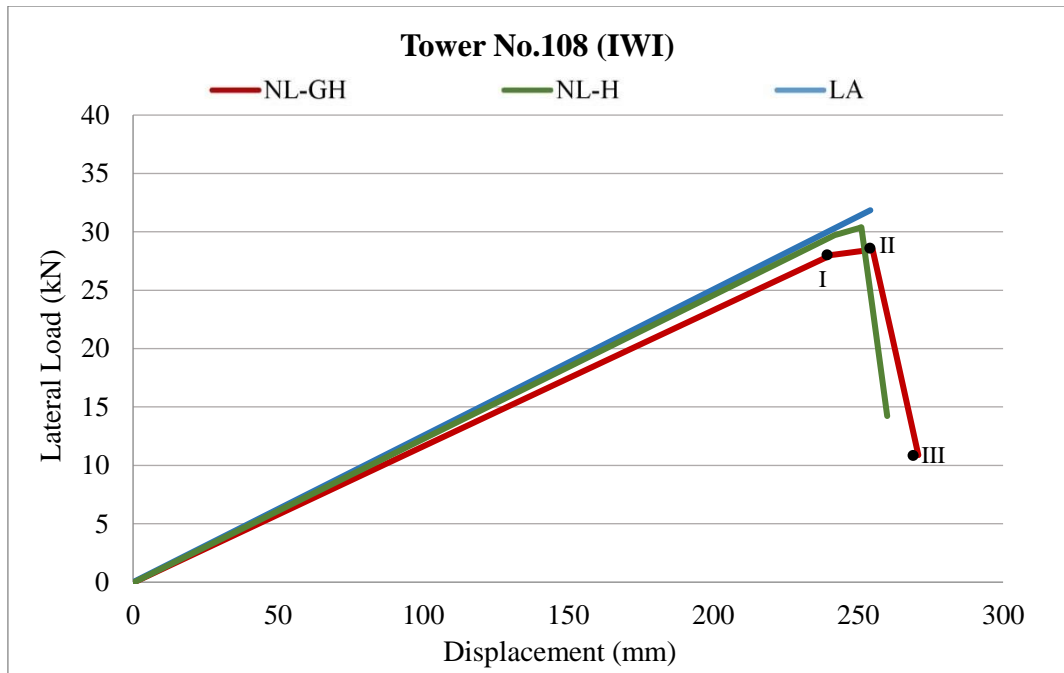


Figure 4.11. Load-displacement response of Tower No.108 under IWI loading case

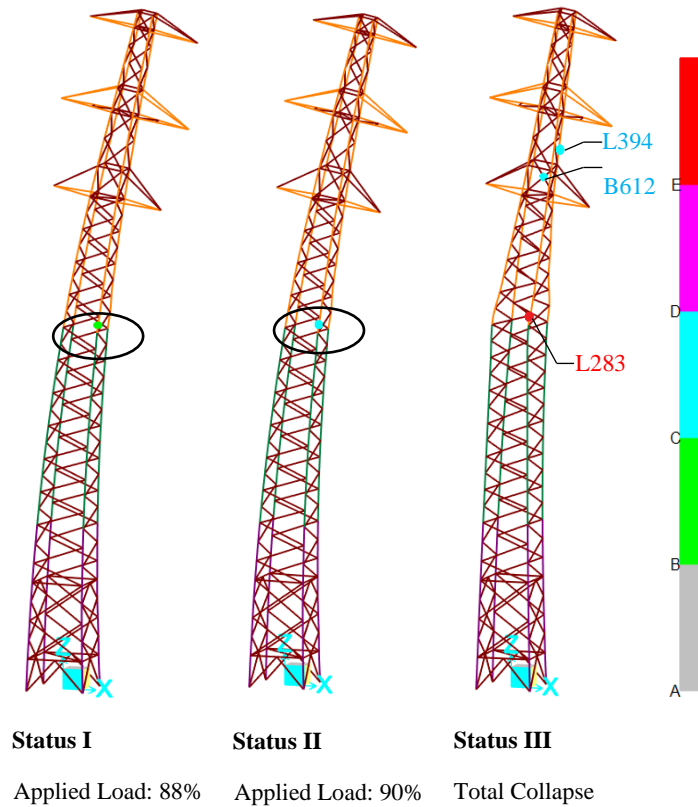


Figure 4.12. Progression of damage in Tower No.108 under IWI loading case

Figures 4.7 to Figure 4.12 reveal that, in all three investigated towers the first hinging appeared in L283 leg member due to buckling. This leg member is located where the L60x6 cross section changes to L50x5 along the tower height. In addition to L283, L394 leg member and B612 brace member, which are located between middle and bottom crossarm, also buckled after the ultimate capacity is reached. In No.106 and No.107 towers, L394 leg member reached its buckling capacity before the buckling of B612 brace member. Also, in No.106 tower an additional brace member, B618 reached its buckling limit prior to collapse. No failed horizontal members were observed in the towers under the IWI loading case.

The load-carrying capacity of the towers under IWI loading case represents the maximum wind load that can be carried by the towers before the total failure occur, since the pushover load simulates the transverse wind loads on the conductors, insulators, and tower body. In this regard, it can be stated that wind speeds corresponding the total collapse are 52.5 km/h, 54.5 km/h and 57.0 km/h for No.106, No.107, and No.108 towers, respectively according to Eqn. (3.2).

A comparison of the three capacity curves obtained from pushover analysis of each tower indicates that the tower response with no geometric nonlinearity effect follows the linear load-displacement behavior up to the initiation of first hinging. As evident in the plots, presence of geometric nonlinearity in the analysis resulted in a decrease in stiffness of the towers. In pushover curves of NL-GH under IWI loading case, the elastic stiffness is decreased up to the initiation of first hinging by 8.0%, 6.6%, and 8.3% in the transverse direction for No.106, No.107, and No.108 towers, respectively.

The load-carrying capacities of No.106, No.107, and No.108 towers from linear and nonlinear analyses under IWI loading case are summarized in Table 4.1. The linear load capacities were determined by considering the first occurrence of member overloading within the towers, while the nonlinear load capacities correspond to the collapse condition. It should be noted that both geometric and material effects were considered in nonlinear analyses.

A nonlinear geometry usually results in larger deformations and member forces, which expedite the failure of towers. Material nonlinearity, on the other hand, allows the formation of plastic hinging in multiple members before the total collapse of towers. During this damage progression stage, the towers still possess a load resisting ability, even though it is usually small. As discussed earlier, in the nonlinear analysis conducted under IWI loading case towers exhibit very limited ductility and suffered from a sudden collapse. As a result of such nonductile response, limited damage progression occurred within the towers prior to collapse. In this case, the detrimental effect of geometric nonlinearity became more dominant and the load capacities determined from nonlinear analysis remained below the elastic capacities. The values presented in Table 4.1 represent 7.9%, 3.5%, and 4.1% reduction in load capacities, respectively for No.106, No.107, and No.108 towers. A slight increase in displacement values from nonlinear analysis compared to the linear case is also valid for all three towers.

Table 4.1 Load-carrying capacities and ultimate displacements under IWI loading case

Tower	Linear Analysis (LA)		Nonlinear Analysis (NL-GH)	
	Load capacity (kN)	Displacement (mm)	Load capacity (kN)	Displacement (mm)
106	29.1	349.1	26.8	353.9
107	28.6	200.5	27.6	212.1
108	29.5	239.2	28.4	255.0

Analysis results indicate that all three towers collapsed due to buckling of the same members. Therefore, similar failure mechanisms and load-carrying capacities were determined for the towers as shown in Figure 4.13. The displacements in the direction perpendicular to the power line (i.e., direction parallel to crossarms) represents a measure of the tower stiffness. The difference between the lateral stiffness of the towers is due to the length of the towers being different. As presented

in Table 3.3, these towers are of the same type but differ from each other according to their geometrical configuration and height.

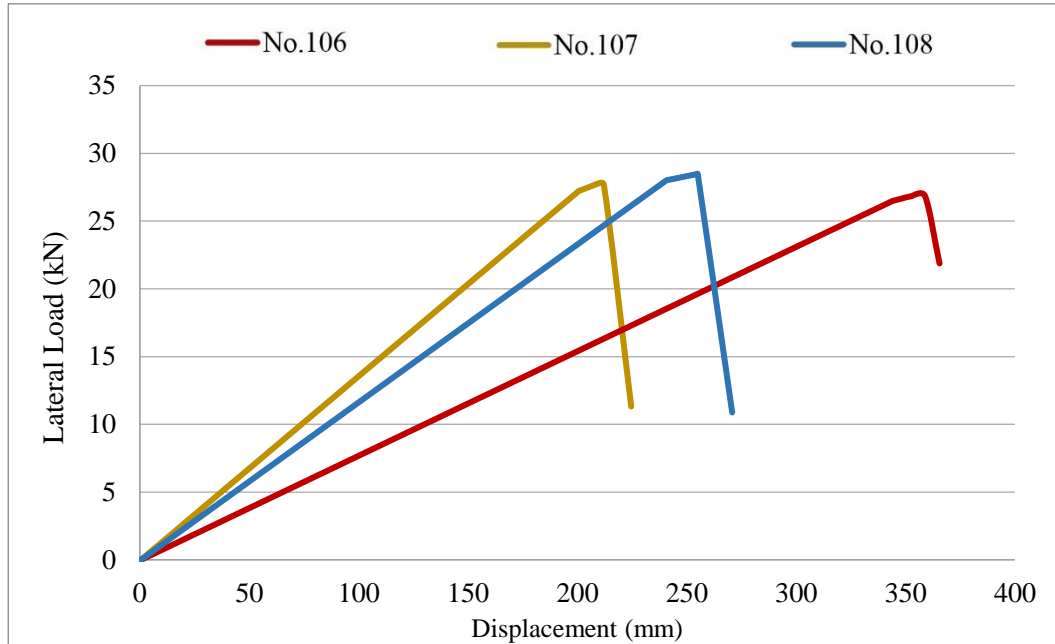


Figure 4.13. Pushover curves of the towers under IWI loading case

4.2.2 Middle Conductor Break (MCB) Load Case

Results of the pushover analyses conducted on No.106, No.107, and No.108 towers under MCB loading case are presented as the total lateral load in the line direction (i.e., direction perpendicular to crossarms) versus the lateral displacement of Joint 171 (Figure 4.2).

Pushover curves of the failed towers are illustrated in Figure 4.14, Figure 4.16, and Figure 4.18. Similar to the case for IWI loading case, three pushover curves are provided for each tower: linear analysis (LA), analysis with only material nonlinearity (NL-H), and analysis with material and geometric nonlinearity (NL-GH). The progression of damage within each tower during analyses is presented in Figures 4.15, 4.17, and 4.19. Members that underwent damage in each tower at the

end of the analysis are indicated in the figures, with “*L*” indicating leg members, “*B*” indicating brace members, and “*H*” indicating horizontal members.

Numerical results reveal that, the failure mode observed under MCB loading case is different than the one observed under IWI loading case. As evident in the figures, member failures are localized in the region between the lower and middle crossarm, with no damage in body part of the towers. Another observation is that under MCB loading case more hinges are observed to develop in the towers compared to IWI loading case. The primary reason for the collapse of towers is buckling of L394 leg member in tower No.106 and buckling of B627 brace member in tower No.107. In tower No.108 the main mechanism that triggers the collapse is bolt bearing damage of B631 brace member under compression.

In No.106 tower, first hinging was developed due to buckling of H717 horizontal member, which is located on middle crossarm, and then buckling of L394 leg member, which is located between the lower and middle crossarms. As the applied load increased, B631 brace member, which is located just below the middle crossarm, developed hinging due to bolt bearing. The load-carrying ability of the towers continues to increase until the formation of hinging in multiple members. After the ultimate capacity is reached, total collapse occurred by strength loss on L394 leg member.

In No.107 tower, even bolt bearing capacity was reached in B629 and B633 brace members under tension forces, the tower failed due to buckling of B624 and B627 brace members. No leg member failures were observed in this tower.

Response of tower No.108 remained linear until B631 brace member reached its bolt bearing capacity. After that B629 brace member and H717 horizontal member, located in the middle of the cage, also developed hinging due to bolt bearing failure. With further loading, L394 leg member reached its buckling capacity, and then B629 and B635 brace members underwent bolt bearing failure.

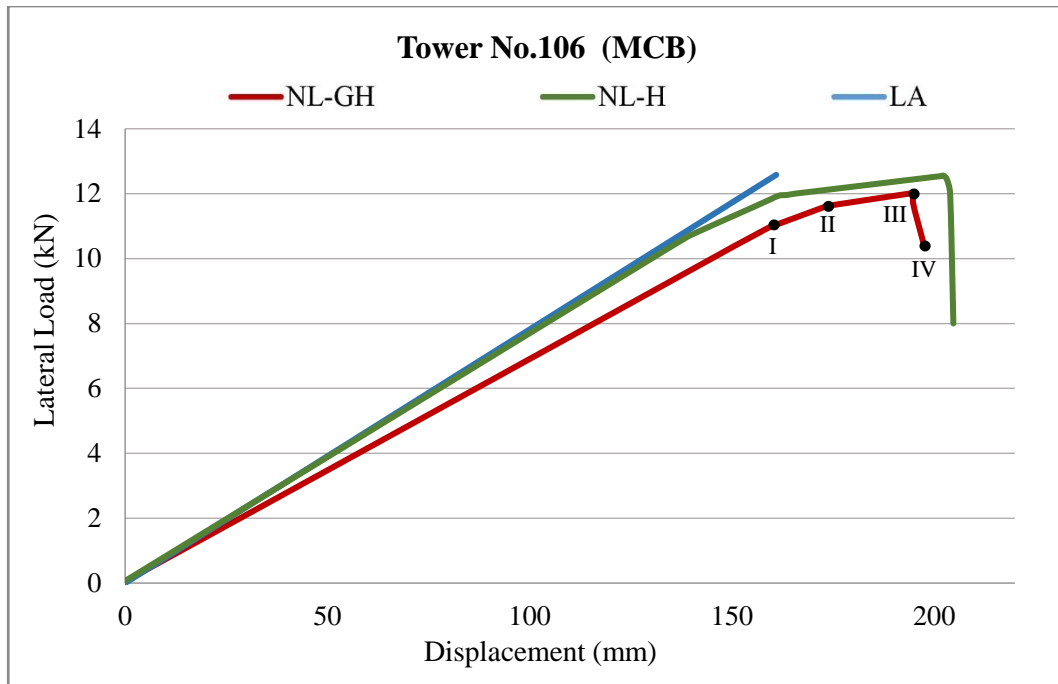


Figure 4.14. Load-displacement response of Tower No.106 under MCB loading case

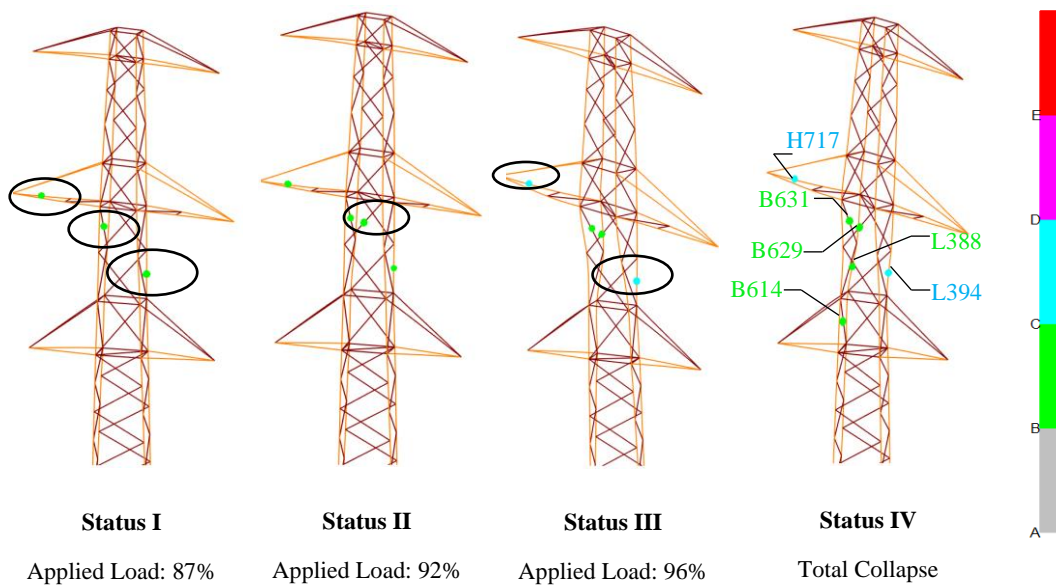


Figure 4.15. Progression of damage in Tower No.106 under MCB loading case

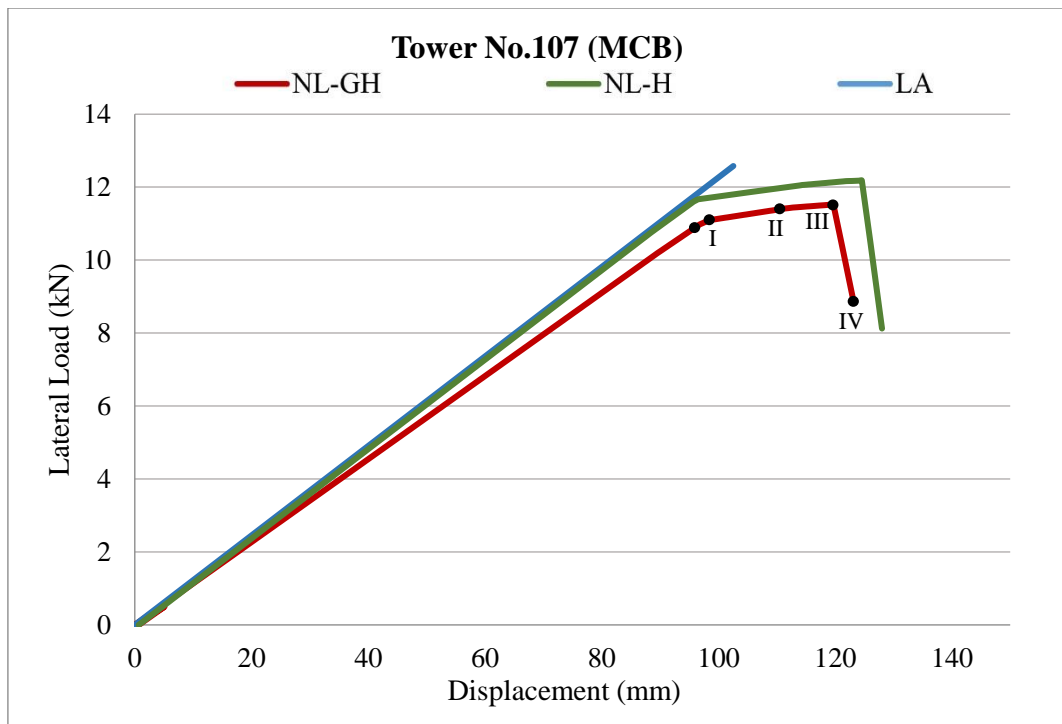


Figure 4.16. Load-displacement response of Tower No.107 under MCB loading case

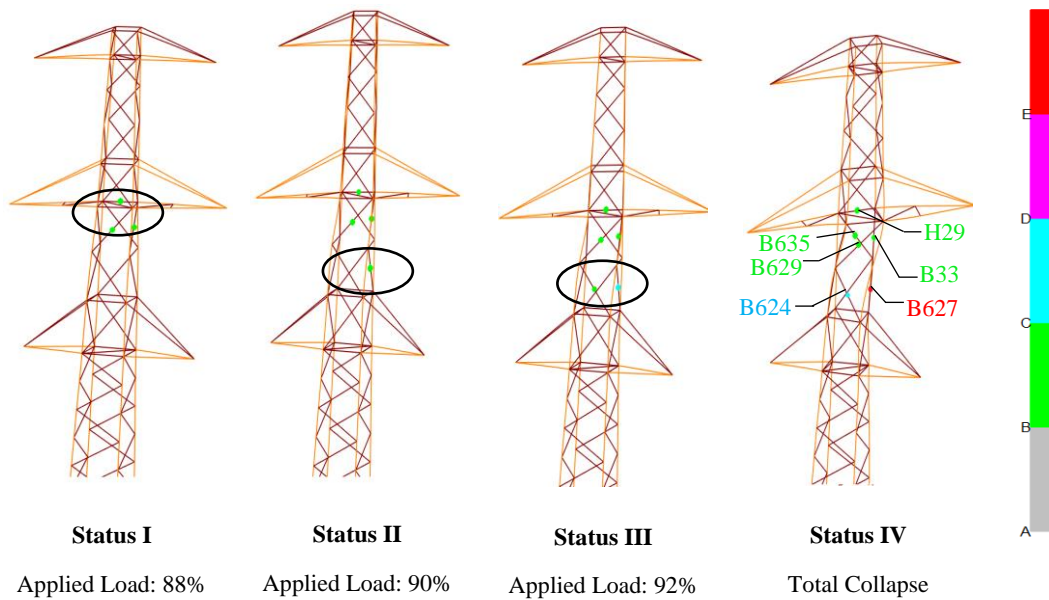


Figure 4.17. Progression of damage in Tower No.107 under MCB loading case

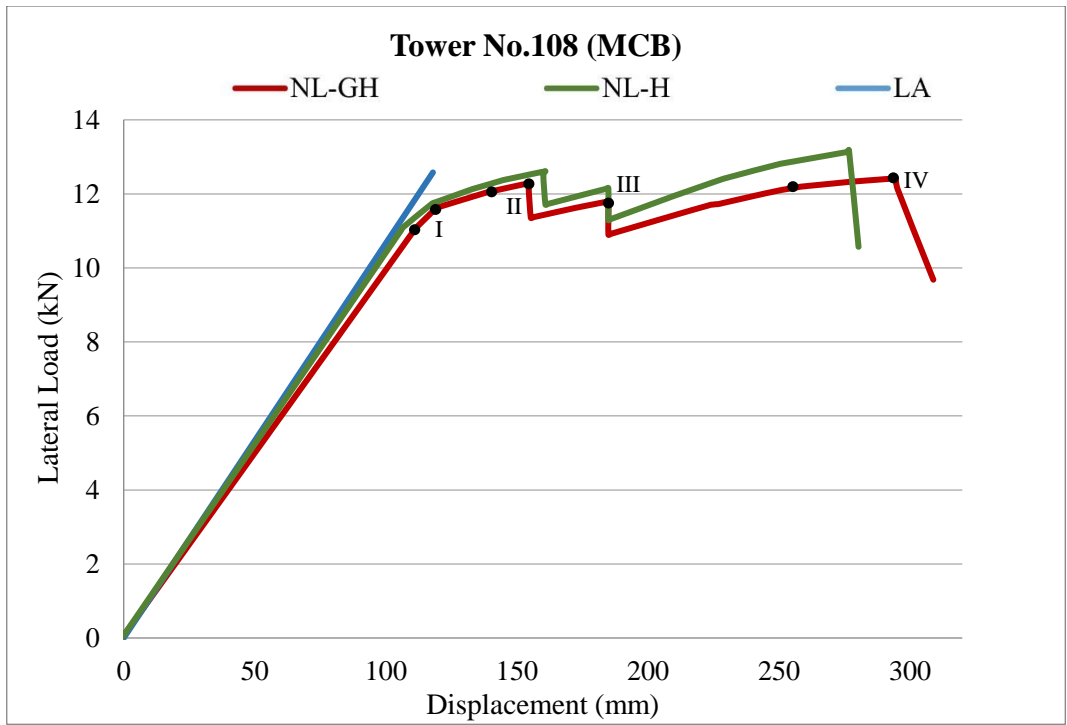


Figure 4.18. Load-displacement response of Tower No.108 under MCB loading case

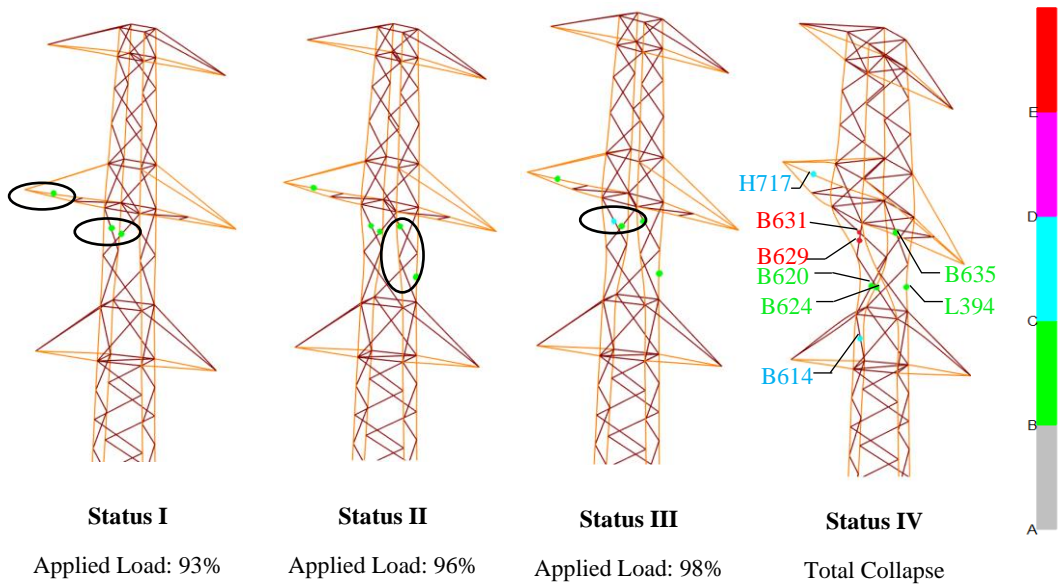


Figure 4.19. Progression of damage in Tower No.108 under MCB loading case

It is interesting to note that No.106 and No.107 towers showed very similar failure paths, while considerable differences are observed in the response of No.108 tower. The reason for this difference is related with the progression of failure in the towers. For No.106 and No.107 towers member buckling occurred at the analysis step before the total collapse condition, while for No.108 tower member damage at the same analysis step includes bolt bearing deformation. This behavior provides a more ductile failure mechanism compared to sudden collapse due to member buckling. This type of ductile response of No.108 tower compared to the other towers is also evident in load-displacement plots presented in Figure 4.20. The relatively lower stiffness of No.106 tower is due to this tower being longer than the others.

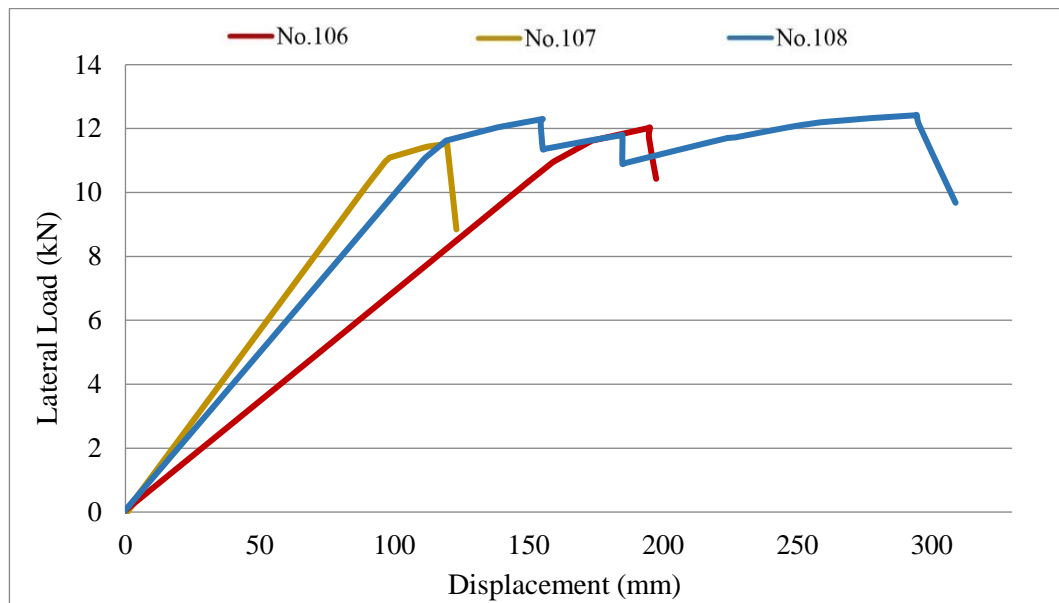


Figure 4.20. Pushover curves of the towers under MCB loading case

As mentioned earlier for the IWI loading case, lateral stiffness of the towers decreased with the inclusion of geometric nonlinearity in the analysis. Similar observation is valid for the MCB loading case as well. In this loading case, the elastic stiffness decreased up to the initiation of first hinging by 12.1%, 8.9% and 7.3% for No.106, No.107 and No.108 towers, respectively.

The load-carrying capacities of No.106, No.107, and No.108 towers from linear and nonlinear analyses under MCB loading case are summarized in Table 4.2. Nonlinear

analysis considering both geometric and material effects predicted 11.1% and 11.7% higher load capacities compared to linear analysis, respectively for No.106 and No.108 towers, while the same capacities were obtained for No.107 tower. The linear load capacities were determined by considering the first occurrence of member overloading within the towers. However, nonlinear analyses demonstrated that the load-carrying ability of towers continues to increase until several members develop plastic hinging. Formation of multiple hinging, on the other hand, results in significant deformation within the towers, as evident in the displacement values provided in Table 4.2. It was discussed earlier that IWI loading case resulted in smaller load capacities from nonlinear analysis compared to the linear case. The reason for such a behavior was the detrimental effect of geometric nonlinearity being more pronounced than the favorable effect provided by ductile damage progression within the tower system. Under MCB loading case, on the other hand, the latter effect was more significant due to ductile response resulting from bolt bearing deformation of tower members.

Table 4.2 Load-carrying capacities and ultimate displacements under MCB load case

Tower	Linear Analysis (LA)		Nonlinear Analysis (NL-GH)	
	Load capacity (kN)	Displacement (mm)	Load capacity (kN)	Displacement (mm)
106	10.8	149.1	12.0	195.2
107	11.6	99.6	11.6	119.7
108	11.1	109.3	12.4	294.5

4.2.3 Comparison of Numerically Predicted and Observed Failures

As mentioned earlier, site observations indicate that the overall failure of No.107 and No.108 towers is localized in leg members located in tower body, while for No.106 tower the overall failure location is between the lower and middle crossarms. Numerical analyses demonstrate that these failure modes result from IWI loading

case in No.107 and No.108 towers, and MCB loading case in No.106 tower. Comparison of the observed and predicted failures in each of the investigated towers are presented in Figure 4.21, Figure 4.22, and Figure 4.23. Predicted total collapse patterns of all three towers by nonlinear analyses agree well with the failure patterns observed at the site.

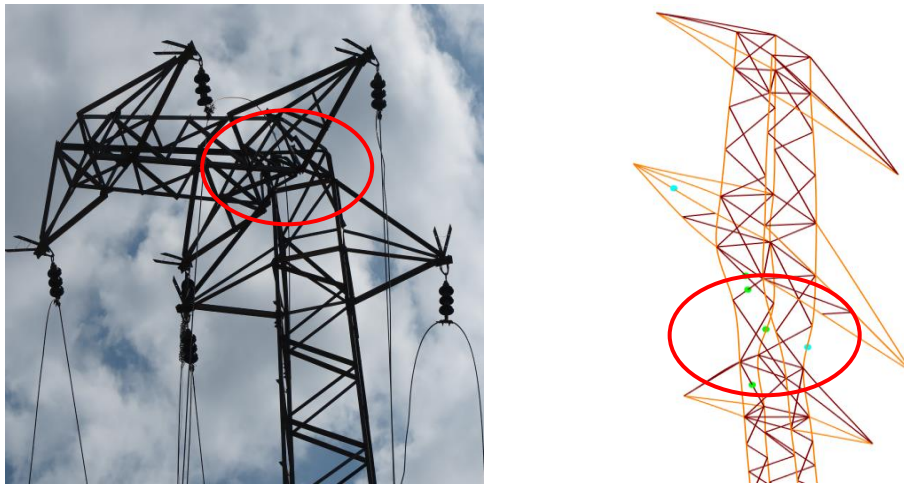


Figure 4.21. Observed and predicted collapse of No.106 tower

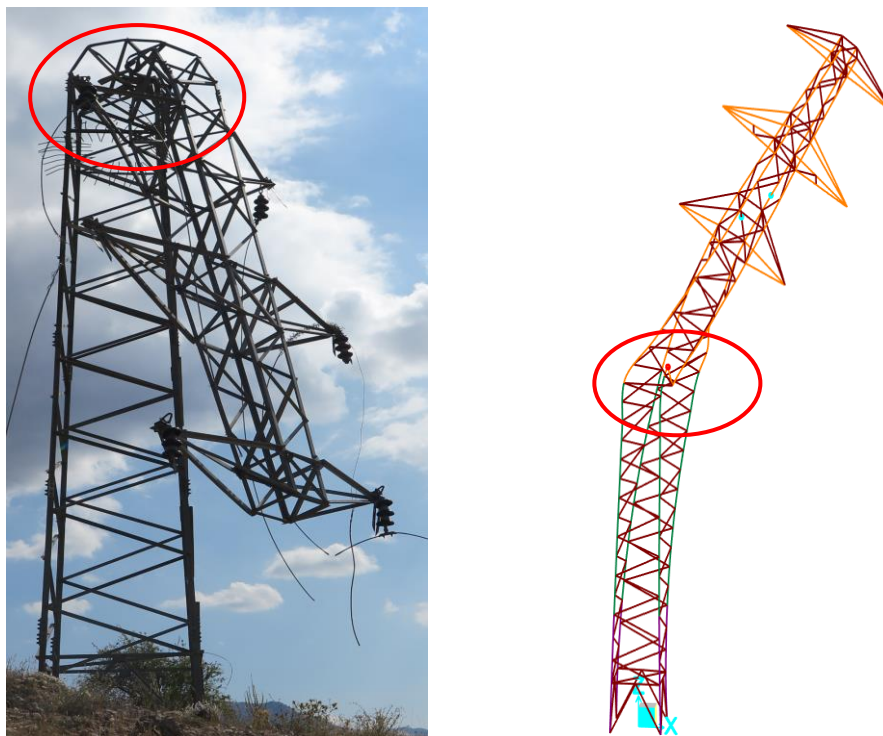


Figure 4.22. Observed and predicted collapse of No.107 tower

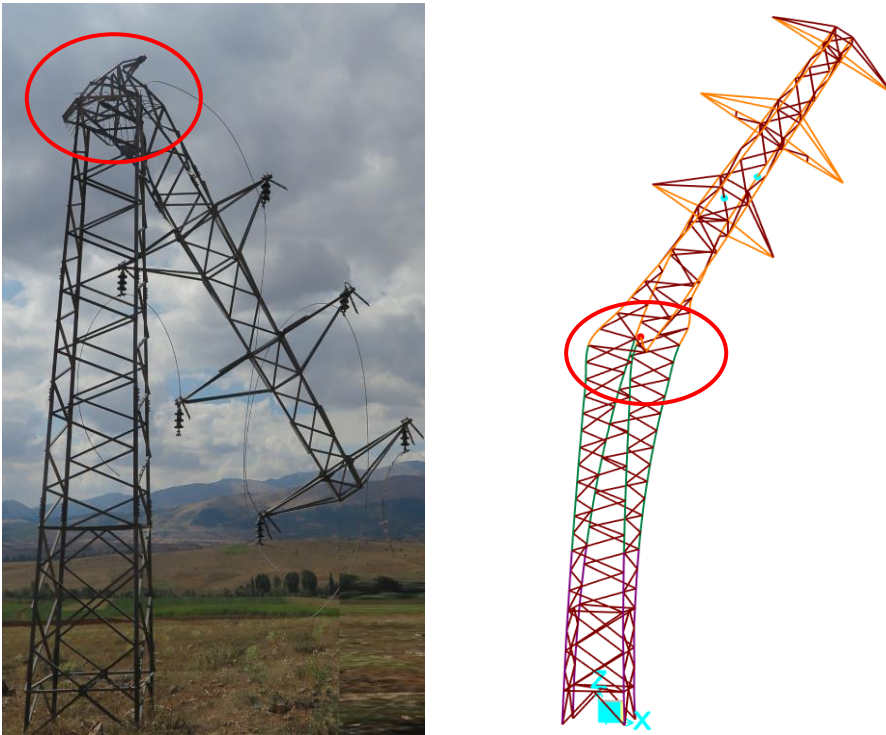


Figure 4.23. Observed and predicted collapse of No.108 tower

CHAPTER 5

CONCLUSIONS

Steel lattice towers are backbones in operation of power systems by providing the essential supports to the conductors along the power transmission/distribution line. Safety of these structures has a great significance in order to keep power systems functioning properly. Despite their crucial function, these structures are susceptible to damage and sometimes total collapse as a result of environmental overloading. In this thesis, a detailed failure investigation on the recent collapse of 34.5 kV voltage capacity distribution towers in Tufanbeyli district was conducted. The main focus of the investigation was on revealing the root cause of the tower failures and determining the safety levels of the remaining towers.

Due to the design and construction of the investigated towers dating back to the 1970s, it was deemed necessary to check the structural behavior of the towers under design loads. In this context, towers were analyzed in order to evaluate the compliance of their structural design according to the current design practice. Loading cases as specified by the Technical Specification by Turkish Power Distribution Agency (TEDAŞ, 2008) for suspension and tension towers were considered to determine member forces. Member capacities were evaluated following the regulations of ASCE10-15 (2015) and considering the nominal material properties.

Failure condition analyses of the towers were conducted by considering the loading cases of conductor break and ice with wind. Measured material capacities for tower steel members and conductors were incorporated in these analyses in an attempt to accurately simulate the actual conditions. The actual loading conditions that the towers were likely to experience on the day of the incident were predicted based on meteorological data. For the cases where conductor break was reported in the field,

the force in the conductor just before the collapse of the investigated towers was considered to be equal to the experimentally determined ultimate tensile capacity of the conductors. The actual ice loading on conductors were also determined by considering the condition that the tensile force in the ice-covered conductor is equal to the experimentally determined ultimate tensile capacity of the conductors.

After the failure conditions of the towers were clarified, further studies were performed with nonlinear analyses on three of the collapsed towers. For this purpose, pushover analyses incorporating nonlinear material and geometric effects were conducted and the progression of damage within the towers were determined under the loading cases of conductor break and ice with wind. Failure modes predicted by these nonlinear pushover analyses agreed well with the tower failure patterns observed at the site.

Based on the results presented in this study, the following conclusions can be made for the investigated towers:

- Numerical results obtained from linear analyses revealed that under design level loads and the specified loading cases the towers possess the safety level intended by the related design documents. Member axial forces in suspension towers remained significantly below the expected capacity of the corresponding members under longitudinal wind with no ice and conductor break loading cases. On the other hand, considerably high capacity ratios, were calculated under transverse wind with no ice loading case. Moreover, under this loading case, the locations of the members with the maximum capacity ratio correspond to the locations where the leg member's cross section changes from L60x6 to L50x5. For tension towers the maximum demand occurs under the unbalanced loading and transverse wind with no ice loading cases. Under these loading cases, the governing limit states for tower members were observed to be buckling and net section yielding. In general, the tension towers possess smaller capacity ratios than the suspension towers, indicating a higher safety level for the investigated tension towers.

- Failure condition analyses indicated the main cause of collapse of the investigated towers to be excessive ice accumulation on conductors with 50-60 km/h wind speed, which resulted in breakage of a conductor in some towers. At the time of the incident ice weights determined based on the measured conductor tensile capacity are 3.4-5.7 times what is specified by the design documents. Increased weight of the conductors due to ice accumulation imposes additional vertical loading at crossarm ends. Ice accumulation around conductors also increases the wind area and leads to larger horizontal loading to be imposed on towers.
- According to nonlinear pushover analyses, tower response under ice+wind loading case is governed by deformation of leg members in the region where leg member cross-section changes along the tower height. For conductor break loading case the response is governed by both brace members and leg members near crossarm locations. Failure is initiated either due to buckling or bolt bearing in tower members.
- Bolt bearing failure provides a more ductile failure mechanism and resulted in relatively large displacement capacity compared to sudden collapse due to member buckling.
- Geometric nonlinearity has a marked effect on lateral stiffness of towers. Reduction in stiffness is 6.6-8.3% and 7.3-12.1% under ice+wind and conductor break loading cases, respectively.
- In design of steel lattice distribution towers, it is necessary to consider the coexistence of wind and ice loading. The current Turkish design code cannot represent the appropriate loading conditions that the towers underwent and therefore, the design code has to be revised in order to include more realistic loading cases.

In conclusion, to evaluate the performance of the failed towers, the actual loading conditions should be considered. In this way, ultimate displacements of joints and

the percentage of loading for collapse can be determined accurately. As evident by results, pushover analysis incorporating nonlinear material and geometric effects is capable of estimating the capacity of tower structures accurately and simulating the structural behavior up to the onset of collapse. This study attempts to accurately evaluate the performance of the towers using different analysis techniques. Numerical results may serve to simulate failure scenarios in existing distribution towers.

REFERENCES

- Al-Bermani, F. G. A., & Kitipornchai, S. (1992). Nonlinear Analysis of Transmission Towers. *Engineering Structures*, 14(3), 139–152. [https://doi.org/10.1016/S1018-3639\(18\)30988-7](https://doi.org/10.1016/S1018-3639(18)30988-7)
- Al-Bermani, F., Mahendran, M., & Kitipornchai, S. (2004). Upgrading of Transmission Towers Using a Diaphragm Bracing System. *Engineering Structures*, 26(6), 735–744. <https://doi.org/10.1016/j.engstruct.2004.01.004>
- Alam, M. J. (1993). *Methodologies For Reliability-Based Design Of Transmission Line Systems*. Anna University.
- Alminhana, F., Al-Bermani, F., & Mason, M. (2018). Cascading Collapse of Transmission Lines. *Proceedings of the Institution of Civil Engineers: Engineering and Computational Mechanics*, 171(3), 115–132. <https://doi.org/10.1680/jencm.18.00010>
- American Society of Civil Engineers. (2010). *Guidelines for Electrical Transmission Line Structural Loading* (Third Edit). Reston, VA.
- American Society of Civil Engineers. (2015). *Design of Latticed Steel Transmission Structures*. <https://doi.org/10.1061/9780784413760>
- Anagnostatos, S. D., Halevidis, C. D., Polykrati, A. D., Bourkas, P. D., & Karagiannopoulos, C. G. (2013). Examination of the 2006 blackout in Kefallonia Island, Greece. *International Journal of Electrical Power and Energy Systems*, 49, 122–127. <https://doi.org/10.1016/j.ijepes.2012.12.003>
- Cai, Y., Xie, Q., & Xue, S. (2016). Effects of Additional Diaphragms on the Wind-Resistant Performance of Power Transmission Tower. *The 2016 World Congress on Advances in Civil, Environmental, and Materials Research (ACEM16)*. Jeju Island, Korea.

- CENELEC. (2012). *Overhead electrical lines exceeding AC 1 kV - Part 1 : General requirements - Common specifications (EBS EN 50341-1)*. Brussels.
- Da Silva, J. G. S., Vellasco, P. C. G. D. S., De Andrade, S. A. L., & De Oliveira, M. I. R. (2005). Structural Assessment of Current Steel Design Models for Transmission and Telecommunication Towers. *Journal of Constructional Steel Research*, 61(8), 1108–1134. <https://doi.org/10.1016/j.jcsr.2005.02.009>
- Edgar, T. H., & Sordo, E. (2017). Structural Behaviour of Lattice Transmission Towers Subjected to Wind Load. *Structure and Infrastructure Engineering*, 13(11), 1462–1475. <https://doi.org/10.1080/15732479.2017.1290120>
- FEMA. (2000). *FEMA 356 Prestandard and Commentary for the Seismic Rehabilitation of Buildings*. Washington D.C.
- Fu, X., & Li, H. N. (2018). Uncertainty Analysis of the Strength Capacity and Failure Path for a Transmission Tower Under a Wind Load. *Journal of Wind Engineering and Industrial Aerodynamics*, 173(December 2017), 147–155. <https://doi.org/10.1016/j.jweia.2017.12.009>
- Fu, X., Li, H. N., & Wang, J. (2019). Failure Analysis of a Transmission Tower Subjected to Combined Wind and Rainfall Excitations. *Structural Design of Tall and Special Buildings*, 28(10), 1–19. <https://doi.org/10.1002/tal.1615>
- Fu, X., Wang, J., Li, H. N., Li, J. X., & Yang, L. D. (2019). Full-Scale Test and Its Numerical Simulation of a Transmission Tower Under Extreme Wind Loads. *Journal of Wind Engineering and Industrial Aerodynamics*, 190(April), 119–133. <https://doi.org/10.1016/j.jweia.2019.04.011>
- Fu, Z., Tian, L., & Liu, J. (2022). Seismic Response and Collapse Analysis of a Transmission Tower-Line System Considering Uncertainty Factors. *Journal of Constructional Steel Research*, 189(June 2021), 107094. <https://doi.org/10.1016/j.jcsr.2021.107094>
- Jian, M. J., Zhang, D. Q., & Zhang, G. C. (2013). Finite Element Analysis for the

- Collapse Accident of One 110kV Transmission Tower. *Advanced Materials Research*, 690 693, 1940–1944.
<https://doi.org/10.4028/www.scientific.net/AMR.690-693.1940>
- Jiang, W. Q., Wang, Z. Q., McClure, G., Wang, G. L., & Geng, J. D. (2011). Accurate Modeling of Joint Effects in Lattice Transmission Towers. *Engineering Structures*, 33(5), 1817–1827.
<https://doi.org/10.1016/j.engstruct.2011.02.022>
- Klinger, C., Mehdiانpour, M., Klingbeil, D., Bettge, D., Häcker, R., & Baer, W. (2011). Failure Analysis on Collapsed Towers of Overhead Electrical Lines in the Region Münsterland (Germany) 2005. *Engineering Failure Analysis*, 18(7), 1873–1883. <https://doi.org/10.1016/j.engfailanal.2011.07.004>
- Li, J. X., Li, H. N., & Fu, X. (2017). Stability and Dynamic Analyses of Transmission Tower-Line Systems Subjected to Conductor Breaking. *International Journal of Structural Stability and Dynamics*, 17(6).
<https://doi.org/10.1142/S0219455417710134>
- Li, J. X., Li, H. N., & Fu, X. (2018). Dynamic Behavior of Transmission Tower-Line Systems Subjected to Insulator Breakage. *International Journal of Structural Stability and Dynamics*, 18(3).
<https://doi.org/10.1142/S0219455418500360>
- Li, J. X., Wang, S. H., & Fu, X. (2020). Dynamic Response of Tower-Line System Induced by Insulator Breakage Considering the Collision between the Conductor and the Ground Surface. *Journal of Performance of Constructed Facilities*, 34(1), 04019098. [https://doi.org/10.1061/\(asce\)cf.1943-5509.0001367](https://doi.org/10.1061/(asce)cf.1943-5509.0001367)
- Long, X., Wang, W., & Fan, J. (2018). Collapse Analysis of Transmission Tower Subjected to Earthquake Ground Motion. *Modelling and Simulation in Engineering*, 2018. <https://doi.org/10.1155/2018/2687561>
- Lu, C., Ma, X., & Mills, J. E. (2014). The Structural Effect of Bolted Splices on

- Retrofitted Transmission Tower Angle Members. *Journal of Constructional Steel Research*, 95, 263–278. <https://doi.org/10.1016/j.jcsr.2013.12.011>
- Manis, P., & Bloodworth, A. G. (2017). Climate Change and Extreme Wind Effects on Transmission Towers. *Proceedings of the Institution of Civil Engineers: Structures and Buildings*, 170(2), 81–97. <https://doi.org/10.1680/jstbu.16.00013>
- Mara, T. G., & Hong, H. P. (2013). Effect of Wind Direction on the Response and Capacity Surface of a Transmission Tower. *Engineering Structures*, 57, 493–501. <https://doi.org/10.1016/j.engstruct.2013.10.004>
- Mills, J. E., Ma, X., & Zhuge, Y. (2012). Experimental Study on Multi-Panel Retrofitted Steel Transmission Towers. *Journal of Constructional Steel Research*, 78, 58–67. <https://doi.org/10.1016/j.jcsr.2012.06.004>
- Pan, H., Tian, L., Fu, X., & Li, H. (2020). Sensitivities of the Seismic Response and Fragility Estimate of a Transmission Tower to Structural and Ground Motion Uncertainties. *Journal of Constructional Steel Research*, 167, 105941. <https://doi.org/10.1016/j.jcsr.2020.105941>
- Rao, N. P., & Kalyanaraman, V. (2001). Non-Linear Behaviour of Lattice Panel of Angle Towers. *Journal of Civil Constructional Steel Research*, 57, 1337–1357.
- Shukla, V. K., Selvaraj, M., & Kumar, K. V. (2021). Failure Analysis of a Cruciform-Leg Transmission Line Tower. *International Journal of Steel Structures*, 21(2), 539–548. <https://doi.org/10.1007/s13296-021-00454-5>
- Tapia-Hernández, E., Ibarra-González, S., & De-León-Escobedo, D. (2017). Collapse Mechanisms of Power Towers Under Wind Loading. *Structure and Infrastructure Engineering*, 13(6), 766–782. <https://doi.org/10.1080/15732479.2016.1190765>
- TEDAŞ. (2000). *Dağıtım Hatları Proje Teknik Klavuzu Yayın: 1-1/A*. Tedaş Proje

ve Tesis Dairesi Başkanlığı.

TEDAŞ. (2008). *YG Dağıtım Hatları Proje Teknik Şartnamesi*. Tedaş Proje ve Tesis Dairesi Başkanlığı.

TEİAŞ. (n.d.). *154 kV Proje Teknik Şartnamesi*. TEİAŞ Genel Müdürlüğü.

Tian, L., Ma, R., & Qu, B. (2018). Influence of Different Criteria For Selecting Ground Motions Compatible with IEEE 693 Required Response Spectrum on Seismic Performance Assessment of Electricity Transmission Towers. *Engineering Structures*, 156(November 2017), 337–350.
<https://doi.org/10.1016/j.engstruct.2017.11.046>

Tian, L., Ma, R. S., Li, H. N., & Wang, Y. (2016). Progressive Collapse of Power Transmission Tower-Line System under Extremely Strong Earthquake Excitations. *International Journal of Structural Stability and Dynamics*, 16(7), 1–21. <https://doi.org/10.1142/S0219455415500303>

Tian, L., Pan, H., Ma, R., & Qiu, C. (2017). Collapse Simulations of a Long Span Transmission Tower-Line System Subjected to Near-Fault Ground Motions. *Earthquake and Structures*, 13(2), 211–220.
<https://doi.org/10.12989/eas.2017.13.2.211>

Vincent, P., Huet, C., Charbonneau, M., Guilbault, P., Lapointe, M., & Banville, D. (2004). Testing and Numerical Simulation of Overhead Transmission Line Dynamics under Component Failure Conditions. *Conférence Internationale Des Grands Réseaux Élect*, 1–8.

Wang, S. L., Lin, Q. X., & Qian, Y. (2014). Research on the Dynamic Characteristics of Strain Tower in Heavy Icing Area Based on SAP2000. *Advanced Materials Research*, 986–987, 681–684.
<https://doi.org/10.4028/www.scientific.net/AMR.986-987.681>

Xie, Q., & Sun, L. (2012). Failure Mechanism and Retrofitting Strategy of Transmission Tower Structures Under Ice Load. *JCSR*, 74, 26–36.

<https://doi.org/10.1016/j.jcsr.2012.02.003>

Yang, W., Li, X., & Yang, Y. (2016). Analysis of Weak Parts of Narrow Transmission Towers and the Reinforcement Measure. *Proceedings - 2015 6th International Conference on Intelligent Systems Design and Engineering Applications, ISDEA 2015*, 143–146. <https://doi.org/10.1109/ISDEA.2015.45>

Zhang, J., & Xie, Q. (2019). Failure Analysis of Transmission Tower Subjected to Strong Wind Load. *Journal of Constructional Steel Research*, 160, 271–279. <https://doi.org/10.1016/j.jcsr.2019.05.041>

Zhuge, Y., Mills, J. E., & Ma, X. (2012). Modelling of Steel Lattice Tower Angle Legs Reinforced for Increased Load Capacity. *Engineering Structures*, 43, 160–168. <https://doi.org/10.1016/j.engstruct.2012.05.017>

APPENDICES

A. Appendix A - Schematic Figures of RU and DU Type of Towers

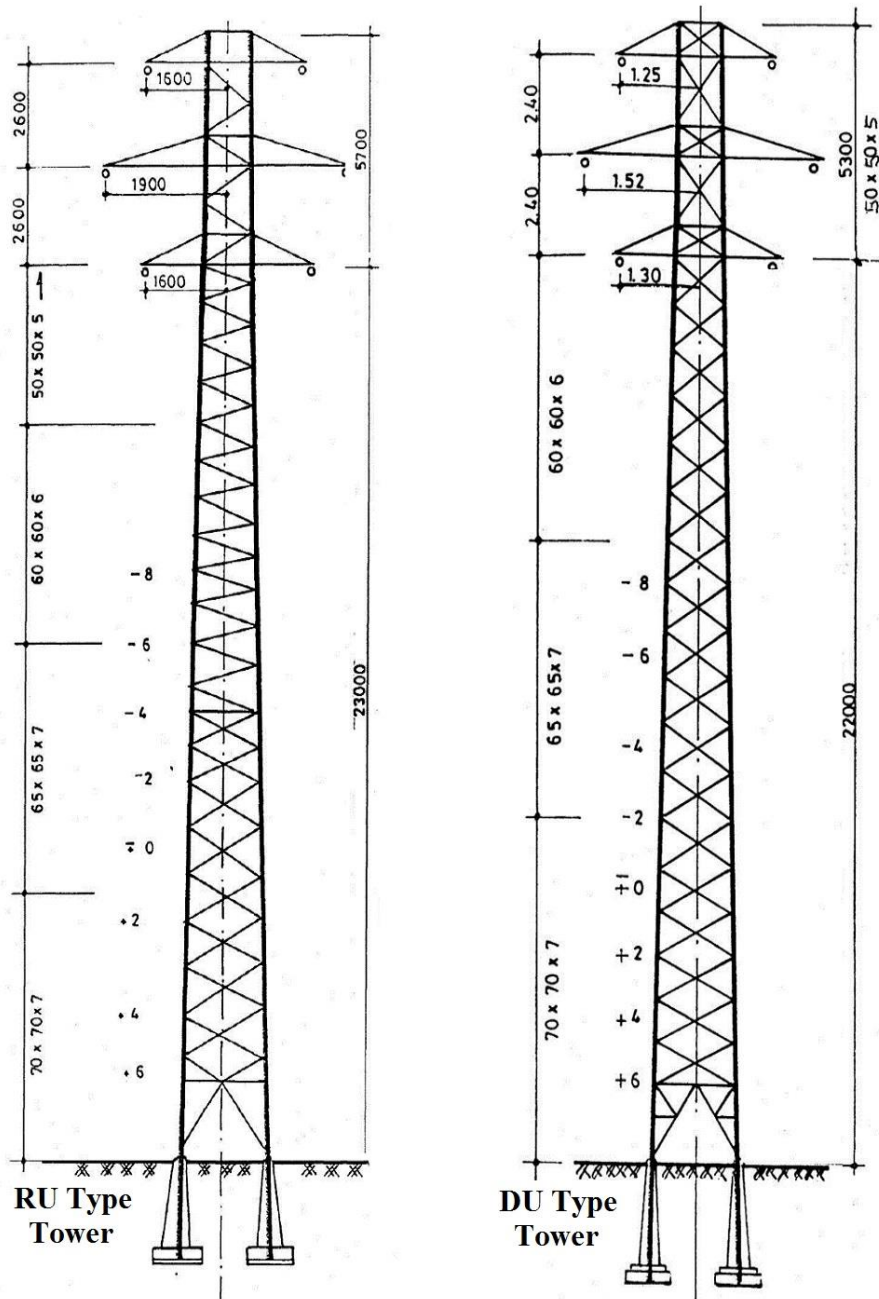


Figure A.1. Schematic figures of RU and DU type towers

B. Appendix B - Investigated Failed Towers During Site Visit



Figure B.1. No.106 tower (Torsional deformation of the tower cage between the middle and bottom crossarms)



Figure B.2. No.107 tower (Buckling of leg members in tower body)



Figure B.3. No.108 tower (Buckling of leg members in tower body)

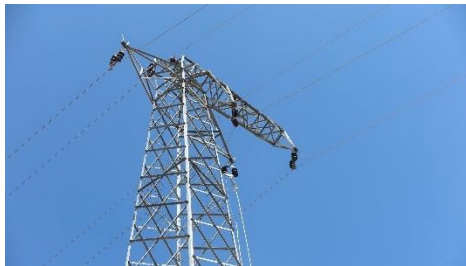


Figure B.4. No.116 tower (Torsional deformation of the tower cage between the middle and bottom crossarms)



Figure B.5. No.127 tower (Deformation of the tower cage)

C. Appendix C – Structural Properties of No.106 Tower

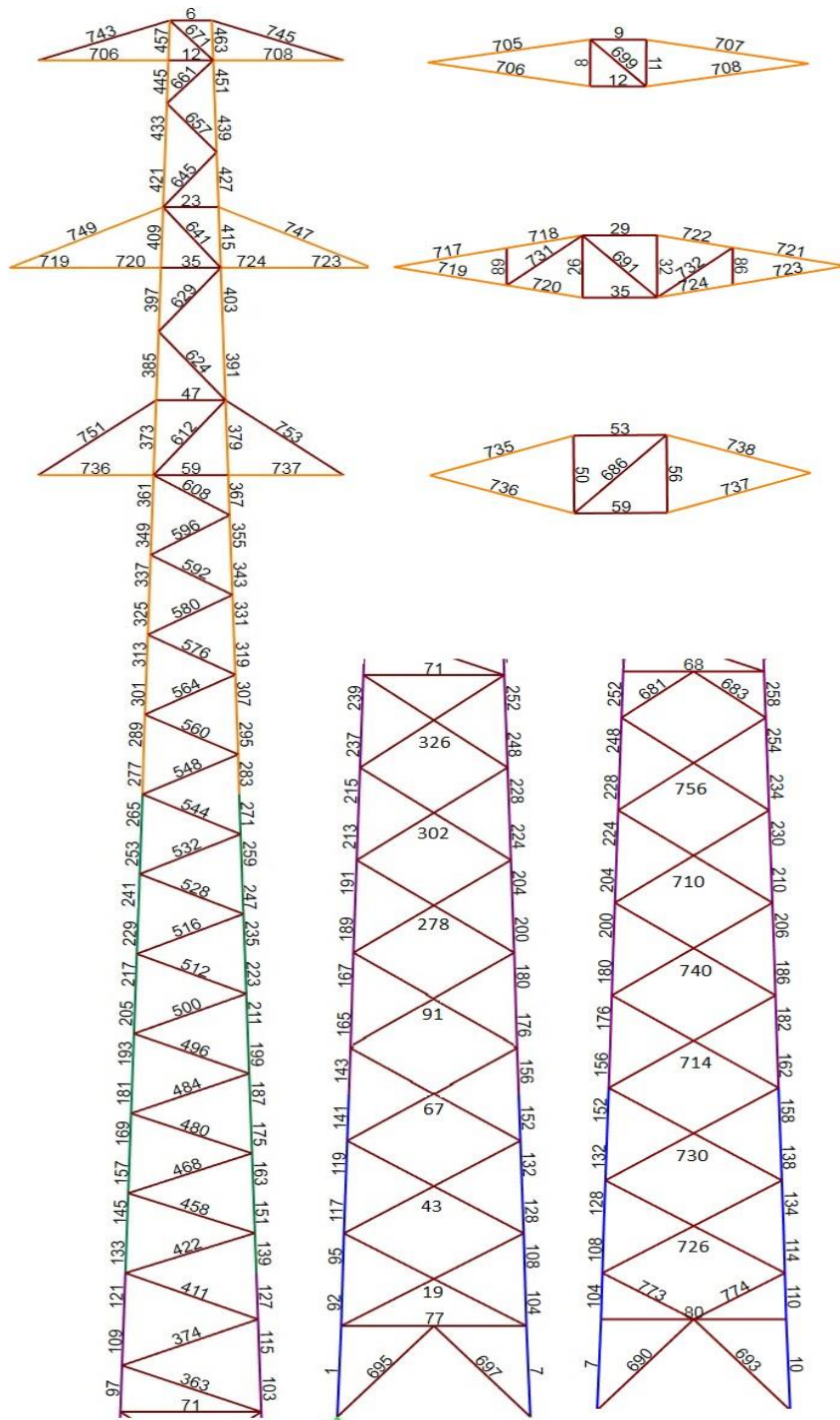


Figure C.1. Structural members of No.106 tower

Table C.1. Design limit states and load capacities of structural members (ASCE. 2015)

Member	Length (m)	Design Limit States (kN)				Design Capacity (kN)	
		Buckling	Bolt Shear	Bolt Bearing	Tensile Yielding	Compression	Tension
463	0.50	139.72	280.48	158.40	106.64	139.72	106.64
451	0.54	107.59	381.70	184.80	100.44	107.59	100.44
439	0.61	96.30	381.70	184.80	100.44	96.30	100.44
427	0.69	81.71	381.70	184.80	100.44	81.71	100.44
415	0.76	68.04	381.70	184.80	100.44	68.04	100.44
403	0.80	61.41	381.70	184.80	100.44	61.41	100.44
391	0.86	53.14	381.70	184.80	100.44	53.14	100.44
379	0.94	44.48	381.70	184.80	100.44	44.48	100.44
367	0.50	113.42	381.70	184.80	100.44	113.42	100.44
355	0.50	113.42	381.70	184.80	100.44	113.42	100.44
343	0.50	113.42	381.70	184.80	100.44	113.42	100.44
331	0.50	113.42	381.70	184.80	100.44	113.42	100.44
319	0.50	113.42	381.70	184.80	100.44	113.42	100.44
307	0.50	113.42	381.70	184.80	100.44	113.42	100.44
295	0.50	113.42	381.70	184.80	100.44	113.42	100.44
283	0.50	113.42	381.70	184.80	100.44	113.42	100.44
271	0.50	177.57	381.70	221.76	154.38	177.57	154.38
259	0.50	177.57	381.70	221.76	154.38	177.57	154.38
247	0.50	177.57	381.70	221.76	154.38	177.57	154.38
235	0.50	177.57	381.70	221.76	154.38	177.57	154.38
223	0.50	177.57	381.70	221.76	154.38	177.57	154.38
211	0.50	177.57	381.70	221.76	154.38	177.57	154.38
199	0.50	177.57	381.70	221.76	154.38	177.57	154.38
187	0.50	177.57	381.70	221.76	154.38	177.57	154.38

Table C.1. (cont'd) Design limit states and load capacities of structural members
(ASCE, 2015)

Member	Length (m)	Design Limit States (kN)				Design Capacity (kN)	
		Buckling	Bolt Shear	Bolt Bearing	Tensile Yielding	Compression	Tension
175	0.50	177.57	381.70	221.76	154.38	177.57	154.38
163	0.50	177.57	381.70	221.76	154.38	177.57	154.38
151	0.50	177.57	381.70	221.76	154.38	177.57	154.38
139	0.50	177.57	381.70	221.76	154.38	177.57	154.38
127	0.58	218.83	381.70	258.72	202.43	218.83	202.43
115	0.58	218.83	381.70	258.72	202.43	218.83	202.43
103	0.58	218.83	381.70	258.72	202.43	218.83	202.43
252	0.58	218.83	381.70	258.72	202.43	218.83	202.43
248	0.58	218.83	381.70	258.72	202.43	218.83	202.43
228	0.58	218.83	381.70	258.72	202.43	218.83	202.43
224	0.58	218.83	381.70	258.72	202.43	218.83	202.43
204	0.58	218.83	381.70	258.72	202.43	218.83	202.43
200	0.58	218.83	381.70	258.72	202.43	218.83	202.43
180	0.58	218.83	381.70	258.72	202.43	218.83	202.43
176	0.58	218.83	381.70	258.72	202.43	218.83	202.43
156	0.58	218.83	381.70	258.72	202.43	218.83	202.43
452	0.58	244.42	381.70	258.72	224.13	244.42	224.13
132	0.58	244.42	381.70	258.72	224.13	244.42	224.13
128	0.58	244.42	381.70	258.72	224.13	244.42	224.13
108	0.58	244.42	381.70	258.72	224.13	244.42	224.13
104	0.58	244.42	381.70	258.72	224.13	244.42	224.13
7	1.14	245.91	381.70	258.72	224.13	245.91	224.13
671	0.68	67.73	35.06	31.68	70.59	31.68	31.68
651	0.73	63.46	35.06	31.68	70.59	31.68	31.68

Table C.1. (cont'd) Design limit states and load capacities of structural members
(ASCE. 2015)

Member	Length (m)	Design Limit States (kN)				Design Capacity (kN)	
		Buckling	Bolt Shear	Bolt Bearing	Tensile Yielding	Compression	Tension
657	0.80	56.54	35.06	31.68	70.59	31.68	31.68
645	0.89	47.77	35.06	31.68	70.59	31.68	31.68
641	0.97	40.05	35.06	31.68	70.59	31.68	31.68
629	1.03	35.48	35.06	31.68	70.59	31.68	31.68
624	1.11	30.66	35.06	31.68	70.59	30.66	31.68
612	1.21	25.96	35.06	31.68	70.59	25.96	31.68
608	0.94	42.60	35.06	31.68	70.59	31.68	31.68
596	0.97	40.39	35.06	31.68	70.59	31.68	31.68
592	0.99	38.31	35.06	31.68	70.59	31.68	31.68
580	1.02	36.38	35.06	31.68	70.59	31.68	31.68
576	1.04	34.57	35.06	31.68	70.59	31.68	31.68
564	1.07	32.89	35.06	31.68	70.59	31.68	31.68
560	1.10	31.31	35.06	31.68	70.59	31.31	31.68
548	1.12	30.08	35.06	31.68	70.59	30.08	31.68
544	1.14	28.91	35.06	31.68	70.59	28.91	31.68
532	1.17	27.59	35.06	31.68	70.59	27.59	31.68
528	1.20	26.35	35.06	31.68	70.59	26.35	31.68
516	1.22	25.19	35.06	31.68	70.59	25.19	31.68
512	1.25	24.09	35.06	31.68	70.59	24.09	31.68
500	1.28	23.07	35.06	31.68	70.59	23.07	31.68
496	1.31	22.10	35.06	31.68	70.59	22.10	31.68
484	1.33	21.19	35.06	31.68	70.59	21.19	31.68
480	1.36	20.33	35.06	31.68	70.59	20.33	31.68
468	1.39	19.52	35.06	31.68	70.59	19.52	31.68

Table C.1. (cont'd) Design limit states and load capacities of structural members
(ASCE. 2015)

Member	Length (m)	Design Limit States (kN)				Design Capacity (kN)	
		Buckling	Bolt Shear	Bolt Bearing	Tensile Yielding	Compression	Tension
458	1.42	18.76	35.06	31.68	70.59	18.76	31.68
422	1.45	18.04	35.06	31.68	70.59	18.04	31.68
411	1.51	16.64	35.06	31.68	70.59	16.64	31.68
374	1.54	15.94	35.06	31.68	70.59	15.94	31.68
363	1.57	15.30	35.06	31.68	70.59	15.30	31.68
326	1.91	41.57	35.06	31.68	70.59	31.68	31.68
683	0.95	81.55	35.06	31.68	70.59	31.68	31.68
302	1.96	39.24	35.06	31.68	70.59	31.68	31.68
756	1.93	40.39	35.06	31.68	70.59	31.68	31.68
278	2.02	37.07	35.06	31.68	70.59	31.68	31.68
710	1.99	38.14	35.06	31.68	70.59	31.68	31.68
740	2.04	36.12	35.06	31.68	70.59	31.68	31.68
91	2.07	35.19	35.06	31.68	70.59	31.68	31.68
714	2.10	34.30	35.06	31.68	70.59	31.68	31.68
67	2.12	33.43	35.06	31.68	70.59	31.68	31.68
730	2.15	32.53	35.06	31.68	70.59	31.68	31.68
726	2.21	30.90	35.06	31.68	70.59	30.90	31.68
43	2.18	31.66	35.06	31.68	70.59	31.66	31.68
774	1.12	76.40	35.06	31.68	70.59	31.68	31.68
19	2.24	30.17	35.06	31.68	70.59	30.17	31.68
697	1.52	60.30	35.06	31.68	70.59	31.68	31.68
6	0.44	83.55	35.06	31.68	70.59	31.68	31.68
745	1.48	17.13	70.12	63.36	70.59	17.13	63.36
708	1.39	48.69	95.42	92.40	90.40	48.69	90.40

Table C.1. (cont'd) Design limit states and load capacities of structural members
(ASCE. 2015)

Member	Length (m)	Design Limit States (kN)				Design Capacity (kN)	
		Buckling	Bolt Shear	Bolt Bearing	Tensile Yielding	Compression	Tension
12	0.47	81.91	35.06	31.68	70.59	31.68	31.68
23	0.58	74.98	35.06	31.68	70.59	31.68	31.68
747	1.80	28.83	70.12	79.20	114.81	28.83	70.12
723	0.97	35.70	95.42	92.40	90.40	35.70	90.40
724	0.65	35.71	95.42	92.40	90.40	35.71	90.40
35	0.63	71.65	35.06	31.68	70.59	31.68	31.68
47	0.73	63.53	35.06	31.68	70.59	31.68	31.68
753	1.60	14.82	70.12	63.36	70.59	14.82	63.36
737	1.27	57.85	95.42	92.40	90.40	57.85	90.40
59	0.78	58.47	35.06	31.68	70.59	31.68	31.68
71	1.48	62.48	35.06	31.68	70.59	31.68	31.68
77	1.94	40.10	35.06	31.68	70.59	31.68	31.68
699	0.66	68.65	35.06	31.68	70.59	31.68	31.68
691	0.89	48.13	35.06	31.68	70.59	31.68	31.68
686	1.11	30.84	35.06	31.68	70.59	30.84	31.68

Table C.2. Hinge properties of structural members under tension

Member	Hinge Properties in Tension							
	<u>B</u>		<u>C</u>		<u>D</u>		<u>E</u>	
	Q_y (kN)	Δ (mm)	Q_u (kN)	Δ (mm)	Q (kN)	Δ (mm)	Q (kN)	Δ (mm)
463	106.64	0.53	151.36	6.36	85.31	6.36	85.31	7.95
451	100.44	0.54	142.56	6.47	80.35	6.47	80.35	8.09
439	100.44	0.61	142.56	7.31	80.35	7.31	80.35	9.14
427	100.44	0.69	142.56	8.27	80.35	8.27	80.35	10.33
415	100.44	0.76	142.56	9.11	80.35	9.11	80.35	11.38
403	100.44	0.80	142.56	9.59	80.35	9.59	80.35	11.98
391	100.44	0.86	142.56	10.30	80.35	10.30	80.35	12.88
379	100.44	0.94	142.56	11.26	80.35	11.26	80.35	14.08
367	100.44	0.50	142.56	5.99	80.35	5.99	80.35	7.49
355	100.44	0.50	142.56	5.99	80.35	5.99	80.35	7.49
343	100.44	0.50	142.56	5.99	80.35	5.99	80.35	7.49
331	100.44	0.50	142.56	5.99	80.35	5.99	80.35	7.49
319	100.44	0.50	142.56	5.99	80.35	5.99	80.35	7.49
307	100.44	0.50	142.56	5.99	80.35	5.99	80.35	7.49
295	100.44	0.50	142.56	5.99	80.35	5.99	80.35	7.49
283	100.44	0.50	142.56	5.99	80.35	5.99	80.35	7.49
271	154.38	0.54	219.12	6.45	123.50	6.45	123.50	8.06
259	154.38	0.54	219.12	6.45	123.50	6.45	123.50	8.06
247	154.38	0.54	219.12	6.45	123.50	6.45	123.50	8.06
235	154.38	0.54	219.12	6.45	123.50	6.45	123.50	8.06
223	154.38	0.54	219.12	6.45	123.50	6.45	123.50	8.06
211	154.38	0.54	219.12	6.45	123.50	6.45	123.50	8.06
199	154.38	0.54	219.12	6.45	123.50	6.45	123.50	8.06
187	154.38	0.54	219.12	6.45	123.50	6.45	123.50	8.06

Table C.2. (cont'd) Hinge properties of structural members under tension

Member	Hinge Properties in Tension							
	<u>B</u>		<u>C</u>		<u>D</u>		<u>E</u>	
	Q_y (kN)	Δ (mm)	Q_u (kN)	Δ (mm)	Q (kN)	Δ (mm)	Q (kN)	Δ (mm)
175	154.38	0.54	219.12	6.45	123.50	6.45	123.50	8.06
163	154.38	0.54	219.12	6.45	123.50	6.45	123.50	8.06
151	154.38	0.54	219.12	6.45	123.50	6.45	123.50	8.06
139	154.38	0.54	219.12	6.45	123.50	6.45	123.50	8.06
127	202.43	0.64	258.72	7.71	161.94	7.71	161.94	9.64
115	202.43	0.64	258.72	7.71	161.94	7.71	161.94	9.64
103	202.43	0.64	258.72	7.71	161.94	7.71	161.94	9.64
252	202.43	0.64	258.72	7.71	161.94	7.71	161.94	9.64
248	202.43	0.64	258.72	7.71	161.94	7.71	161.94	9.64
228	202.43	0.64	258.72	7.71	161.94	7.71	161.94	9.64
224	202.43	0.64	258.72	7.71	161.94	7.71	161.94	9.64
204	202.43	0.64	258.72	7.71	161.94	7.71	161.94	9.64
200	202.43	0.64	258.72	7.71	161.94	7.71	161.94	9.64
180	202.43	0.64	258.72	7.71	161.94	7.71	161.94	9.64
176	202.43	0.64	258.72	7.71	161.94	7.71	161.94	9.64
156	202.43	0.64	258.72	7.71	161.94	7.71	161.94	9.64
452	224.13	0.66	258.72	7.90	179.30	7.90	179.30	9.88
132	224.13	0.66	258.72	7.90	179.30	7.90	179.30	9.88
128	224.13	0.66	258.72	7.90	179.30	7.90	179.30	9.88
108	224.13	0.66	258.72	7.90	179.30	7.90	179.30	9.88
104	224.13	0.66	258.72	7.90	179.30	7.90	179.30	9.88
7	224.13	1.30	258.72	15.55	179.30	15.55	179.30	19.44
671	31.68	0.33	31.68	3.99	25.34	3.99	25.34	4.98
651	31.68	0.36	31.68	4.29	25.34	4.29	25.34	5.36

Table C.2. (cont'd) Hinge properties of structural members under tension

Member	Hinge Properties in Tension							
	<u>B</u>		<u>C</u>		<u>D</u>		<u>E</u>	
	Q_y (kN)	Δ (mm)	Q_u (kN)	Δ (mm)	Q (kN)	Δ (mm)	Q (kN)	Δ (mm)
657	31.68	0.39	31.68	4.73	25.34	4.73	25.34	5.91
645	31.68	0.44	31.68	5.24	25.34	5.24	25.34	6.55
641	31.68	0.48	31.68	5.72	25.34	5.72	25.34	7.15
629	31.68	0.51	31.68	6.08	25.34	6.08	25.34	7.60
624	31.68	0.55	31.68	6.54	25.34	6.54	25.34	8.18
612	31.68	0.59	31.68	7.11	25.34	7.11	25.34	8.88
608	31.68	0.46	31.68	5.55	25.34	5.55	25.34	6.94
596	31.68	0.47	31.68	5.70	25.34	5.70	25.34	7.12
592	31.68	0.49	31.68	5.85	25.34	5.85	25.34	7.31
580	31.68	0.50	31.68	6.00	25.34	6.00	25.34	7.51
576	31.68	0.51	31.68	6.16	25.34	6.16	25.34	7.70
564	31.68	0.53	31.68	6.32	25.34	6.32	25.34	7.89
560	31.68	0.54	31.68	6.47	25.34	6.47	25.34	8.09
548	31.68	0.55	31.68	6.60	25.34	6.60	25.34	8.25
544	31.68	0.56	31.68	6.74	25.34	6.74	25.34	8.42
532	31.68	0.57	31.68	6.90	25.34	6.90	25.34	8.62
528	31.68	0.59	31.68	7.06	25.34	7.06	25.34	8.82
516	31.68	0.60	31.68	7.22	25.34	7.22	25.34	9.02
512	31.68	0.61	31.68	7.38	25.34	7.38	25.34	9.22
500	31.68	0.63	31.68	7.54	25.34	7.54	25.34	9.43
496	31.68	0.64	31.68	7.70	25.34	7.70	25.34	9.63
484	31.68	0.66	31.68	7.87	25.34	7.87	25.34	9.83
480	31.68	0.67	31.68	8.03	25.34	8.03	25.34	10.04
468	31.68	0.68	31.68	8.20	25.34	8.20	25.34	10.25

Table C.2. (cont'd) Hinge properties of structural members under tension

Member	Hinge Properties in Tension							
	<u>B</u>		<u>C</u>		<u>D</u>		<u>E</u>	
	Q_y (kN)	Δ (mm)	Q_u (kN)	Δ (mm)	Q (kN)	Δ (mm)	Q (kN)	Δ (mm)
458	31.68	0.70	31.68	8.36	25.34	8.36	25.34	10.45
422	31.68	0.71	31.68	8.53	25.34	8.53	25.34	10.66
411	31.68	0.74	31.68	8.88	25.34	8.88	25.34	11.10
374	31.68	0.76	31.68	9.07	25.34	9.07	25.34	11.34
363	31.68	0.77	31.68	9.26	25.34	9.26	25.34	11.57
326	31.68	0.94	31.68	11.23	25.34	11.23	25.34	14.04
683	31.68	0.47	31.68	5.62	25.34	5.62	25.34	7.02
302	31.68	0.96	31.68	11.56	25.34	11.56	25.34	14.46
756	31.68	0.95	31.68	11.40	25.34	11.40	25.34	14.25
278	31.68	0.99	31.68	11.90	25.34	11.90	25.34	14.87
710	31.68	0.98	31.68	11.73	25.34	11.73	25.34	14.66
740	31.68	1.00	31.68	12.05	25.34	12.05	25.34	15.07
91	31.68	1.02	31.68	12.21	25.34	12.21	25.34	15.26
714	31.68	1.03	31.68	12.37	25.34	12.37	25.34	15.46
67	31.68	1.04	31.68	12.53	25.34	12.53	25.34	15.66
730	31.68	1.06	31.68	12.70	25.34	12.70	25.34	15.88
726	31.68	1.09	31.68	13.03	25.34	13.03	25.34	16.29
43	31.68	1.07	31.68	12.87	25.34	12.87	25.34	16.09
774	31.68	0.55	31.68	6.59	25.34	6.59	25.34	8.24
19	31.68	1.10	31.68	13.19	25.34	13.19	25.34	16.48
697	31.68	0.75	31.68	8.99	25.34	8.99	25.34	11.24
6	31.68	0.22	31.68	2.59	25.34	2.59	25.34	3.24
745	63.36	1.46	63.36	17.50	50.69	17.50	50.69	21.88
708	90.40	1.24	92.40	14.94	72.32	14.94	72.32	18.67

Table C.2. (cont'd) Hinge properties of structural members under tension

Member	Hinge Properties in Tension							
	<u>B</u>		<u>C</u>		<u>D</u>		<u>E</u>	
	Q_y (kN)	Δ (mm)	Q_u (kN)	Δ (mm)	Q (kN)	Δ (mm)	Q (kN)	Δ (mm)
12	31.68	0.23	31.68	2.77	25.34	2.77	25.34	3.46
23	31.68	0.29	31.68	3.42	25.34	3.42	25.34	4.28
747	70.12	1.25	70.12	15.06	56.10	15.06	56.10	18.82
723	90.40	0.87	92.40	10.44	72.32	10.44	72.32	13.05
724	90.40	0.58	92.40	7.00	72.32	7.00	72.32	8.75
35	31.68	0.31	31.68	3.69	25.34	3.69	25.34	4.61
47	31.68	0.36	31.68	4.28	25.34	4.28	25.34	5.35
753	63.36	1.57	63.36	18.82	50.69	18.82	50.69	23.52
737	90.40	1.14	92.40	13.70	72.32	13.70	72.32	17.13
59	31.68	0.38	31.68	4.61	25.34	4.61	25.34	5.76
71	31.68	0.73	31.68	8.70	25.34	8.70	25.34	10.88
77	31.68	0.95	31.68	11.44	25.34	11.44	25.34	14.30
699	31.68	0.33	31.68	3.92	25.34	3.92	25.34	4.90
691	31.68	0.44	31.68	5.22	25.34	5.22	25.34	6.53
686	31.68	0.54	31.68	6.52	25.34	6.52	25.34	8.15

Table C.3. Hinge properties of structural members under compression

Member	Hinge Properties in Compression							
	<u>B</u>		<u>C</u>		<u>D</u>		<u>E</u>	
	Q_y (kN)	Δ (mm)	Q_u (kN)	Δ (mm)	Q (kN)	Δ (mm)	Q (kN)	Δ (mm)
463	139.72	0.69	139.72	1.04	27.94	1.04	27.94	6.95
451	107.59	0.58	107.59	0.87	21.52	0.87	21.52	5.78
439	96.30	0.58	96.30	0.88	19.26	0.88	19.26	5.84
427	81.71	0.56	81.71	0.84	16.34	0.84	16.34	5.60
415	68.04	0.51	68.04	0.77	13.61	0.77	13.61	5.14
403	61.41	0.49	61.41	0.73	12.28	0.73	12.28	4.88
391	53.14	0.45	53.14	0.68	10.63	0.68	10.63	4.54
379	44.48	0.42	44.48	0.62	8.90	0.62	8.90	4.16
367	113.42	0.56	113.42	0.85	22.68	0.85	22.68	5.64
355	113.42	0.56	113.42	0.85	22.68	0.85	22.68	5.64
343	113.42	0.56	113.42	0.85	22.68	0.85	22.68	5.64
331	113.42	0.56	113.42	0.85	22.68	0.85	22.68	5.64
319	113.42	0.56	113.42	0.85	22.68	0.85	22.68	5.64
307	113.42	0.56	113.42	0.85	22.68	0.85	22.68	5.64
295	113.42	0.56	113.42	0.85	22.68	0.85	22.68	5.64
283	113.42	0.56	113.42	0.85	22.68	0.85	22.68	5.64
271	177.57	0.62	177.57	0.93	35.51	0.93	35.51	6.18
259	177.57	0.62	177.57	0.93	35.51	0.93	35.51	6.18
247	177.57	0.62	177.57	0.93	35.51	0.93	35.51	6.18
235	177.57	0.62	177.57	0.93	35.51	0.93	35.51	6.18
223	177.57	0.62	177.57	0.93	35.51	0.93	35.51	6.18
211	177.57	0.62	177.57	0.93	35.51	0.93	35.51	6.18
199	177.57	0.62	177.57	0.93	35.51	0.93	35.51	6.18
187	177.57	0.62	177.57	0.93	35.51	0.93	35.51	6.18

Table C.3. (cont'd) Hinge properties of structural members under compression

Member	Hinge Properties in Compression							
	<u>B</u>		<u>C</u>		<u>D</u>		<u>E</u>	
	Q_y (kN)	Δ (mm)	Q_u (kN)	Δ (mm)	Q (kN)	Δ (mm)	Q (kN)	Δ (mm)
175	177.57	0.62	177.57	0.93	35.51	0.93	35.51	6.18
163	177.57	0.62	177.57	0.93	35.51	0.93	35.51	6.18
151	177.57	0.62	177.57	0.93	35.51	0.93	35.51	6.18
139	177.57	0.62	177.57	0.93	35.51	0.93	35.51	6.18
127	218.83	0.69	218.83	1.04	43.77	1.04	43.77	6.95
115	218.83	0.69	218.83	1.04	43.77	1.04	43.77	6.95
103	218.83	0.69	218.83	1.04	43.77	1.04	43.77	6.95
252	218.83	0.69	218.83	1.04	43.77	1.04	43.77	6.95
248	218.83	0.69	218.83	1.04	43.77	1.04	43.77	6.95
228	218.83	0.69	218.83	1.04	43.77	1.04	43.77	6.95
224	218.83	0.69	218.83	1.04	43.77	1.04	43.77	6.95
204	218.83	0.69	218.83	1.04	43.77	1.04	43.77	6.95
200	218.83	0.69	218.83	1.04	43.77	1.04	43.77	6.95
180	218.83	0.69	218.83	1.04	43.77	1.04	43.77	6.95
176	218.83	0.69	218.83	1.04	43.77	1.04	43.77	6.95
156	218.83	0.69	218.83	1.04	43.77	1.04	43.77	6.95
452	244.42	0.72	244.42	1.08	48.88	1.08	48.88	7.18
132	244.42	0.72	244.42	1.08	48.88	1.08	48.88	7.18
128	244.42	0.72	244.42	1.08	48.88	1.08	48.88	7.18
108	244.42	0.72	244.42	1.08	48.88	1.08	48.88	7.18
104	244.42	0.72	244.42	1.08	48.88	1.08	48.88	7.18
7	245.91	1.42	245.91	2.13	49.18	2.13	49.18	14.22
671	31.68	0.33	31.68	3.99	25.34	3.99	25.34	4.98
651	31.68	0.36	31.68	4.29	25.34	4.29	25.34	5.36

Table C.3. (cont'd) Hinge properties of structural members under compression

Member	Hinge Properties in Compression							
	<u>B</u>		<u>C</u>		<u>D</u>		<u>E</u>	
	Q_y (kN)	Δ (mm)	Q_u (kN)	Δ (mm)	Q (kN)	Δ (mm)	Q (kN)	Δ (mm)
657	31.68	0.39	31.68	4.73	25.34	4.73	25.34	5.91
645	31.68	0.44	31.68	5.24	25.34	5.24	25.34	6.55
641	31.68	0.48	31.68	5.72	25.34	5.72	25.34	7.15
629	31.68	0.51	31.68	6.08	25.34	6.08	25.34	7.60
624	30.66	0.53	30.66	0.79	6.13	0.79	6.13	5.28
612	25.96	0.49	25.96	0.73	5.19	0.73	5.19	4.85
608	31.68	0.46	31.68	5.55	25.34	5.55	25.34	6.94
596	31.68	0.47	31.68	5.70	25.34	5.70	25.34	7.12
592	31.68	0.49	31.68	5.85	25.34	5.85	25.34	7.31
580	31.68	0.50	31.68	6.00	25.34	6.00	25.34	7.51
576	31.68	0.51	31.68	6.16	25.34	6.16	25.34	7.70
564	31.68	0.53	31.68	6.32	25.34	6.32	25.34	7.89
560	31.31	0.53	31.31	0.80	6.26	0.80	6.26	5.33
548	30.08	0.52	30.08	0.78	6.02	0.78	6.02	5.23
544	28.91	0.51	28.91	0.77	5.78	0.77	5.78	5.12
532	27.59	0.50	27.59	0.75	5.52	0.75	5.52	5.00
528	26.35	0.49	26.35	0.73	5.27	0.73	5.27	4.89
516	25.19	0.48	25.19	0.72	5.04	0.72	5.04	4.78
512	24.09	0.47	24.09	0.70	4.82	0.70	4.82	4.68
500	23.07	0.46	23.07	0.69	4.61	0.69	4.61	4.58
496	22.10	0.45	22.10	0.67	4.42	0.67	4.42	4.48
484	21.19	0.44	21.19	0.66	4.24	0.66	4.24	4.39
480	20.33	0.43	20.33	0.64	4.07	0.64	4.07	4.30
468	19.52	0.42	19.52	0.63	3.90	0.63	3.90	4.21

Table C.3. (cont'd) Hinge properties of structural members under compression

Member	Hinge Properties in Compression							
	<u>B</u>		<u>C</u>		<u>D</u>		<u>E</u>	
	Q_y (kN)	Δ (mm)	Q_u (kN)	Δ (mm)	Q (kN)	Δ (mm)	Q (kN)	Δ (mm)
458	18.76	0.41	18.76	0.62	3.75	0.62	3.75	4.13
422	18.04	0.40	18.04	0.61	3.61	0.61	3.61	4.05
411	16.64	0.39	16.64	0.58	3.33	0.58	3.33	3.89
374	15.94	0.38	15.94	0.57	3.19	0.57	3.19	3.80
363	15.30	0.37	15.30	0.56	3.06	0.56	3.06	3.73
326	31.68	0.94	31.68	11.23	25.34	11.23	25.34	14.04
683	31.68	0.47	31.68	5.62	25.34	5.62	25.34	7.02
302	31.68	0.96	31.68	11.56	25.34	11.56	25.34	14.46
756	31.68	0.95	31.68	11.40	25.34	11.40	25.34	14.25
278	31.68	0.99	31.68	11.90	25.34	11.90	25.34	14.87
710	31.68	0.98	31.68	11.73	25.34	11.73	25.34	14.66
740	31.68	1.00	31.68	12.05	25.34	12.05	25.34	15.07
91	31.68	1.02	31.68	12.21	25.34	12.21	25.34	15.26
714	31.68	1.03	31.68	12.37	25.34	12.37	25.34	15.46
67	31.68	1.04	31.68	12.53	25.34	12.53	25.34	15.66
730	31.68	1.06	31.68	12.70	25.34	12.70	25.34	15.88
726	30.90	1.06	30.90	1.59	6.18	1.59	6.18	10.59
43	31.66	1.07	31.66	1.61	6.33	1.61	6.33	10.72
774	31.68	0.55	31.68	6.59	25.34	6.59	25.34	8.24
19	30.17	1.05	30.17	1.57	6.03	1.57	6.03	10.47
697	31.68	0.75	31.68	8.99	25.34	8.99	25.34	11.24
6	31.68	0.22	31.68	2.59	25.34	2.59	25.34	3.24
745	17.13	0.39	17.13	0.59	3.43	0.59	3.43	3.94
708	48.69	0.67	48.69	1.01	9.74	1.01	9.74	6.70

Table C.3. (cont'd) Hinge properties of structural members under compression

Member	Hinge Properties in Compression							
	<u>B</u>		<u>C</u>		<u>D</u>		<u>E</u>	
	Q_y (kN)	Δ (mm)	Q_u (kN)	Δ (mm)	Q (kN)	Δ (mm)	Q (kN)	Δ (mm)
12	31.68	0.23	31.68	2.77	25.34	2.77	25.34	3.46
23	31.68	0.29	31.68	3.42	25.34	3.42	25.34	4.28
747	28.83	0.52	28.83	0.77	5.77	0.77	5.77	5.16
723	35.70	0.34	35.70	0.52	7.14	0.52	7.14	3.44
724	35.71	0.23	35.71	0.35	7.14	0.35	7.14	2.30
35	31.68	0.31	31.68	3.69	25.34	3.69	25.34	4.61
47	31.68	0.36	31.68	4.28	25.34	4.28	25.34	5.35
753	14.82	0.37	14.82	0.55	2.96	0.55	2.96	3.67
737	57.85	0.73	57.85	1.10	11.57	1.10	11.57	7.31
59	31.68	0.38	31.68	4.61	25.34	4.61	25.34	5.76
71	31.68	0.73	31.68	8.70	25.34	8.70	25.34	10.88
77	31.68	0.95	31.68	11.44	25.34	11.44	25.34	14.30
699	31.68	0.33	31.68	3.92	25.34	3.92	25.34	4.90
691	31.68	0.44	31.68	5.22	25.34	5.22	25.34	6.53
686	30.84	0.53	30.84	0.79	6.17	0.79	6.17	5.29